International Scientific-Technical and Production Journal

CONTENTS

BRAZING OF TITANIUM ALLOYS
BY USING ALUMINIUM-BASE FILLER ALLOYS

V.F. KHORUNOV, V.V. VORONOV and **S.V. MAKSYMOVA**

E.O. Paton Electric Welding Institute, NASU, Kiev, Ukraine

Investigations on brazing of titanium alloy samples by using different compositions of aluminium filler alloys were carried out. Silicon-free aluminium filler alloys were found to be acceptable for producing the brazed joints on titanium alloys. The 670−690 °C brazing temperature range is optimal for the selected filler alloys.

Keywords: brazing, titanium alloys, aluminium alloys, commercial brazing filler alloys, wetting, microstructure, mechanical properties

Since the 1960s, Al-base filler alloys have been widely used for brazing of titanium alloys. Pure aluminium or alloys of the Al−Si, Al−Si−Cu and Al−Mg systems are mainly applied as brazing filler alloys [7]. Compositions of some Al-base filler alloys are given in Table 1.

Key advantages of aluminium filler alloys are low melting temperature, low specific weight, good compatibility with titanium alloys base metal and, in particular, good wetting and flowing into the gap. Therefore, special consideration has been given to the aluminium filler alloys since the time when the Ti-base alloys have found application in aerospace engineering.

An important drawback of the Al-base filler alloys is their active reaction with the base metal. Even a relatively short time of contact of titanium with molten aluminium may lead to a deep erosion of the base metal. Silicon is added to the Al-base filler alloys to reduce reactivity of pure aluminium and decrease the brazing temperature (hence, decrease the probability of formation of intermetallics). But in this case silicides may form at the titanium alloy−filler alloy interface. However, the main problem is the Al_2O_3 film on the aluminium filler alloys, which prevents their spreading over the base metal.

Despite a large amount of the investigations conducted in Eastern Europe and particularly in Ukraine to study brazing of titanium by using aluminium filler alloys, brazing of titanium with this type of the filler alloys failed to receive acceptance. There are publications on development of new aluminium filler alloys for brazing of titanium alloys [7], this evidencing the industrial demand for commercial medium-melting point filler alloys for brazing of titanium and its alloys.

Wide application of aluminium filler alloys in this case is hindered by a low strength of the resulting brazed joints, which is much lower than that of the joints brazed with titanium filler alloys. One of the promising areas of using aluminium filler alloys is brazing of lamellar-ribbed thin-walled structures and thin-walled honey-

Table 1. List of standard aluminium-base brazing filler alloys

| Grade of filler alloy	Manufacturing country	Composition of filler alloy	T_{br}, °C
AD1	USSR	Al−0.4Si−0.3Fe	665
AL2	Same	Al−13Si	560−700
AVCON 48	USA	Al−4.8Si−3.8Cu−0.2Fe−0.2Ni	610−680
AA3003	Same	Al−1Mn−0.6Si−0.7Fe	660−670
TiBrazeAl-600	»	Al−12Si−0.8Fe	590−610
TiBrazeAl-630	»	Al−1.5Mg−4Cu−2Ni	630−660
TiBrazeAl-640	»	Al−(4.4−5.2)Mg−(0.7-1)Mn−0.2Cr	640−660
TiBrazeAl-642	»	Al−5.3Si−0.8Fe−0.3Cu−0.2Ti	650−680
TiBrazeAl-645	»	Al−(4.3−5.5)Mg−0.25Si−0.4Fe−0.2Ti−0.2Cr	640−660
TiBrazeAl-655	»	Al−6.3Cu−0.3Mn−0.2Si−0.2Ti−0.2Zr	650−670
TiBrazeAl-665	»	Al−2.5Mg−0.2Si−0.4Fe−0.2Cr	660−680

comb panels for aerospace engineering, where a relatively low strength of the seams is acceptable, which is confirmed, in particular, in study [7]. The choice of the aluminium filler alloys is favoured by their good wetting and spreading over the titanium substrate at a comparatively low temperature, as well as the possibility of achieving a low level of erosion of the base metal in brazing. Therefore, all drawbacks in this case are surpassed by the advantages, such as a lower cost, higher affordability and better workability of the aluminium filler alloys compared to the titanium and silver ones.

The purpose of this study was to generate data on advantages and drawbacks of different compositions of aluminium filler alloys for brazing of titanium, as well to compare modern commercial and experimental filler alloys with widely used aluminium alloys AD1 and AMg6.

Low titanium alloy OT4 was used as a base metal. Two groups of aluminium filler alloys for brazing of titanium were investigated: in the first group silicon was used as a depressant, and in the second group the depressant was magnesium.

The first group included standard alloy AL2, modern commercial filler alloy TiBrazeAl-642 and experimental alloys Al−12Si−1Mg, Al−12Si−0.3Li and Al−5Si−1.5V produced by the powder metallurgy method. The second group included alloy AMg6 and modern commercial filler alloy TiBrazeAl-665. Low alloy AD1 was investigated for comparison.

Experiments on selection of optimal parameters of heating for brazing were carried out in vacuum furnace SGV 2,4-2/15-I3 at a vacuum level of $5 \cdot 10^{-5}$ mm Hg. For additional cleaning of the brazing atmosphere, brazing was performed in vacuum in the titanium container with a getter.
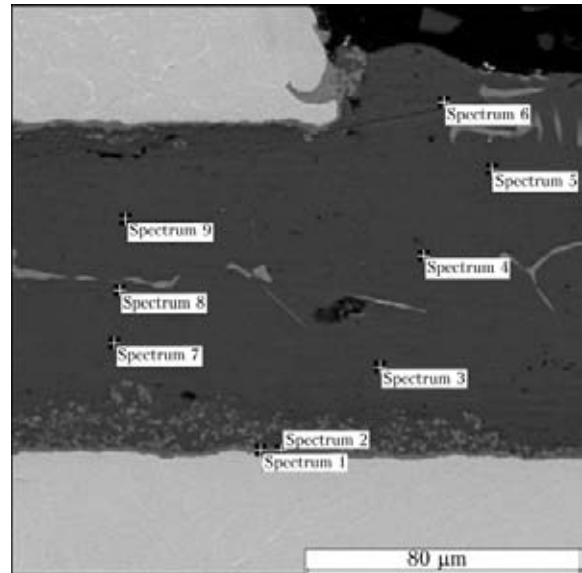
Figure 1. Microstructure of fillet region of the brazed joint on titanium alloy OT4 made by using filler alloy AMg6

Table 2 gives contact angles of the alloys on a substrate of titanium alloy OT4, which were measured by using software AutoCad 2002LT. Increase in the temperature of brazing of titanium alloys was accompanied by substantial improvement of wetting and spreading of the filler alloys over the substrate. However, it should be noted that Si-containing filler alloys TiBrazeAl-642, Al−13Si and Al−12Si−0.3Li featured a poor spreading over the surface of the titanium samples up to a temperature of 700 °C (at 740 °C, spreading of all the filler alloys was so high that it caused flowing out of a filler alloy from the gaps, the contact angle in this case being approximately 0°). At the same time, filler alloy AD1 and the Mg-containing filler alloys (AMg6 and TiBrazeAl-665) satisfactorily wetted titanium even at 670 °C.

Metallographic examinations of the brazed joints made by using the Mg-containing aluminium filler alloys showed the presence of a

Table 2. Dependence of contact angles on brazing temperature

Filler alloy	T_L, °C	Temperature of heating for brazing, °C			
		600	630	670	700
		Contact angles, deg			
AD1 (Al−0.4Si−0.3Fe)	660	−	−	60	~15
AMg6 (Al−6Mg−0.6Mn−0.4Si−0.4Fe−0.1Ti)	632	−	−	20	7−10
TiBrazeAl-642 (Al−5.3Si−0.8Fe−0.3Cu−0.2Ti)	630	−	−	40	~10
AL2 (Al−13Si)	578	90	90	55	~25
TiBrazeAl-665 (Al−2.5Mg−0.2Si−0.4Fe−0.2Cr)	650	−	−	25	8−10
Al−12Si−0.3Li	580	90	60	45	~10
Al−12Si−1Mg	575	−	85	40	~15
Al−5Si−1.5V	630	−	−	40	~10
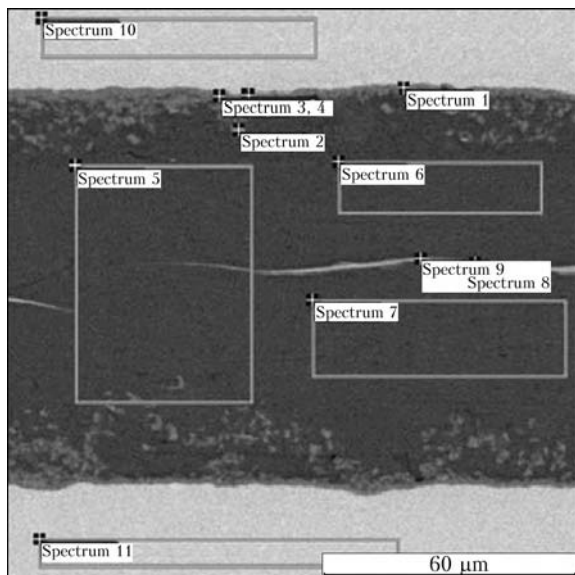
Figure 2. Microstructure of region of the brazed joint on titanium alloy OT4 made by using filler alloy AMg6

Table 3. Chemical heterogeneity of fillet region of the brazed joint on titanium alloy OT4 made by using filler alloy AMg6, wt.%

Spectrum number	O	Mg	Al	Si	Ti	Mn	Fe
1	1.76	–	48.67	1.05	47.95	0.57	–
2	1.62	–	50.89	1.06	45.83	0.60	–
3	1.13	0.43	97.01	–	0.79	0.64	–
4	0.77	0.49	97.84	–	0.25	0.65	–
5	1.24	0.28	97.78	–	0.13	0.57	–
6	3.01	0.15	95.68	–	0.15	0.69	0.32
7	1.07	0.53	97.01	–	0.77	0.62	–
8	1.78	0.71	96.59	–	0.28	0.63	–
9	1.31	0.71	96.71	–	0.64	0.63	–

continuous intermetallic interlayer at the filler alloy–base metal interface (T_{br} = 685 °C, vacuum — $5 \cdot 10^{-5}$ mm Hg, t = 3 min). Composition of the interlayer varied from (wt.%) 48.67Al–47.95Ti–1.05Si–0.57Mn in the fillet region (see spectrum 1 in Figure 1; Table 3) to 72.68Al–20.75Ti–1.33Mg–0.74Si–0.36Mn (spectrum 2 in Figure 2; Table 4). In the first case it corresponded approximately to a composition of intermetallic compound $TiAl_2$, and in the second case — to $TiAl_3$.

Also, one should note a low content of magnesium in the brazed seams, i.e. maximum 1.5 wt.% (see Tables 3 and 4). This can be explained by evaporation of magnesium from the seam metal during heating and melting of a filler alloy in vacuum. Very likely that it is this fact that caused destruction of the aluminium oxide film on the surface of the filler alloy, which made wetting of the base metal with the filler alloy melt much easier. The destructed oxide film was distributed over the entire seam (see oxygen content in spectra 1–9 in Figure 1 and Table 3;

spectra 5–9 in Figure 2 and Table 4), except for the intermetallic interlayer at the filler alloy–base metal interface.

Light phase inclusions along the seam axis were compounds of aluminium with iron and silicon, which were present in alloy AMg6 in small quantities.

Metallographic examinations of the joints brazed by using the Si-containing aluminium filler alloys showed that the brazed joints were characterised by a poor quality and the presence of cracks in the seams and fillet regions. Solidification of silicide in the form of a continuous strip was observed along the seam on both interfaces with the base metal. Such peculiarities of formation of the brazed seams did not allow providing of sound brazed joints and avoiding formation of silicides and cracks (Figure 3).

Strength tests of the overlap joints on alloy OT4 brazed by using commercial filler alloys Ti-BrazeAl-665 and TiBrazeAl-642, as well as alloys AD1 and AMg6 were carried out to evaluate the level of strength of the brazed joints. Thickness of the filler alloy foils was 100 μm for TiBrazeAl-665 and TiBrazeAl-642, and 60 μm for AD1 and

Figure 3. Microstructure of region of the brazed joint on titanium alloy OT4 made by using filler alloy Al–5Si–1.5V

Table 4. Chemical heterogeneity of region of the brazed joint on titanium alloy OT4 made by using filler alloy AMg6, wt.%

Spectrum number	O	Mg	Al	Si	Ti	Mn	Fe
1	–	0.46	64.12	1.32	33.55	0.30	0.25
2	4.14	1.33	72.68	0.74	20.75	0.36	–
3	–	–	54.42	1.34	43.83	0.41	–
4	–	0.75	68.94	1.10	28.78	0.43	–
5	1.16	1.43	96.22	–	0.60	0.59	–
6	1.12	1.25	96.35	–	0.74	0.54	–
7	1.23	1.46	96.47	–	0.30	0.54	–
8	1.64	0.96	81.16	0.48	0.30	1.99	10.13
9	1.15	1.05	85.72	0.46	0.30	1.66	9.66
10	–	–	4.49	–	94.95	0.56	–
11	–	–	3.59	–	95.90	0.51	–

AMg6. A filler alloy in the form of a foil was placed in the gap between the samples brazed. The time of holding at a brazing temperature was 3 min, and the brazing temperature was 685 °C. Additionally, brazing of the samples by using the AMg6 filler alloy was carried out at a temperature of 720 °C. The mechanical test results are shown in Figure 4.

Based on the data presented, it can be noted that strength of the joints made by using Mg-containing filler alloys TiBrazeAl-642 and AMg6 was almost identical and equal to 82−83 MPa, whereas strength of the joints made by using Si-containing filler alloy TiBrazeAl-665 was low, which could be due to solidification of silicide in the form of a continuous strip at the filler alloy−base metal interface.

It should be noted that the evaluated strength value (83 MPa) of the joints brazed by using commercial filler alloys TiBrazeAl-665 (Al−2.5Mg−0.3Cr) turned out to be lower than that claimed by the manufacturer (about 98 MPa) [7]. The attempts to achieve the claimed values failed, and after changing the configuration of the samples brazed, which was aimed at decreasing the bending component of stresses in shear tests, the determined strength value of the brazed joints was the same 83 MPa. Probably, in our experiments we omitted some know-how of the authors.

Increase in the brazing temperature had an extremely negative effect on strength of the joints brazed with aluminium filler alloys. For example, a twofold decrease in strength was revealed in brazing with alloy AMg6 at a temperature of 720 °C (see pos. 3 in Figure 4). In this case the decrease can be explained by growth of the Ti_3Al interlayer because of intensification of the reactivity of aluminium with respect to titanium with increase in the temperature and extension of the time of contact of the molten filler alloy with the titanium substrate.

The obtained strength value (about 83 MPa) of the brazed joints made by using aluminium filler alloys is sufficient for brazing of lamellar-ribbed structures and sheet parts with a large contact area. The main advantage of the aluminium filler alloys in this case will be, as mentioned above, the workability, low cost and affordability.

Analysis of the results obtained shows that the 680−690 °C brazing temperature is acceptable for producing the brazed joints on titanium alloys by using the Si-free aluminium filler alloys, such as alloys AD1, AMg6 and TiBrazeAl-642. The time of holding in brazing of titanium by using the above filler alloys should be as short as pos-
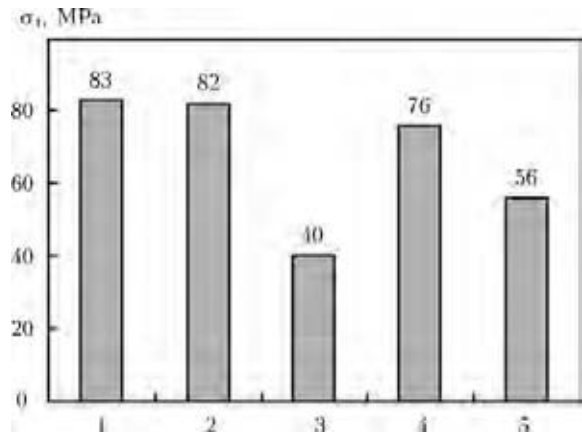
Figure 4. Strength of the overlap joints on alloy OT4 (holding time − 3 min) made by using the following filler alloys: 1 − TiBrazeAl-642; 2, 3 − AMg6; 4 − AD1; 5 − TiBrazeAl-665 (1, 2, 4, 5 − T_{br} = 685; 3 − 720 °C)

sible to prevent formation of brittle intermetallic interlayers.

CONCLUSIONS

1. Si-free brazing filler alloys, e.g. AD1, AMg6, TiBrazeAl-642, were found to be acceptable for producing the brazed joints on titanium alloys. The best results were obtained with the Al−Mg system based filler alloys (AMg6, TiBrazeAl-642).

2. The 680−700 °C brazing temperature range is optimal for the chosen filler materials. The holding time in brazing of titanium with the given filler alloys should be as short as possible to prevent formation of brittle intermetallic interlayers.

3. When using filler alloys based on the Al−Si system, formation of silicides, in addition to the Al- and Ti-base intermetallic interlayers, occurs in the brazed seams. They have the form of a continuous strip propagating along the seam on the side of the base metal, this leading to origination of defects in the form of cracks.

1. Lashko, N.F., Lashko, S.V. (1977) *Brazing of metals*. Moscow: Mashinostroenie.
2. Wells, R.R. (1975) Low temperature large-area brazing of damage tolerant structure. *Welding J.*, 54(**10**), 348−356.
3. Kimbal, C.E. (1980) Aluminum brazed titanium acoustic structures. *Ibid.*, 59(**10**), 26−30.
4. Nesterov, A.F., Studenov, G.V. (1987) Brazing of overlap titanium joints with aluminium filler alloys. In: *Proc. of Seminar on Increase in Quality and Efficiency of Welding Production at Moscow Enterprises* (Moscow, 1987).
5. Nesterov, A.F., Dolgov, Yu.S., Telkov, A.M. (1985) Brazing of titanium structures with aluminium filler alloys. In: *Filler alloys for brazing of current materials*. Ed. by A.A. Rossoshinsky. Kiev: PWI.
6. Sokolova, N.M., Perevezentsev, V.N. (1989) Brazing with aluminium filler alloys: Progress. In: *Advanceed brazing methods*: Transact. Ed. by V.F. Khorunov. Kiev: PWI.
7. Shapiro, A.E., Flom, Y.A. Brazing of titanium at temperatures below 800 °C: Review and prospective applications. *http*://www.titanium-brazing.com/publications/DVS-Manuscript_1020-Copy-19-07.pdf

STRUCTURE AND PROPERTIES OF WELDED JOINTS ON TITANIUM ALLOYS CONTAINING SILICON ADDITIONS

L.I. MARKASHOVA, S.V. AKHONIN, G.M. GRIGORENKO, M.G. KRUGLENKO, A.S. KUSHNARYOVA and **I.K. PETRICHENKO**

E.O. Paton Electric Welding Institute, NASU, Kiev, Ukraine

Structural-phase transformations in specimens of electron beam welded joints on two experimental heat-resistant pseudo- α and α + β multi-component titanium alloys containing silicon additions were investigated. Specific (differentiated) contributions of different types of structures and phase formations in the near-weld zone to strength values and distribution of local internal stresses in the welding zones under investigation were analytically estimated.

Compared to aluminium alloys, steels and nickel superalloys, high values of strength, specific strength and corrosion resistance of titanium alloys over a wide temperature range favour their increasingly wider application in aircraft and space engineering, ship building, chemical industry, etc. The use of titanium alloys grows due to high reliability of this class of materials at increased and high (of the order of 600–650 °C) temperatures, as well as in high-temperature and aggressive environments, this allowing replacement of parts and components of steels and other structural materials by titanium ones (parts of cases of rocket engines and nuclear power plants, disks and blades of compressors, steam turbines, turbine and gas-turbine engines, heat exchangers, etc.). Heat-resistant titanium alloys are receiving an increasing acceptance in motor car construction, this leading to a substantial increase in power of automobile engines [1–3].

However, complication of service conditions related to increase in the level of working temperatures and necessity to extend the life of parts and mechanisms requires not only improvement of composition and technology of treatment of initial materials, but also finding a solution to the problem of their weldability. The latter is of special importance in manufacture of long and complex-configuration structures, as well as in repair-and-renewal operations, including, for example, reconditioning of worn-out engine blades.

As increase in service properties and level of working temperatures of any structure can be achieved, first of all, by appropriate alloying, as well as by providing the required structural state of the employed metals, alloys and their welded joints, the focus in this study is on conducting more comprehensive investigations of structural-phase changes depending on alloying with silicon, and on evaluating the chemical composition → structure → properties relationship for titanium alloys and their welded joints.

In this connection, considering the complexity of the processes and mutual effect of alloying and phase formation under different technological conditions of the thermal-deformation effect (welding, heat treatment), it seems expedient not only to perform appropriate experimental studies of structural-phase changes (chemical composition, character of grain, sub-grain and dislocation structure, and phase precipitates differing in composition, morphology and distribution) under certain welding conditions, but also to evaluate the effect of specific structural-phase components on changes in mechanical characteristics of the welded joints that are most significant for service conditions, such as strength, ductility and crack resistance values. This will make it possible to determine the role of structural and phase components not only in strengthening of metal, but also as a factor affecting the processes of accumulation of local internal stresses, value and extent of this type of stresses, as well as the possibility of their plastic relaxation, which is an indicator of crack resistance of a material under service conditions.

Materials and procedures. The investigation objects in this study are electron beam welded (EBW) joints on two heat-resistant multi-component titanium alloys. Both alloys contain silicon as an alloying element, and belong to pseudo-α (alloy 1) and α + β (alloy 2) titanium alloys (Table).

The basic experimental information on structural-phase composition of metal of a welded joint was generated by using optical, analytic scanning microscopy (SEM-515, PHILIPS, Holland) and microdiffraction transmission electron microscopy (JEM-200 CX, JEOL, Japan) with accelerating voltage of 200 kV. Thin foils for transmission microscopy were prepared by the two-stage method, i.e. preliminary electropolishing and subsequent multiple ion thinning by ionised argon flows in a specially developed unit [4]. The latter allowed not only widening the investigation fields (increasing statistics), but also making all structural and phase components of a material being analysed «transparent» for electrons.

Investigation results. The optical metallography methods were used to reveal structure, presence and arrangement of cold cracks in the EB welded joints on two experimental titanium alloys in the most problematic zone of a welded joint, i.e. HAZ [5–7], which in fact is a near-weld zone (NWZ), whose size and structure are determined by the thermal cycle of welding, and where the most dramatic changes in structure are expected to take place, allowing for high cooling rates characteristic of EBW.

Cold cracks were found to form in the welded joints on the investigated alloys after welding, the rate of formation of this type of cracks in the welded joints on experimental alloy 1 being much higher (Figure 1, a, b) than in the welded joints on alloy 2.

Also, as shown by metallographic examinations of structure, coarse equiaxed polyhedral

Chemical composition of experimental heat-resistant alloys

Alloy	Content of alloying elements, wt.%							Coefficient of stability of β-phase K_β
	Al	Sn	Zr	Mo	V	Nb	Si	
1	5.2	3.3	4.2	0.1	0.6	0.8	0.6	0.07
2	4.3	4.4	6.0	1.6	0.7	4.3	0.4	0.33

primary β-grains up to 0.5 mm in size form in NWZ of the welded joints on alloy 1 (Figure 1, c). In NWZ of the welded joints on alloy 2 the primary structure is heterogeneous: along with large regions of polyhedral grains 0.2 mm in size (Figure 1, d), there are regions of fine 20–60 μm equiaxed grains surrounded by coarse grains (Figure 1, e). Formation of chains of fine equiaxed grains was observed also in the HAZ regions located at a distance from the weld (Figure 1, f). As a rule, they extend along the base metal rolling direction (normal to the weld axis). Often, location of fine grains coincides with localisation of clusters of dispersed precipitates, most probably silicide ones. Intragranular structure in NWZ of alloy 1 consists of a coarse-acicular α′-phase. In NWZ of alloy 2, the martensitic α′-phase has a fine-acicular structure (see Figure 1, c, d). In addition to the martensitic phase, NWZ of both alloys may contain the retained β-phase, the amount of which, according to the chemical composition, is very insignificant in alloy 1, and higher in alloy 2 than in alloy 1.

More detailed structural-phase examinations of HAZ of the welded joints on titanium alloys by using microdiffraction transmission electron
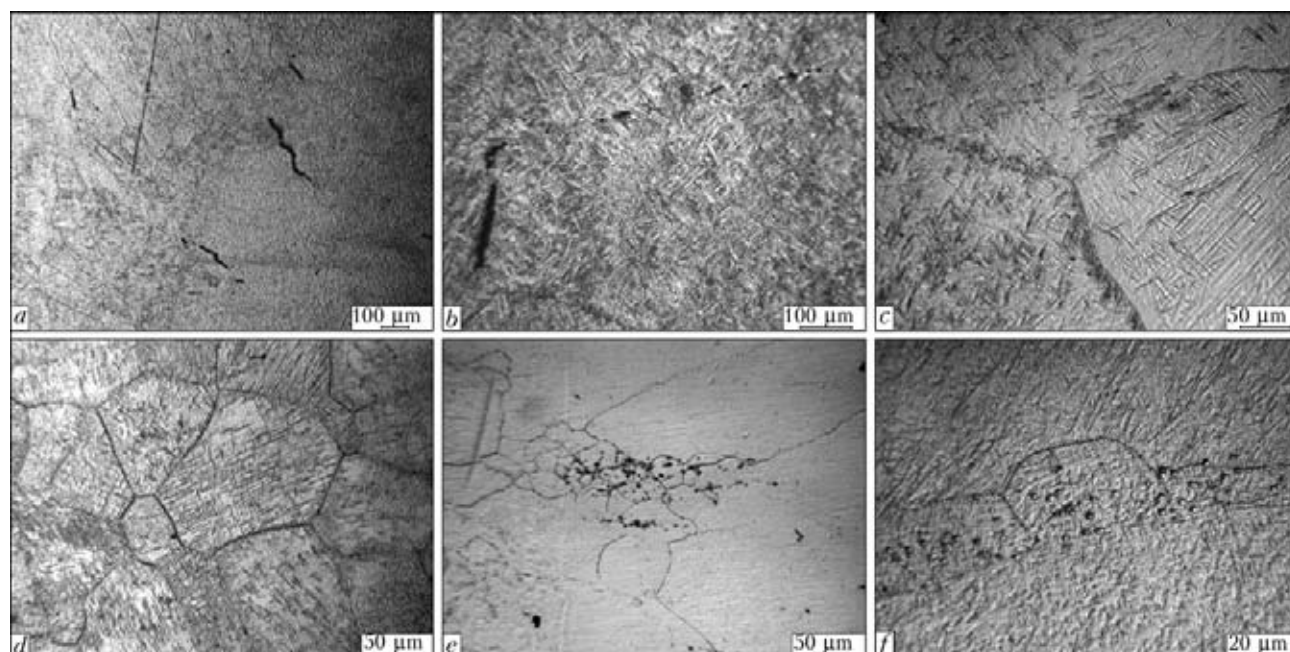
Figure 1. Microstructures of HAZ metal on experimental heat-resistant alloys after EBW: a, b — alloy 1, cracks in HAZ metal; c — alloy 1, NWZ; d, e — alloy 2, NWZ; f — alloy 2, HAZ region located at distance from the weld
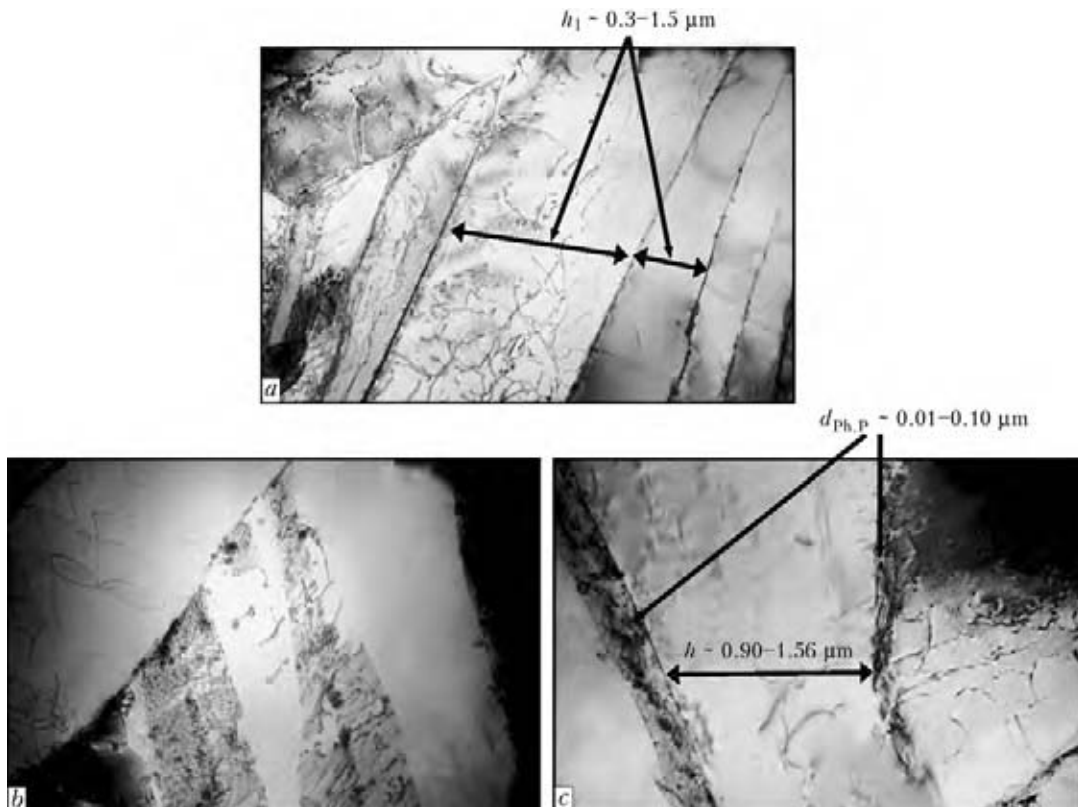
Figure 2. Microstructure of experimental alloy 1, NWZ: a — well-defined orientation of laminae of mainly α-component of structure at comparatively low density and uniform distribution of dislocations (lamina width h_l ~ 0.3−1.5 μm), ×20,000; b, c — phase formation in internal volumes and in boundary regions of α-laminated structures, ×30,000

microscopy were carried out to determine composition of the forming phases, as well as their sizes, morphology and structural zones of their localisation (internal volumes or grain-boundary regions).

Welded joint on experimental heat-resistant alloy 1. Structure of NWZ of the EB welded joint on alloy 1 consists mainly of the laminated α′-phase and a very small amount of the laminated β-phase, which differ in length l_l of a submicron sized (approximately from 0.3 to 1.5 μm) form with cross section h_l (Figure 2, a). Moreover, the laminated structural components differ greatly in their internal structure. The major part of this type of structures (consisting mostly of the α′-phase, according to the microdiffraction analysis) is characterised by a minimal dislocation density (ρ ~ 10^9 cm^{-2}) in the internal volume of the uniformly distributed laminae. The other part of the laminated structures (their quantity being much lower) radically differs both in dislocation density and distribution. For example, in this type of the laminated structures the dislocation density is higher approximately by an order of magnitude (ρ ~ $(7-8) \cdot 10^{10}$ cm^{-2}). The distribution of crystalline lattice defects in some cases is more or less uniform (Figure 2, a, b), whereas in other cases the complex dislocation configurations in the form of blocks or cells, as

well as an intralaminar dispersed (d_s ~ 0.1 μm) sub-structure (Figure 3, a) are detected. The structure with a clearly defined intralaminar substructure is most pronounced in the dark field imaging mode (Figure 3, c).

It should be noted that structures with a high dislocation and phase precipitate density correspond not only to the β-phases, but also partially to the α′-phases.

Examinations of thin foils allowed generating the detailed information on the phase precipitates forming in the welded joint, which differ in size, morphology, stoichiometric composition and localisation zones (along the boundaries of the laminated structures, in internal volumes, in sub-structure, etc.).

Phase precipitates of fine sizes ($d_{Ph.P}$ ~ 0.01−0.10 μm) forming in narrow grain-boundary interlayers and along the interlaminar boundaries (see Figure 2, c), the composition of which corresponds mainly to stoichiometry Ti_5Si_3 (Figure 3, b), are most distinct. The fine phase precipitates form also in internal volumes of the α′- and β-laminae, in the bulk of which fragmentation of the intralaminar structure and formation of sub-structures take place (Figure 3, $a-c$). The phases forming in this type of the structures are detected primarily in the zones of intralaminar sub-structural boundaries, and are characterised
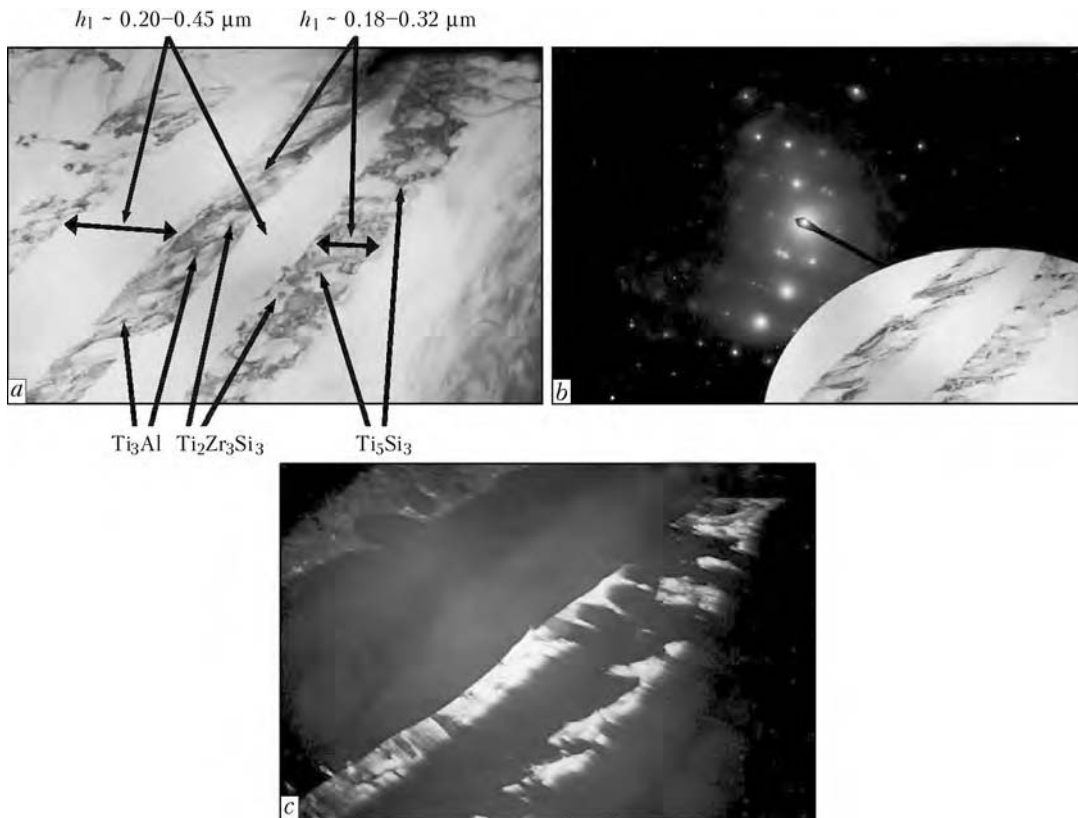
Figure 3. Microstructure of experimental alloy 1, NWZ: a — fine structure of laminae with sub-structure, ×37,000; b — microdiffraction reflection; c — dark-field image of specific (marked with arrows in Figure 3, a) phase formations, ×3000

by the finest sizes, i.e. $d_{Ph.P} \sim 0.01-0.02$ μm. As can be seen, such phases are the phases bordering the sub-structure. In addition to the fine equiaxed phase precipitates, there are also precipitates of an extended form, when $l_{Ph.P} >> h_{Ph.P}$ at $l_1 \sim$ $\sim 0.7-0.8$ μm, propagating along this type of the sub-structural boundaries (Figure 3, a, b). Stoichiometric composition of the fine phase precipitates bordering the intralaminar sub-structure becomes a bit wider: in addition to the noted Ti_5Si_3 composition, there are also phases of other compositions, including such elements as aluminium and zirconium, i.e. Ti_3Al and $Ti_2Zr_3Si_3$ phases (Figure 3, $a-c$; Figure 4, a).

The most active development of phase formation is characteristic of the laminated structures of comparatively coarse (in cross section) sizes ($h_1 \sim 0.4-1.5$ μm). Besides, the active phase formation in such zones is accompanied by occurrence of the following important factors. Firstly, coarsening of the phase formations takes place, i.e. size of the phase formations $d_{Ph.P}$ amounts to about $0.1-0.2$ μm, this being an order of magnitude higher than size of the intralaminar sub-boundary phases observed in the laminated structures of a smaller cross section (see Figure 4, a). Secondly, no ordering can be seen in distribution of coarse, mainly silicide phases in the bulk of the massive α′-laminae: the forming phases are

distributed chaotically, and they are not related either to structural boundaries, or grain and sub-grain boundaries. Moreover, formation of intra-volume phases in the said cases is accompanied by a substantial increase, i.e. up to (7-8)·10^10 cm^{-2}, of the dislocation density in the phase formation zone propagating along the entire length of the laminae (Figure 4, b, c). Therefore, a distinctive feature of the structure of the metal under investigation is formation of extended, special α-lamina structural zones saturated with coarse globular phase precipitates surrounded by dense dislocation clusters.

As follows from the results of investigations of the dislocation structure and phase formation processes, a substantial difference between the structural-phase states of the α′- and β-laminated structures is observed in the welded joints on experimental alloy 1. There occurs parallel formation of the laminated structures dramatically differing in their structural-phase states, such as almost dislocation-free laminae containing no phase precipitates, along with laminae characterised by a high dislocation density and saturation of the internal volumes with chaotically distributed precipitates of a rather coarse size. It is likely that formation of the substantially graded (as to phase precipitates and dislocation density) laminae is attributable to the type of the crys-
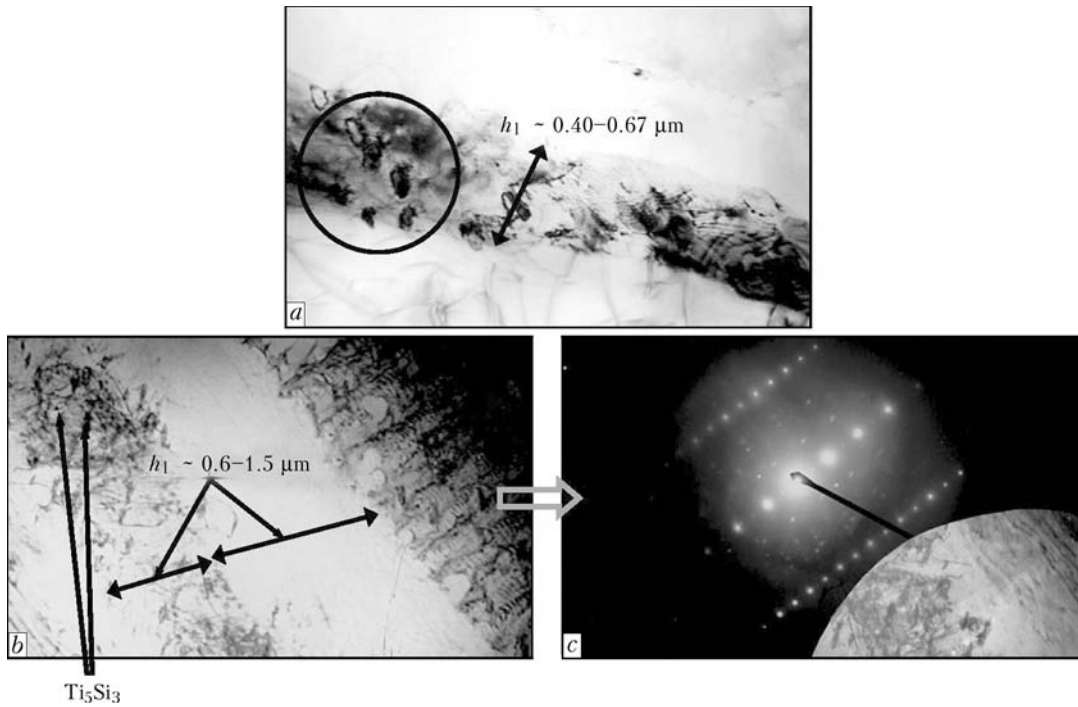
Figure 4. Microstructure of experimental alloy 1, NWZ: a — phase formation in β-laminae, ×50,000; b — extended dramatic gradients of dislocation density along the laminated structures, ×30,000; c — combined microdiffraction reflections of specific phases in α′-lamina structures

talline lattice corresponding to the β- and α-formations in titanium alloys. For instance, the β-phase having the bcc lattice (comprising up to 48 sliding systems) has an almost unlimited possibility for initiation, sliding and redistribution of dislocations, which are known to serve as active channels for transportations of alloying elements and, hence, activation of the phase formation processes. The α-structure having the hcp lattice is characterised by a very limited quantity of the sliding systems. Predominantly, this is one basal (0001) plane, and deformation in metal with this type of the lattice is realised due to twinning, which hampers dislocation initiation and sliding and, therefore, phase formation.

Most probably, it is different peculiarities in realisation of the deformation processes (through dislocation sliding or twinning) and, as a result, different phase formation possibilities for the main phase components (α- and β-phases) that explain formation of the extended laminated structures characterised by sharp gradients of the dislocation density and saturation with phase precipitates. The presence of the graded structural-phase formations, which are substantially different in the quantity and degree of dispersion of the silicide phases, including in dislocation density, is likely to serve as a base for formation in metal of this type of the corresponding sharply graded mechanical characteristics, such as gradients of strength properties ($\sigma_{0.2}$ and σ_t) in the related laminated structures.

Therefore, it was found that NWZ of alloy 1 is characterised by the presence of the extended α′- and β-laminated phase formations, sharply graded in dislocation density, as well as in quantity and size of the forming silicide and intermetallic phase precipitates:

• α′ — laminated phase components (hcp lattice) characterised by a minimal intralaminar dislocation density and an insignificant quantity of phase precipitates in laminae;

• β — laminated structures (bcc lattice) and a small part of the α′-phase characterised by a dramatic increase in the general dislocation density, formation of the sub-structure, very intensive development of the phase formation processes (growth of size and quantity of phases) and distribution of the silicide and intermetallic phases in zones of the dislocation clusters.

Welded joint on experimental heat-resistant alloy 2. Metal structure in NWZ of the EB welded joint on experimental alloy 2, similar to experimental alloy 1, is represented by different phases (α′- and β-phases), which differ both in size and fine structure of the phase formations and in size and distribution of the silicide and intermetallic precipitates originating during the welding process.

For example, cross section size h_1 of laminae of the martensitic α′-phase is much smaller (approximately 2−3 times) compared to that of the laminated structures of the corresponding zone of the welded joint on experimental alloy 1, and

$h_1 \sim 0.24{-}0.50\ \mu m$
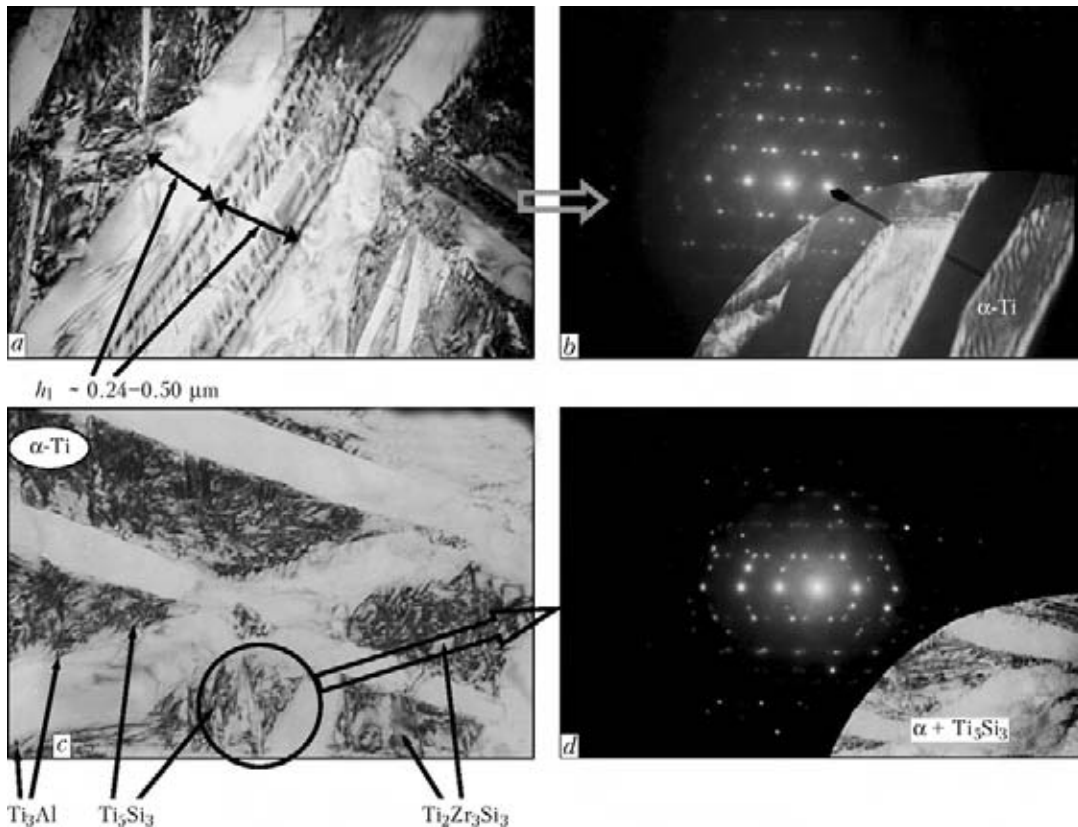
Figure 5. Microstructure of experimental alloy 2, NWZ: *a*, *c* — fine structure of laminated phases of the martensitic type (*a* — ×50,000; *c* — ×37,000); *b*, *d* — microdiffraction reflections of phase precipitates

is equal to $0.2{-}0.5\ \mu m$ (Figure 5, *a*). In addition, no dramatic changes in thickness of the laminae are observed. In this case, and this should be emphasised, structure of the α'- and β-phases is characterised by the presence of the acicular and fine intralaminar sub-structure. The dislocation density equal to $\rho \sim (8{-}9){\cdot}10^{10}\ cm^{-2}$ is uniformly distributed.

As to the phase precipitates, structural examinations and parallel analysis of microdiffraction reflections (Figure 5, *b*, *d*; Figure 6, *b*, *d*) show formation of primarily fine $(0.01{-}0.02 \times 0.02{-}0.06\ \mu m)$ and comparatively more uniformly distributed silicide and intermetallic phases in NWZ of the welded joint on alloy 2, compared to the welded joint on alloy 1. Moreover, the forming phases are distributed mainly in internal volumes of the laminated structures, first of all along the sub-structural boundaries, i.e. they are phase precipitates that border the intralaminar sub-structural elements (Figures 5 and 6). This character of distribution of the fine phase precipitates should promote not only fixation of the formed intralaminar sub-structure, but also consolidation of the thus fixed structure up to a temperature of dissolution of the grain-boundary distributed phases. Besides, this type of the structural state (fine fragments with grain-boundary fixing phases) is more or less uniformly distributed in the entire volume of the NWZ metal.

Analysis of microdiffraction reflections of the structures being investigated reveals diversity of stoichiometric compositions of the phase precipitates forming in NWZ of the joints on alloy 2. These are mostly phases of the Ti_5Si_3, $Ti_2Zr_3Si_3$ and Ti_3Al types (Figure 5, *d*; Figure 6, *b*). As seen, compositions of the precipitated silicides and intermetallics hardly differ from those detected in NWZ of the welded joint on alloy 1. However, morphology of this type of the phases, their size and distribution are substantially different. In the welded joint on alloy 2, silicides and intermetallics are finer, have a rod-like or globular shape (see dark-field image in Figure 6, *b*), and are distributed more uniformly in the bulk of metal, which seems to be caused by a structural state of the NWZ metal of the welded joint on this alloy, i.e. by a comparatively more uniform and finer structure of α'-martensite. However, despite a more favourable change in structural-phase state of the NWZ metal on alloy 2, including dispersion and uniformity of structure, formation of fine precipitates along the structural boundaries and absence of the laminated structure that is dramatically graded in its structural-phase state, the presence of a pronounced extension of the laminated structures will lead, though to a smaller degree (compared to the NWZ state in alloy 1), to decrease in
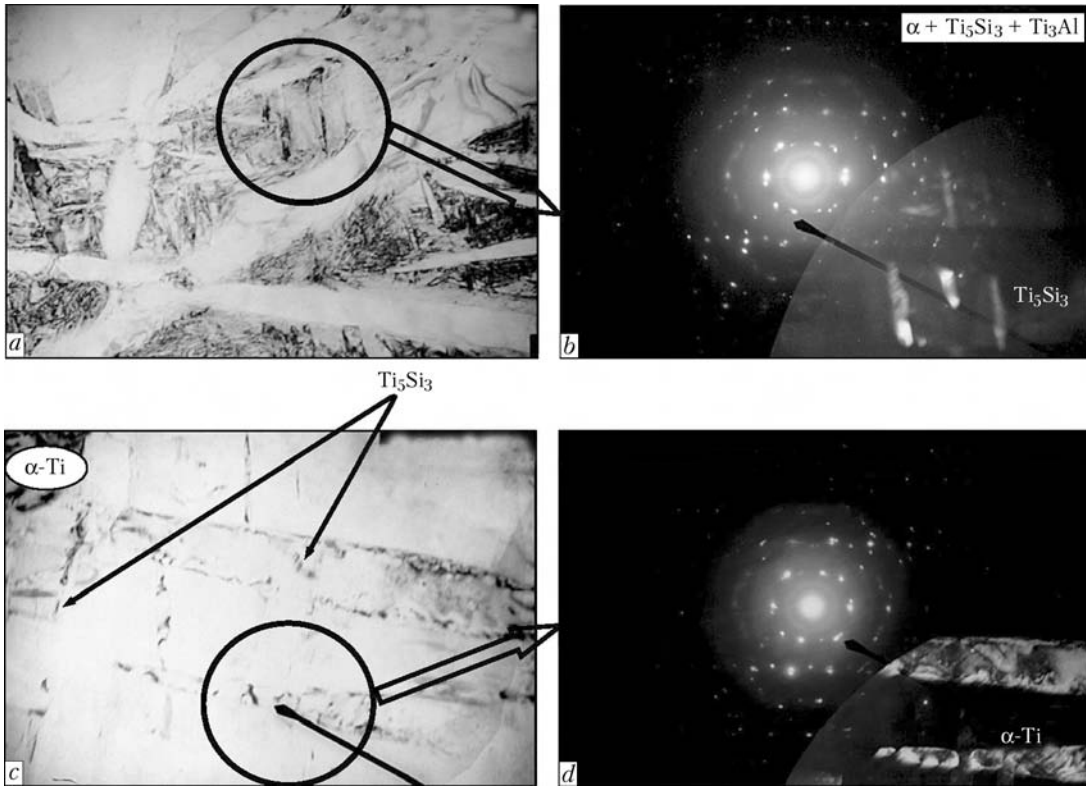
Figure 6. Microstructure of experimental alloy 2, NWZ: a, c — distribution of phase precipitates differing in morphology and size, ×50,000; b, d — microdiffraction reflections of specific zones of phase precipitates

ductility values and, accordingly, to increase in susceptibility of the welded joint to cracking.

Therefore, NWZ of the welded joint on experimental alloy 2 is characterised by formation of the extended phases of the laminated type (α'-martensite and β-phase) having, like in alloy 1, a laminated morphology, but considerably differing (approximately 2–3 times) in width of the laminated structures, finer acicular α'-martensitic structure and intralaminar sub-structure, as well as more uniform distribution of dislocations in the entire volume of the NWZ metal.

Differences are observed also in the process of formation of the silicide and intermetallic phases: at a similar stoichiometric composition (like in case of alloy 1) the phases are smaller in size and are uniformly distributed in the entire volume, their localisation occurring mainly along the sub-structure boundaries.

Additional fractographic examinations of fractures of the EB welded joints on experimental
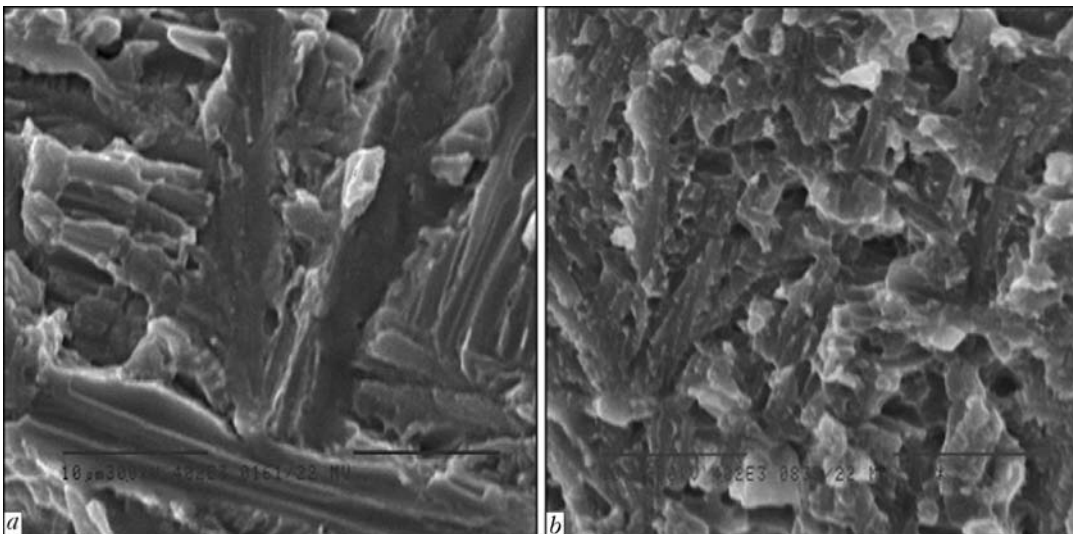
Figure 7. Microstructures of fracture surfaces on titanium alloys (×4020): a — brittle cleavage in laminated structures with intravolume phase precipitates (welded joint on experimental alloy 1); b — quasi-brittle fracture in martensitic component (welded joint on experimental alloy 2)
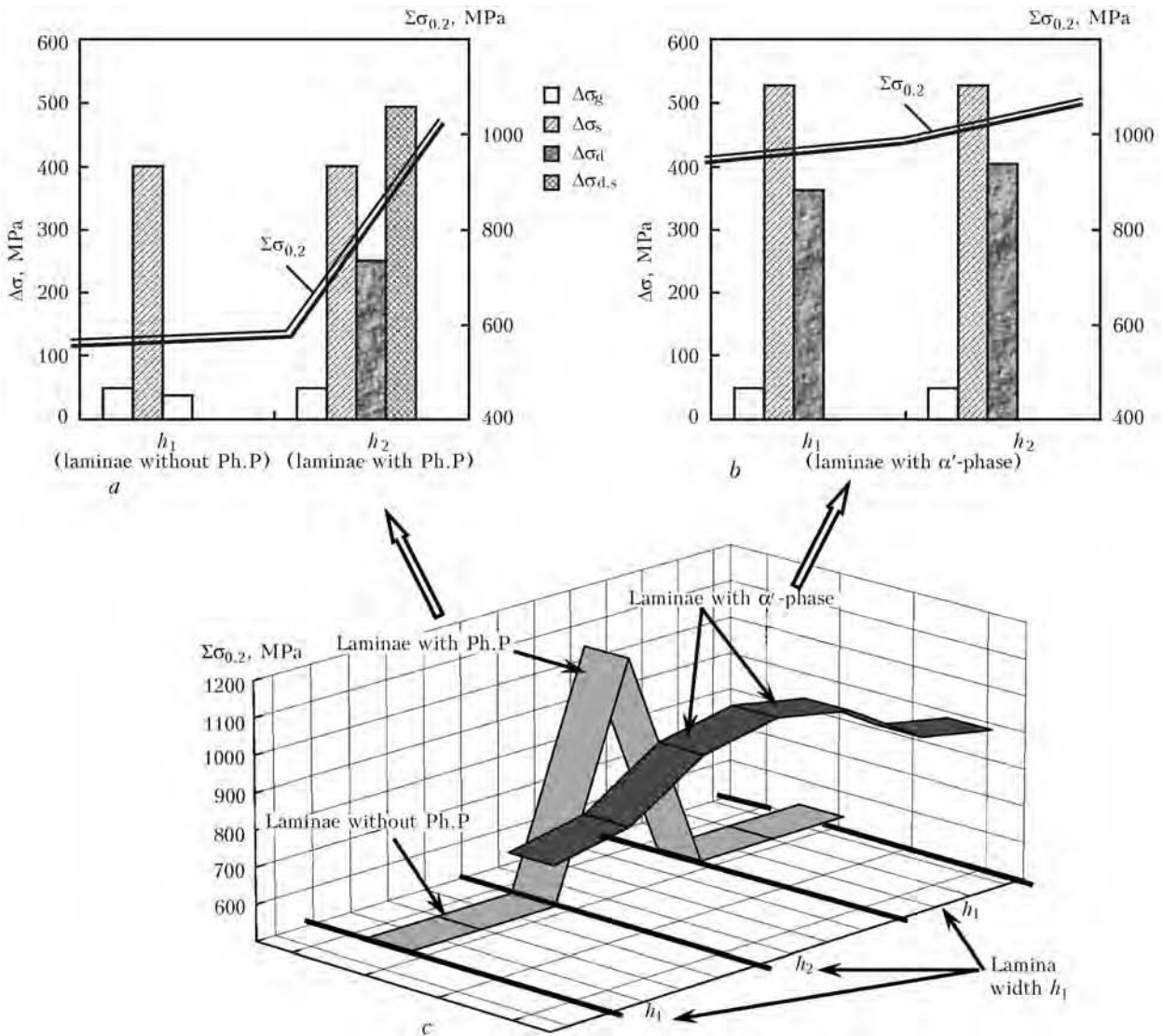
Figure 8. Contribution of different components of structural strengthening (grain, sub-grain, dislocation and dispersion): *a* — alloy 1; *b* — alloy 2; *c* — calculated value of yield strength $\Sigma\sigma_{0.2}$

alloys 1 and 2 showed that the fracture zone of the welded joints on experimental alloy 1 is characterised by the presence of regions of the extended transcrystalline brittle cleavage in a direction of the laminated structures (Figure 7, *a*). In contrast to this, the welded joints on experimental alloy 2 feature a more homogeneous quasibrittle fracture of the intragranular type (Figure 7, *b*) with dispersed fragments ($d_f \sim 2$–5 μm) corresponding in size to sub-structural components in α'-martensite.

A substantial effect on quality of the welded joint is exerted by distribution and localisation of internal stresses in the HAZ metal of the alloys investigated. Stresses of this type related to non-uniformity of heating and structural-phase transformations lead to a dramatic decrease in ductility, and in some cases to cold cracking, which occurs under the conditions of EBW of experimental heat-resistant alloys. Therefore, analysis of the role of different structural factors inducing

or blocking formation of internal stresses is also of an important practical interest.

The package of the conducted experimental studies made it possible, firstly, to analytically estimate specific (differentiated) contributions of different structural-phase factors and parameters forming in welded joints of the investigated alloys to changes in strength characteristics $\sigma_{0.2}$, and, secondly, to reveal the structural factors determining the character and distribution of internal stresses τ_{in}, which are potential sources of initiation and propagation of cracks in the investigated structural microregions [8–12].

Analytical estimates of strength $\sigma_{0.2}$ were made according to the Archard equation that includes the known Hall–Petch, Orowan and other dependences [13–20]:

$$\Sigma\Delta\sigma_{0.2} = \Delta\sigma_0 + \Delta\sigma_{s.s} + \Delta\sigma_g + \Delta\sigma_s + \Delta\sigma_d + \Delta\sigma_{d.s},$$

where $\Delta\sigma_0$ is the resistance of the metal lattice to movement of free dislocations (friction stress

of the lattice or Peierls–Nabarro stress); $\Delta\sigma_{s.s}$ is the strengthening of solid solution with alloying elements and impurities (solid solution strengthening); $\Delta\sigma_g$, $\Delta\sigma_s$ is the strengthening due to a change in size of grain and sub-grain (Hall–Petch dependences, grain and sub-grain strengthening); $\Delta\sigma_d$ is the dislocation strengthening caused by the inter-dislocation interaction; and $\Delta\sigma_{d.s}$ is the strengthening provided by the dispersed particles according to the Orowan dependence (dispersion strengthening).

It was shown as a result that the HAZ metal of the welded joint on experimental alloy 1 features the dramatically graded (approximately 1.8 times) change in yield strength ($\Delta\sigma_{0.2} \sim 570-1010$ MPa) that depends on the structural-phase state of the laminated structures. A dramatic increase in $\Delta\sigma_{0.2}$, which is characteristic of the laminated structures with a high dislocation density ($\rho \sim (7-8)\cdot10^{10}$ cm^{-2}) and most saturated with the phase precipitates, leads to a growth of dislocation ($\Delta\sigma_d \sim 250$ MPa) and dispersion ($\Delta\sigma_{d.s} \sim 375-500$ MPa) strengthening (Figure 8, a, c).

NWZ of alloy 2 is characterised by a high level and more uniform distribution of strength properties ($\Delta\sigma_{0.2} \sim 910-1040$ MPa) in the forming martensitic phases of the laminated type (Figure 8, b, c), this being related to their finer structure. In this case, a certain increase in strengthening is caused by dispersion of the substructure ($\Delta\sigma_s \sim 530$ MPa), and a comparatively uniform increase in general dislocation density in the bulk of metal leads to strengthening of an order of $\Delta\sigma_d \sim 360$ MPa (Figure 8, b).

Furthermore, internal stresses τ_{in} in HAZ of the joints were determined by examinations of the dislocation structure [21, 22]:

$$\tau_{in} = Gbh\rho/[\pi(1 - \nu)],$$

where G is the shear modulus; b is the Burgers vector; $h = 2\cdot10^{-5}$ cm is the foil thickness; ν is the Poisson ratio; and ρ is the dislocation density.

The investigations conducted showed (Figure 9, a) that the HAZ metal of alloy 1 is characterised by a dramatically graded (approximately 10 times) distribution of internal stresses, directed along the laminae (from 10–100 to 750–860 MPa), this being related to a change of the dislocation density in different types of the laminae, i.e. with low ($\rho \sim 10^9-10^{10}$ cm^{-2}) and high ($\rho \sim (7-8)\cdot10^{10}$ cm^{-2}) dislocation densities. However, there are also regions with an even higher local dislocation density ($\rho \sim 2\cdot10^{11}$ cm^{-2}), where local internal stresses $\tau_{in/l}$ amount to about 2000 MPa.

HAZ of alloy 2 is characterised by a comparatively uniform distribution of internal stresses
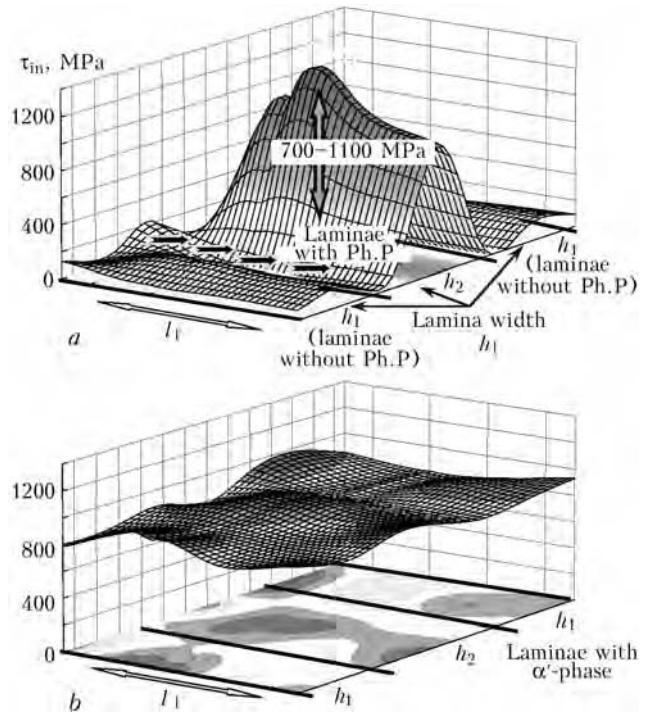
Figure 9. Level of local internal stresses forming in laminated structures of NWZ of the welded joints: a — laminated structures graded in distribution of dislocation density, and intravolume phase precipitates (experimental alloy 1); b — martensitic laminated structures (experimental alloy 2)

($\tau_{in} \sim 860-970$ MPa), this corresponding to a uniform dislocation density ($\rho \sim (8-9)\cdot10^{10}$ cm^{-2}) in the intralaminar structures (Figure 9, b).

However, both welded joints on alloy 1 and welded joints on alloy 2 (though to a lower degree) feature a clear relationship of orientation of the distribution of internal stresses and the laminated structures, which can be a cause of formation and propagation of cracks.

CONCLUSIONS

1. As established in the course of the comprehensive investigations of the welded joints on experimental titanium alloys conducted at different structural levels (grain, sub-grain, dislocation), NWZ of the joints on alloys 1 and 2 is characterised by formation of the laminated-type extended structures of the α'- and β-phase components with a similar morphology, but considerably differing in density and distribution of dislocations, as well as in intensity of the processes of formation of phase precipitates of the silicide and intermetallic types.

2. In NWZ of the welded joint on pseudo-α alloy 1, the silicide phase formation occurs most actively in few grains of the β-phase and in a small part of the α'-laminae, which are characterised by a high dislocation density and formation of a sub-structure. At the same time, the

major part of the α′-laminae is characterised by a low dislocation density, uniform distribution of dislocations and absence of silicides and intermetallics in their bulk. Phase precipitates are observed both in the grain-boundary interlayers and along the boundaries between the laminae.

3. The presence of the structural-phase formations in NWZ of alloy 1, which are considerably different in quantity and degree of dispersion of the silicide phases, and in dislocation density, is a base for formation of dramatically graded strength characteristics, as well as internal stresses in the adjoining laminated structures.

4. NWZ of the welded joints on (α + β) titanium alloy of the martensitic type is characterised by formation of finer silicide and intermetallic phase precipitates in the α′- and β-phases, which are mainly uniformly distributed in the bulk of the NWZ metal, i.e. along the sub-boundaries and boundaries of the fine martensitic α′-phase.

5. Analytical estimation of differentiated contribution of different structural-phase factors and parameters forming in the welded joints on the investigated alloys to changes in strength properties ($\sigma_{0.2}$) showed that a substantial change in yield strength $\sigma_{0.2}$ of the adjoining laminated structures occurs in NWZ of the welded joints on alloy 1, i.e. from 570 MPa for the laminated α′-phase with a low dislocation density to 1010 MPa for the laminae with a high dislocation density and silicide precipitates. NWZ of alloy 2 features a higher level and more uniform distribution of strength properties ($\sigma_{0.2}$ changes from 910 to 1040 MPa in the entire volume of the NWZ metal).

6. Estimation of changes in internal stresses τ_{in} in NWZ of the welded joints on the investigated alloys, made on a base of examinations of the dislocation structures, showed that distribution of internal stresses in NWZ of the welded joint on alloy 1 is extremely non-uniform and directed along the laminated structures (τ_{in} changes from 10−100 to 750−860 MPa in the laminae with a high and low dislocation densities). Internal stresses in NWZ of the welded joint on alloy 2 are distributed more uniformly. However, fixation of the direction of the distribution of internal stresses and laminated structures can serve as a cause of a directed propagation of cracks.

7. To eliminate strength and internal stress gradients, it is necessary to achieve formation of a homogeneous uniform dispersed structure.

1. Iliin, A.A., Kolachev, B.A., Polkin, I.S. (2009) *Titanium alloys. Composition, structure, properties*: Refer. book. Moscow: VILS−MATI.

2. Solonin, O.P., Glazunov, S.G. (1976) *Refractory titanium alloys*. Moscow: Metallurgiya.

3. Chechulin, B.B., Ushkov, S.S., Razuvaeva, I.N. et al. (1977) *Titanium alloys in machine-building*. Moscow: Mashinostroenie.

4. Darovsky, Yu.F., Markashova, L.I., Abramov, N.P. et al. (1985) Procedure of thinning of dissimilar welded joint samples for microscopic examinations. *Avtomatich. Svarka*, **12**, 60.

5. Grabin, V.F. (1975) *Principles of metals science and heat treatment of titanium alloy welded joints*. Kiev: Naukova Dumka.

6. Moiseev, V.N., Kulikov, F.R., Kirillov, Yu.G. et al. (1979) *Titanium alloy welded joints*. Moscow: Metallurgiya.

7. Gurevich, S.M., Zamkov, V.N., Blashchuk, B.E. et al. (1986) *Metallurgy and technology of welding of titanium and its alloys*. Kiev: Naukova Dumka.

8. Markashova, L.I., Grigorenko, G.M., Poznyakov, V.D. (2009) Influence of thermal cycles of welding and external loading on structural-phase variations and properties of joints of 17Kh2M steel. *The Paton Welding J.*, **7**, 18−25.

9. Markashova, L.I., Grigorenko, G.M., Arsenyuk, V.V. et al. (2002) Criterion of evaluation of mechanical properties of dissimilar material joints. In: *Proc. of Int. Conf. on Mathematical Modeling and Information Technologies in Welding and Related Processes* (16−20 Sept. 2002, Katsiveli, Ukraine). Kiev: PWI, 107−113.

10. Markashova, L.I., Grigorenko, G.M., Poznyakov, V.D. et al. (2004) Structural approach to evaluation of mechanical properties in HAZ of steel and alloy joints. In: *Proc. of Int. Conf. on Mathematical Modeling and Information Technologies in Welding and Related Processes* (13−17 Sept. 2004, Katsiveli, Ukraine). Kiev: PWI, 174−179.

11. Markashova, L.I., Grigorenko, G.M., Poznyakov, V.D. et al. (2008) Structural factors determining the properties of strength, plasticity and fracture of welded joints. In: *Proc. of Int. Conf. on Mathematical Modeling and Information Technologies in Welding and Related Processes* (27−30 May 2008, Katsiveli, Ukraine). Kiev: PWI, 87−94.

12. Markashova, L.I., Grigorenko, G.M., Poznyakov, V.D. et al. (2009) Structural criterion for evaluation of strength, plasticity, crack resistance of metals, alloys, composite materials and their welded joints. In: *Proc. of 4th Int. Conf. on Fracture Mechanics of Materials and Strength of Structures* (June 2009, Lviv, Ukraine). Lviv: FMI, 447−451.

13. Suzuki, H. (1967) About yield strength of polycrystalline metals and alloys. In: *Structure and mechanical properties of metals*. Moscow: Metallurgiya.

14. Ashby, M.F. (1986) About Orowan stress. In: *Physics of strength and plasticity*. Moscow: Metallurgiya.

15. Goldshtein, M.I., Litvinov, V.S., Bronfin, B.M. (1986) *Physics of metals of high-strength alloys*. Moscow: Metallurgiya.

16. Conrad, H. (1973) Model of deformation strengthening for definition of grain size effect on metal flow stress. In: *Ultrafine grain in metals*. Ed. by L.K. Gordienko. Moscow: Metallurgiya.

17. Armstrong, R.V. (1973) Strength properties of metals with ultrafine grain. *Ibid*.

18. Petch, N.J. (1953) The cleavage strength of polycrystalline. *J. Iron and Steel Inst.*, **173**, 25−28.

19. Orowan, E. (1954) *Dislocation in metals*. New York: AIME.

20. Ashby, M.F. (1983) Mechanisms of deformation and fracture. *Adv. Appl. Mech.*, **23**, 117−177.

21. Koneva, N.A., Lychagin, D.V., Teplyakova, L.A. et al. (1986) Dislocation-disclination sub-structures and strengthening. In: *Theoretical and experimental investigation of disclinations*. Leningrad: LFTI.

22. Conrad, H. (1963) Effect of grain size on the lower yield and flow stress of iron and steel. *Acta Metallurgica*, **11**, 75−77.

COMBINED LASER-MICROPLASMA CLADDING WITH POWDERS OF Ni−Cr−B−Si SYSTEM ALLOYS

**Yu.S. BORISOV, V.Yu. KHASKIN, S.G. VOJNAROVICH, A.N. KISLITSA, A.Yu. TUNIK, L.I. ADEEVA,
E.K. KUZMICH-YANCHUK, A.V. BERNATSKY** and **A.V. SIORA**
E.O. Paton Electric Welding Institute, NASU, Kiev, Ukraine

Structural features of deposited layers produced by the combined laser-microplasma method using powders of the Ni−Cr−B−Si system alloys were investigated. Technological advantages and drawbacks of a combination of laser cladding and microplasma spraying were determined. It was shown that the developed combined laser-microplasma method allows improving the quality of the deposited layers by preserving the key advantages characteristic of the laser powder cladding process.

K e y w o r d s : *combined laser-microplasma cladding, self-fluxing nickel alloy, structure, phase composition, hardness, wear resistance*

Different thermal spraying methods, such as flame, plasma and detonation ones, are applied to deposit coatings of alloys of the Ni−Cr−B−Si system. Spraying and melting can be performed in one (gas powder cladding) or two successive stages (spraying with subsequent melting of the sprayed layer). The sprayed NiCrBSi coatings preserve the main properties of the NiCrBSi alloy (wear and corrosion resistance), but lack the high adhesion strength (normally, less than 35−40 MPa). After melting the strength of adhesion of the NiCrBSi coating layer to the substrate grows to 70−75 MPa [1].

For a number of industrial problems it is desirable that the adhesion strength value be as close as possible to strength of the base metal. In this connection, of an increasing interest now is the process of laser melting of coatings. Advantages of this process include thermal locality and minimal effect on the base metal, as well as small (5−20 μm) size of the transition zone, which minimises penetration of the base metal into the deposited one and favours refining of structure of the material, this resulting in improvement of mechanical properties. However, shrinkage cracks may form in laser melting as a result of dramatically heterogeneous heating, especially of coatings more than 0.5 mm thick, as well as subsequent cooling [2, 3].

It is noted in studies [4−6] that drawbacks characteristic of laser melting can be eliminated by combining plasma and laser heating. One of such processes, which integrates advantages of laser cladding and microplasma spraying, is combined laser-microplasma cladding (CLMPC) [7].

It allows avoidance of drawbacks characteristic of laser cladding (formation of internal pores and microcracks), preparation of the workpiece surface directly during the process of deposition of a material, and fusion of the deposited layers with the base metal.

The purpose of this study was to investigate structural peculiarities of the layers deposited with powders of the Ni−Cr−B−Si system alloys (PG-12N-01 and PG-12N-02) by the CLMPC process, as well as to define technological advantages of combining the laser cladding and microplasma spraying processes.

Investigation procedure. Layers 0.3−1.2 mm thick were deposited on substrates of steels St3 and 38KhN3MFA by the CLMPC method using self-fluxing alloy powders (PG-12N-01 and PG-12N-02). Structure, phase composition and properties of the layers were investigated. An integrated procedure comprising metallography (microscope «Neophot-32» with digital photography attachment), durometric analysis (LECO hardness meter M-400 with loads of 0.25, 0.5 and 1 N) and X-ray phase analysis in monochromatic CuK_α-radiation by using diffractometer DRON-UM1 was applied for investigation of the resulting deposited layers. Graphite single crystal placed on a path of the diffracted beam was used as a monochromator. Diffraction patterns were made by the step scan method in the $20° < 2\theta < 90°$ angle range. The scan step was 0.05°, and the time of exposure at a point was 3−7 s. The data of the diffractometry experiment were processed by using software PowderCell 2.4 for full-profile analysis of X-ray spectra of a mixture of polycrystalline phase components.

Cracking index α the value of which was determined in percent was introduced to compare

the quantity of cracks in clad specimens. The absence of cracks in the deposited layer was taken as zero, and the network of cracks with a pitch of 1 mm was taken as 100 %. The investigations showed that this index can be estimated from formula $\alpha = 3/L$, where L is the distance between the cracks, mm.

Investigation of wear resistance of the deposited layers was carried out by using friction machine 2070 SMT-1 by the disk−pin method without lubrication. Before the investigation the 40 mm diameter specimens were polished to surface finish R_a = 1.6 μm. Material of the mating body was steel 45 heat treated to hardness HRC 55. Prior to the tests, the surfaces were subjected to running-in, the presence of which was fixed from stabilisation of the friction moment in a pair. Relative wear resistance was determined from the loss of weight at sliding speeds of 1.3 m/s in a mode of stepwise loading, the test time at each step being 15 s, and load being 0.2 kN. Wear resistance of the clad specimens compared to that of the base metal was determined by using the in-house friction machine according to the cylinder−pin scheme by the dry friction method. As this machine is a non-standard development, the results obtained by using it were regarded as relative. A specimen of steel 38KhN3MFA after volumetric (furnace) hardening and heat treatment, having hardness HRC 43−44, was chosen as the reference one. Wear of the specimens measured from a change in weight (in grams) was compared with that of the reference specimen. The time of friction was increased to improve accuracy of the measurement results. The mating body was made from hard alloy T15 or steel 45 hardened to HRC 50−55. The specific pressure was set within 11−12 MPa, the rotation speed for a test specimen was 50−1600 rpm, and the linear friction speeds were 0.4−15.0 m/s. In all the cases the specimens were weighed before and after the friction tests by using analytical balance VPR-200 within 0.0005 g.

Materials, equipment and principle of operation of the devices. Self-fluxing nickel alloy powders PG-12N-01 and PG-12N-02 with a particle size of 40−100 μm (TU 48-19-383−84), the chemical compositions of which is given in Table 1, were used as materials for cladding. The powders produced by atomisation in inert gas had particles with a regular round shape, close to the spherical one. The fractional composition of the powders was −40−+100 μm. Hardness of

Table 1. Chemical composition of nickel alloy powders (Ni − base), wt.%

Powder grade	Cr	B	Si	Fe	C
PG-12N-01	8−14	1.7−2.8	1.2−3.2	2−5	0.3−0.6
PG-12N-02	10−16	2.0−4.0	3.0−5.0	3−6	0.4−0.8

the PG-12N-01 powder was HRC 36−45, and T_{melt} = 1080 °C. Hardness of the PG-12N-02 powder was HRC 46−55, and T_{melt} = 1050 °C.

CO_2-laser TR-100 (Rofin-Sinar, Germany) with a power of up to 10 kW was used as a laser radiation source. Radiation of this laser with a power of 2, 3 and 4 kW, combined with the microplasma jet with a power of up to 1.5 kW, was used in the experiments.

The MPN-004 system with the MP-04 microplasmatron developed by the E.O. Paton Electric Welding Institute of the NAS of Ukraine was used to form the microplasma jet (design of the microplasmatron is covered by the Ukrainian patent «Plasmatron for spraying of coatings» No. 2002076032) UA, B23K10/00.

Design and operating parameters of the microplasmatron provide formation of the laminar plasma jet (Reynolds criterion is 0.10-0.55). According to this criterion, the microplasma spraying process is characterised [8] by:

• low thermal power, this making it possible to decrease heating of the substrate and deposit coatings on small-size and thin-walled pieces without substantial local overheating and buckling;

• low level of noise in spraying with the laminar plasma jet, which is no more than 30−50 dB, this allowing avoidance of cumbersome protection chambers;

• small size of the spraying spot (1−5 mm) at a small diameter of the nozzle equal to 1−2 mm.

The latter parameter is the key one for implementation of the laser-microplasma cladding process, as it provides adequacy of the geometric size of the spraying spot to the focal spot of the laser. Therefore, with a spraying spot of about 5 mm, it can be completely overlapped by the focal spot of the laser, the thermal power density in the spot being sufficient for remelting of the sprayed layer and its fusion with the substrate.

Flow diagram of the cladding process is shown in Figure 1. A specimen (plate) was mounted on a working frame approximately at equal angles to axes of the laser beam and plasma jet. The laser beam was fed vertically from above. The plasma jet transporting the cladding powder was directed to the focusing spot normal to the laser beam. The laser beam and microplasma jet action
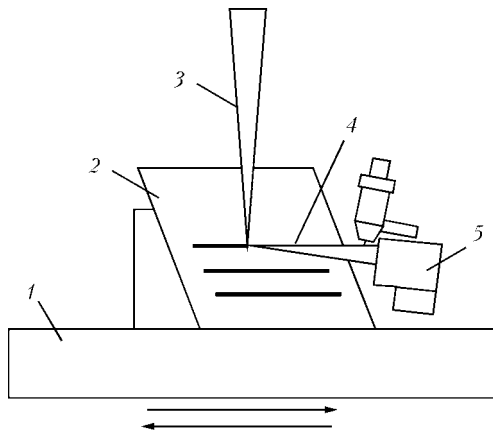
Figure 1. Flow diagram of the combined laser-microplasma cladding process: *1* — frame; *2* — specimen; *3* — laser beam; *4* — plasma jet; *5* — microplasmatron

zones were combined to form the common zone, the frame with the specimen mounted on it being moved relative to this common zone. Additional scanning by using a scanator (Figure 2) was used to smooth down the surface of the deposited layer.

The principle of operation of this device is as follows: DC motor *3* (see Figure 2, *b*), the rotation frequency of which is adjustable within 10–200 rpm, imparts the torque moment to eccentric *2*, whose axis is shifted relative to the motor axis. The eccentric engages holder *1*, thus forcing it to oscillate relative to the semi-axes. The lens fixed in the holder oscillates together with it. This leads to periodic deflections of the radiation focusing axis from the vertical position, which in turn shifts position of the focal spot. As a result, the laser beam focusing spot on a workpiece starts oscillating at a certain frequency depending on the rotation frequency of motor *3*. The amplitude of such oscillations depends on the value of eccentricity, which is set by using

eccentric *2*. Return of the holder back to the initial position is provided by spring *5*, which is constantly kept in the compressed state. The entire structure is mounted on swinging bracket *4*, which makes it possible to arbitrarily select direction of the oscillations relative to the laser treatment direction. This allows both transverse and longitudinal oscillations of the beam.

Experimental. To determine dependence of height h (mm) of the deposited layer on the process parameters, initially the process was performed by depositing single beads on a plate of steel St3 ($\delta = 8$ mm). The following parameters were chosen as the variable ones: laser radiation power P_{laser} (kW), energy input E (J/mm), and specimen movement speed v (m/h). Powder consumption G_p during the experiments was varied within 0.1–0.2 g/s. Other process parameters were kept constant: diameter of the spot of the beam focused on the specimen surface $d_{sp} = 5$–6 mm, plasmatron current $I = 43$ A, voltage $U = 30$ V, plasma gas (argon) flow rate $Q = 80$ l/h, and shielding gas (argon) flow rate $Q_{sh} = 240$ l/h. To optimise the value of overlapping of the beads (according to the criterion of roughness of the resulting coating on a similar plate), several beads were deposited by overlapping 10–50 % of their width.

Decrease in height of the deposited bead with increase in power of the laser beam (Table 2, specimen 1) is related to a burn-off loss of part of the cladding material, as well as to overheating of the base metal and dissolution of part of the deposited bead material in it. Increase in height of the bead (Table 2, specimen 5) is attributable to the noted instability in feeding the powder.

Results and discussions. Based on the experimental results, the mode corresponding to speci-
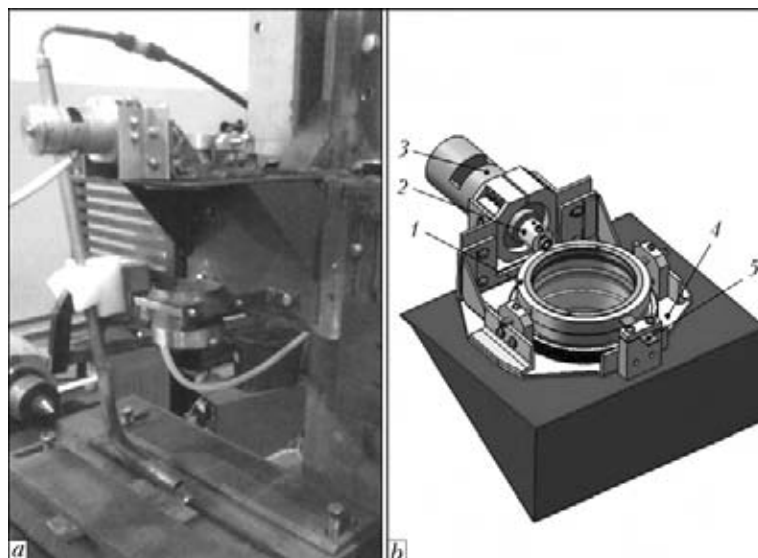
Figure 2. Appearance (*a*) and schematic of structure of the laser radiation scanator (for designations see the text)

Table 2. Effect of power and speed of movement of a specimen in CLMPC on height and quality of the bead deposited with powders PG-12N-02

Specimen number	P_{laser}, kW	v, m/h	E, J/mm	Microstructure, ×20	h, mm	Note
1	4	30	635		0.4	Presence of microcracks
2	3	6.5	2380		1.2	Bead is non-uniform in height
3	3	10	1545		0.8	Bead is uniform
4	3	20	770		0.6	Same
5	3	30	520		1.0	»
6	2	10	1185		0.3	Bead is non-uniform in profile
7	2	20	590		–	Bead is not formed
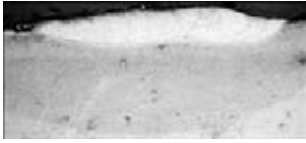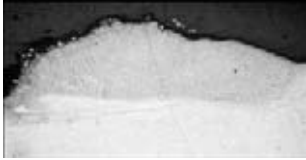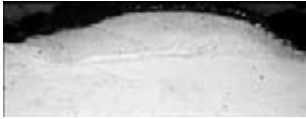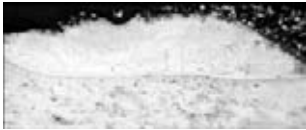
men 4, which provided the defect-free layers at a comparatively low energy input, was chosen to implement the process of laser-microplasma cladding of steels with powders of the Ni−Cr−B−Si system alloys. Decrease in energy input led to formation of such a defect as microcracks (see Table 2, specimens 1 and 5). Further investigations showed that with increase in the powder consumption to G_p = 0.5−0.8 g/s the speed of movement can be increased to 60 m/h, other parameters being kept unchanged. This will provide the deposited beads with the geometry similar to that described in Table 2, along with decrease in the HAZ. In addition, it was established that the acceptable roughness of the deposited layers (about R_a = 200−300 μm) occurs at the coefficient of overlapping of the beads equal to K_{ov} = 25−30 %. It means that at a bead width of

6 mm the transverse movement of a specimen for deposition of each next bead will be not less than 4 mm. Also, it was established that the optimal parameters for laser-microplasma cladding can be provided at an energy input ranging from 500 to 800 J/mm. For comparison, it should be noted that in laser powder cladding the energy input is 120−250 J/mm [9]. This shows that overheating of the deposited layers and increase in size of HAZ should take place in the case of combined cladding, in contrast to laser cladding.

Overheating of the layers deposited by the laser-microplasma method leads to some decrease in their hardness. The higher the energy input in the process and, hence, the higher the temperature in the working zone, the bigger this decrease is. This is explained by the fact that in plasma spraying of self-fluxing alloys at a temperature
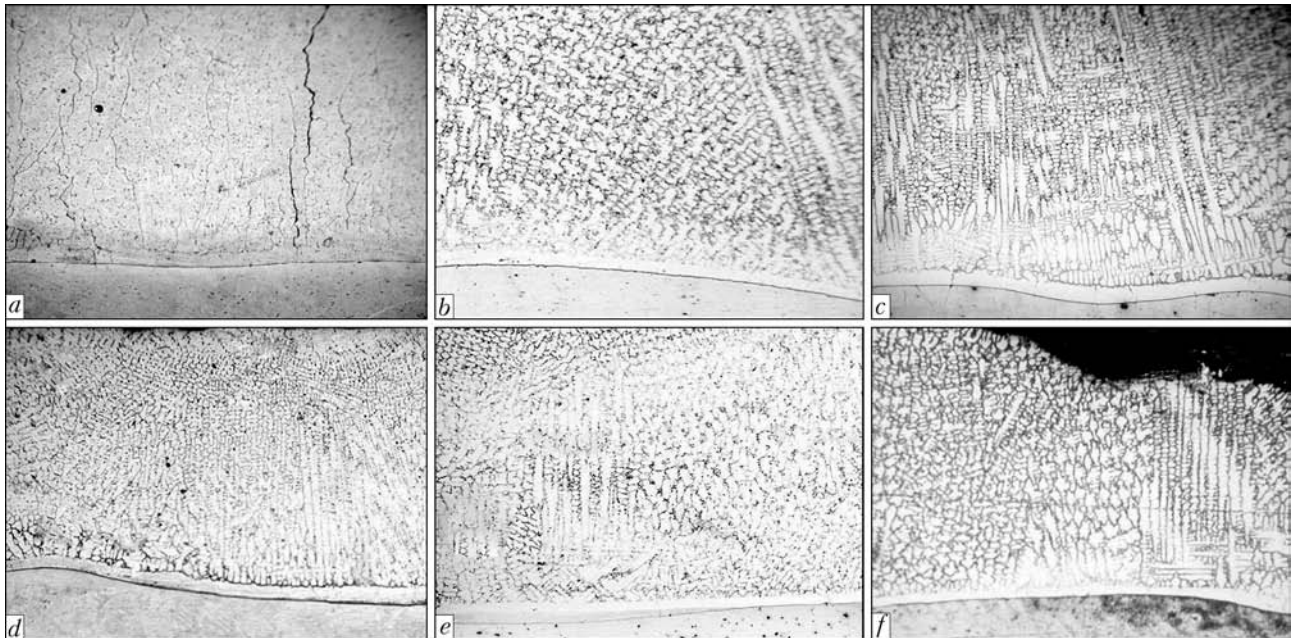
Figure 3. Microstructures (×100) of the layers deposited by the CLMPC method using powder PG-12N-02: *a–f* — specimens 1–6, respectively, from Table 2

close to their melting temperature the burn-off (oxidation) of boron takes place to form B_2O_3. According to the data of study [10], at a temperature of 2000 °C the content of B_2O_3 in the oxide film within the process zone amounts to 81 at.%. Under the combined laser-microplasma process conditions the temperature of the working zone is higher than in plasma spraying, this intensifying burning-off of boron.

As shown by the experiments, in deposition of the layers not less than 0.6 mm high at an energy input ranging from 300 to 400 J/mm the decrease in hardness is minimal. The layers deposited at the above energy inputs have hardness that corresponds to the certificate hardness of the applied cladding alloys. Investigations of the layers produced by the CLMPC method showed that on all the specimens the deposited layers have a sufficiently fine cast structure. Moreover, formation of columnar dendrites of metal, which grew in a direction of heat removal from the zone of fusion with the base metal, takes place in the lower part of the deposited layers. In the upper part of the deposited layers, the columnar dendrites propagate, as a rule, into the zone of finer equiaxed crystals, which is accompanied by some increase in microhardness. The microhardness of the layers deposited at the specimen movement speeds of up to 30 m/h in most cases amounts to about 3000 MPa.

Examinations of structures of the deposited specimens showed the following. Specimen 1 (see Table 2 and Figure 3, *a*) differed from the rest of the specimens in the presence of structural defects, such as transverse cracks in the cast struc-

ture that propagated along the boundaries of dendrites in the deposited metal. HAZ in the base metal was rather big. Its width was 2.5 times bigger than cladding thickness. Specimens 2–4 (see Figure 3, *b–d*) had no cracks and no separations from the substrate. Microcracks similar to those observed in specimen 1 were detected in specimen 5, which can be explained by close energy inputs in cladding of these specimens. Specimens 6 and 7 sprayed at a lower power of the laser were characterised by formation of a lower-quality bead. In all the specimens the deposited metal had the cast dendritic structure, transforming into the fine-crystalline one in the upper part. Interlayers consisting of nickel borides Ni_3B and nickel silicides Ni_2Si and, probably, their eutectics with γ-Ni, as well as chromium carbides $Cr_{23}C_6$ and Cr_7C_3, were located along the boundaries of light dendrites, which were γ-Ni based solid solution.

The feature in common to the specimens is that the dendritic structure of the cladding near the zone of fusion with the base metal was free from inclusion. Structure of the fusion region (white strip) consisted of γ-Ni solid solution and had a decreased hardness, 25 % lower, on the average, than hardness of the cladding. The region located below the fusion zone (HAZ) can be subdivided into two parts as to its depth: a region adjoining the fusion zone, having hardness of 2590–3260 MPa, and a region located below, which adjoins the base metal and has hardness of 1580–1940 MPa. Microhardness of the base metal was 2100–2310 MPa, on the average. Presumably, the presence of the HAZ metal regions
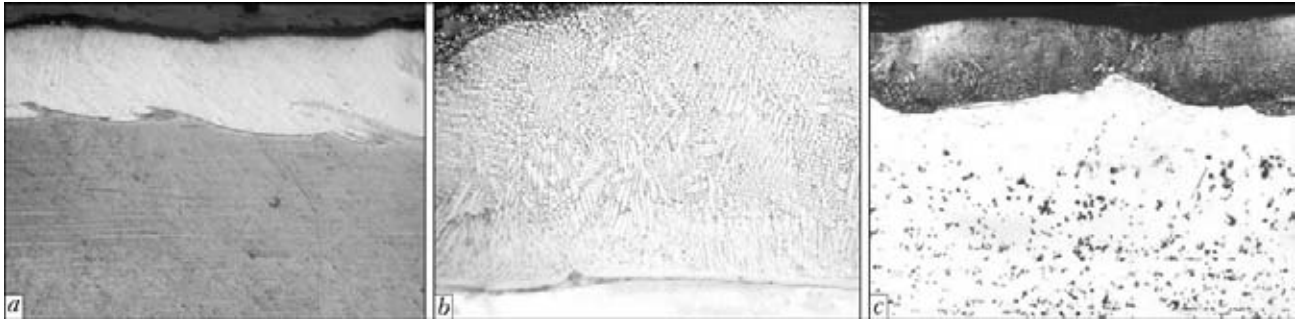
Figure 4. Microstructures of the layers deposited by the CLMPC method using powder PG-12N-02 at a process speed of 20 (*a*, *b*) and 50 (c) m/h with transverse scanning of the laser beam (*a* — ×25; *b* — ×100) and without it (*c* — ×32)

with a different hardness can be explained by a diffusion redistribution of elements. Probably, such alloying elements as carbon, boron and silicon propagated from the deposited layer into that part of HAZ which adjoins the transition part. Moreover, it is likely that carbon from the lower part of HAZ redistributed to the upper part. Size and hardness of the cladding regions and metal depend on the combination of parameters of the laser and microplasma processes, consumption of the additive powder and speed of movement of a specimen in CLMPC.

The experiments showed that increase in the laser beam focusing spot up to values of $d_{sp} = 5-6$ mm leads to the need to use a substantial power of laser radiation (about 3 kW). To decrease the latter and reduce roughness of the surface of the layer, the laser beam was additionally scanned across the cladding with amplitude of 2 mm and frequency of about 20 Hz. The beam was scanned by using a scanator (see Figure 2).

Adding of scanning of the laser beam across the CLMPC direction allowed diameter of the spot focused on the surface treated to be decreased to 4 mm, and laser radiation power to be reduced to 2 kW. Other process parameters were kept constant. Adding of scanning of the laser beam reduced the sensitivity of the deposited layers to cracking. The general trends in formation of structure in these layers remained unchanged (Figure 4, *a*, *b*).

Quality of the resulting layers also depends on the consumption of the additive powder. For example, the CLMPC process without scanning of the laser beam, at the PG-12N-02 powder consumption of $G_p = 1.0-1.2$ g/s, allowed depositing the sound layers 0.5–0.6 mm high at a speed of 50 m/h and at radiation power $P = 3$ kW. In this case the size of HAZ was approximately equal to height of the deposited coating (Figure 4, *c*). Therefore, the indicated consumption of the additive powder materials for CLMPC is 0.8–1.2 g/s.

The results obtained in the above experiments were compared with the results of cladding of

similar materials performed by the laser powder cladding method developed at the E.O. Paton Electric Welding Institute [9]. It turned out that they were rather close in value of irregularities (roughness) and appearance of the clad surfaces. The main difference consisted in sticking of an insignificant quantity of the powder material to the surface in CLMPC.

It was found that the layers of the Ni−Cr−B−Si system alloys deposited by the laser method had a cracking index of about 40−60 % ($\alpha = 0.4-0.6$), whereas the combined cladding allowed decreasing this index from 10−20 % ($\alpha = 0.1-0.2$) to a complete elimination of microcracks.

Both standard friction machine 2070 SMT-1 and in-house friction machine were used to determine wear resistance of the deposited layers.
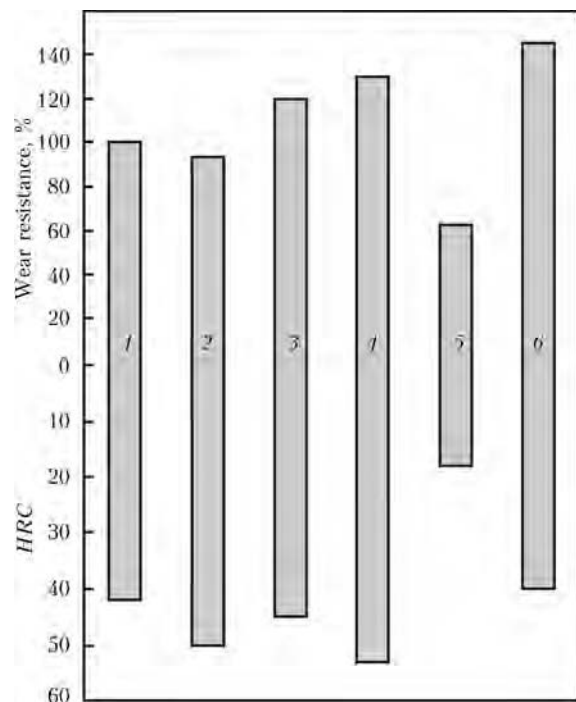
Figure 5. Comparison of wear resistance and hardness *HRC* of Ni−Cr−B−Si system alloys deposited by different methods with those of steel 38KhN3MFA in dry friction: *1* — 38KhN3MFA; *2* — plasma spraying with powder PG-12N-02; *3, 4* — laser cladding with PG-12N-01 and PG-12N-02, respectively; *5, 6* — combined deposition of layers with PG-12N-01 and PG-12N-02

Wear resistance in dry sliding friction was determined in percent, by taking wear resistance of steel 38KhN3MFA with hardness *HRC* 42–43 as 100 %. It was established as result that the wear resistance values in CLMPC can be superior to those characteristic of laser cladding. However, in a case of failure to comply with the thermal conditions, i.e. overheating of specimens at low cladding speeds, the value of wear resistance may decrease to a substantial degree because of weakening of the hard phases. An example of such decrease in wear resistance of metal deposited with powder PG-12N-01 is shown in Figure 5. There this indicator decreased almost to 60 % relative to the same indicator for steel 38KhN3MFA.

CONCLUSIONS

1. The efficiency of applying CLMPC is determined by decrease in the quantity of microcracks in the deposited layers. For instance, the layers of Ni–Cr–B–Si system alloys (PG-12N-01 and PG-12N-02) deposited by the laser method had a cracking index of about 40–60 %, whereas combined cladding of the same alloys allowed decreasing this index from 10–20 % to complete elimination of microcracks.

2. Comparative dry friction tests of specimens of the base metal (steel 38KhN3MFA, whose wear resistance was taken as 100 %) and specimens deposited with the same Ni–Cr–B–Si system alloys showed the possibility of providing wear resistance of an order of 120–130 % in laser powder cladding, and more than 140 % in CLMPC.

3. Along with the above advantages, CLMPC has certain drawbacks compared to laser cladding. The key drawbacks include increase in size of HAZ in the base metal, decrease in hardness of the deposited layers as a result of weakening of metal (burn-off loss (oxidation) of boron and, hence, decrease in the content of the boride phases, as well as coagulation of particles of the

strengthening carbide and silicide phases). The cause is increase in temperature of the working zone due to a substantial growth of the process energy input (to 500–800 J/mm), compared to laser cladding (normally 120–250 J/mm), which is required to achieve the optimal parameters.

4. Further investigations on elimination of the said drawbacks will show expediency of applying laser-microplasma cladding for deposition of wear-resistant coatings both in manufacture and in repair of parts of the shaft type operating in friction pairs (e.g. components of sleeve assembly of internal combustion engines, and running gear of motor and railway transport).

1. Borisov, Yu.S., Kharlamov, Yu.A., Sidorenko, S.L. et al. (1987) *Thermal spray coatings from powder materials*: Refer. Book. Kiev: Naukova Dumka.
2. Grigoriants, A.G., Safonov, A.N., Shibaev, V.V. (1982) Production of wear-resistant chrome-nickel and chrome-boron-nickel coatings by using laser radiation. *Izvestiya Vuzov. Mashinostroenie*, **3**, 87–92.
3. Safonov, A.N., Grigoriants, A.G., Shibaev, V.V. et al. (1984) Investigation of crack formation in laser cladding of chrome-boron-nickel powdered alloys. *Ibid.*, **12**, 64–68.
4. Dilthey, U., Wieschemann, A. (2000) Prospects by combining and coupling laser beam and arc welding processes. *Rivista Italiana della Saldatura*, 52(**6**), 749–759.
5. Coddet, C., Montaron, G., Marchione, T. et al. (1998) Surface preparation and thermal spray in a single step: the PROTAL process. In: *Proc. of 15th ITSC* (Nice, France), Vol. 1, 1321–1325.
6. Krivtsun, I.V. (2002) *Combined laser-arc processes of materials treatment and devices for their realization*: Syn. of Thesis for Dr. of Techn. Sci. Degree. Kiev: PWI.
7. Shelyagin, V.D., Krivtsun, I.V., Borisov, Yu.S. et al. (2006) Laser-arc and laser-plasma welding and coating technologies. *Svarka v Sibiri*, **1**, 32–36.
8. Borisov, Yu.S., Vojnarovich, S.G., Bobrik, V.G. et al. (2000) Microplasma spraying of bioceramic coatings. *The Paton Welding J.*, **12**, 63–67.
9. Velichko, O.A., Avramchenko, P.F., Molchan, I.V. et al. (1990) Laser powder cladding of cylindrical parts. *Avtomatich. Svarka*, **1**, 59–65.
10. Gershenzon, S.M., Borisov, Yu.S., Razikov, M.I. et al. (1978) Interaction of self-fluxing nickel alloys with oxygen. *Svarochn. Proizvodstvo*, **1**, 9–11.

THERMODYNAMIC ANALYSIS OF SLAG MELTS IN MANUFACTURE OF FUSED WELDING FLUXES

L.A. ZHDANOV[1], **A.N. DUCHENKO**[1], **I.A. GONCHAROV**[2], **V.I. GALINICH**[2], **A.V. ZALEVSKY**[2] and **N.Ya. OSIPOV**[3]

[1]NTUU «Kiev Polytechnic Institute», Kiev, Ukraine
[2]E.O. Paton Electric Welding Institute, NASU, Kiev, Ukraine
[3]OJSC «Zaporozhstekloflyus», Zaporozhie, Ukraine

Applicability of equilibrium thermodynamic laws for analysis of physico-chemical reactions was established proceeding from analysis of temperature-time conditions of melting of welding fluxes in arc and open gas furnaces. Thermodynamic analysis of reactions of charge components used in welding flux manufacture was conducted. Techniques to control the process of slag melt refining are determined.

Keywords: *fused welding fluxes, slag melt, sulphur, phosphorus, thermodynamic analysis*

Ukraine today is a leading manufacturer of fused welding fluxes. Such leading scientists as E.O. Paton, K.V. Lyubavsky, B.E. Paton, V.I. Dyatlov, I.I. Frumin, V.V. Podgaetsky, I.K. Pokhodnya and many others participated in development of flux compositions and their manufacturing technology. In connection with depletion of deposits of mineral raw materials traditionally applied in fused flux manufacture, the problem of ensuring the required flux composition and their quality, respectively, became much more acute.

Conducted analysis of charge materials showed that in most of the cases the content of impurities in them is specified by the normative documents (GOST, DSTU, TU). Technical documentation predominantly specifies the content of the main component in the raw material, and in a number of cases does not limit the content of impurities — sulphur, phosphorus, and iron oxides. At the same time, their content in the fluxes is limited. On the other hand, statistical data of incoming inspection of the raw materials are indicative of wide ranges of variation of their impurity content.

The most contaminated are manganese ore and fluorospar concentrates, in which sulphur and phosphorus content reaches 0.3 % in some cases. These materials make up almost half of the charge in manufacture of the most widely accepted fluxes of AN-348-A, OSTs-45 grades. Therefore, it is possible to keep their sulphur and phosphorus content only at the upper admissible level by the technical requirements. Forced application of low-grade ore materials leads to increase of the amount of impurities contributed by them to the melt that in its turn reduces the technological margin on impurities in flux melting.

Therefore, work on investigation of processes running in flux-meting furnaces is urgent for development of recommendations on lowering the impurities in the slag melt.

Fused welding fluxes are made in open gas and arc furnaces [1]. These melting units differ by temperature conditions, lining type, volume, mixing conditions and time of slag melt existence. For open gas furnaces these are: up to 1450 °C temperature, up to 60 t melt volume, and up to 6 h melting time. In the case of arc furnaces slag melt temperature is higher on average and can reach 1800—1900 °C. Melt volume for various types of furnaces can be in the range from 50 kg up to 5 t, and melting time is from 1 up to 2 h. Intensive processes of slag melt mixing proceed in arc furnaces under the impact of the magnetic field and temperature gradient. Thus, equilibrium conditions are in place in both the cases, which are characterized by long-time existence of the melt, large volume and uniformity in local melting regions. All that allows applying the principles and laws of chemical equilibrium thermodynamics for assessment of physico-chemical processes in flux-melting furnaces.

In the general case the melting space of a furnace can be regarded as a closed thermodynamic system that is related to features of mass exchange with the environment. In flux melting by a traditional schematic, uniformly blended charge is fed into the furnace and, as a rule, there is no further adding of charge components to the furnace volume. Mass transfer can be performed only as a result of gas removal from the melting space and transition of compounds from slag into the metal phase.

Melting space, in which charge material components are present in the form of solid and partially molten particles of the slag melt, shot iron and lining, is a heterogeneous system. To perform analysis of such a complex heterogeneous thermodynamic system, the melting space should be separated into certain homogeneous systems (zones), in which chemical reactions will be considered. Zone interaction is performed through interfaces. It is understandable that such a division is conditional, and does not reflect all the diversity of high-temperature processes in the furnace melting space, in particular, kinetics of slag melt homogenizing, hydrodynamic conditions of its existence, process of gas removal from the melt and impact of the electromagnetic field (in flux melting in electric arc furnaces).

Traditionally [2] the process of flux melting is divided into three stages: reaction in the solid state, flux formation and slag melt homogenizing. As a result, the following phases can be singled out in the flux volume:

• solid, in which thermal dissociation and interaction of charge particles take place;

• partially molten dispersed solid-liquid phase, arising as a result of charge heating, eutectic and contact melting;

• slag melt with a certain degree of homogenizing;

• metallic phase (shot iron) forming as a result of chemical reactions in the slag melt;

• gas phase forming as a result of thermal dissociation of charge components and chemical reactions with formation of gaseous products, which float to the slag melt surface in the form of bubbles.

Interfaces are well developed, rather blurred, particularly in the presence of dispersed particles at the beginning of slag melt formation. A certain temperature interval corresponds to each phase in flux manufacture.

The objective of this work was analysis of thermodynamic probability of chemical reaction running in the flux-melting furnace volume, and precising the mechanism of sulphur and phosphorus removal from the slag melt to lower the content of these impurities in the finished flux composition. A characteristic of the probability of reaction running was dependence of Gibbs energy ΔG on temperature. In metallurgy in most of the cases a simplified Gibbs equation is used, which allows for the change of enthalpy and entropy of the reaction, depending on temperature. Heat capacity of initial materials and reaction products in this case is neglected. This is related to the fact that heat capacity contribution to ΔG value

at up to 800−1000 K temperatures is negligible. At temperature rise heat capacity value rises by a logarithmic dependence, and it can change the heat capacity of elements 2 times. One of the calculation methods of allowing for the change of heat capacity value, depending on temperature, is application of Uhlich function

$$M_0 = \ln \frac{T}{298.15} + \frac{298.15}{T} - 1. \qquad (1)$$

As a result, equation for calculation of the change of Gibbs energy becomes

$$\Delta G_T^0 = \Delta H_{298}^0 - T\Delta S_{298}^0 - \Delta Cp_{298}^0 \, TM_0, \qquad (2)$$

where

$$\Delta H_{298}^0 = \sum H_{298 \text{ prod}}^0 - \sum H_{298 \text{ in}}^0; \qquad (3)$$

$$\Delta S_{298}^0 = \sum S_{298 \text{ prod}}^0 - \sum S_{298 \text{ in}}^0; \qquad (4)$$

$$\Delta Cp_{298}^0 = \sum \Delta Cp_{298 \text{ prod}}^0 - \sum \Delta Cp_{298 \text{ in}}^0; \qquad (5)$$

ΔH_{298}^0, ΔS_{298}^0, ΔCp_{298}^0 is the variation of values of thermodynamic characteristic functions of the participants (products and initial materials) of the chemical reaction under standard thermodynamic conditions (at temperature of 298 K and atmospheric pressure of 1 atm ($9.80665 \cdot 10^4$ Pa)).

One of the main problems, arising during thermodynamic metallurgical calculations, is finding the values of enthalpy, entropy and heat capacity of the initial materials and reaction products. Unfortunately, the most fundamental works [3, 4] do not include the data on complex compounds, so that we assumed them on the basis of processing the experimental equations, used in metallurgical calculations [5].

In manufacture of fused welding fluxes for steel welding, the most often used raw materials are manganese ore concentrates, quartz sand, alumina, periclase powders, lime, marble, fluorite, fluorspar, rutile, zirconium concentrates, etc., which contain such chemical compounds as SiO_2, MnO_2, Mn_2O_3, MnO, Fe_2O_3, CaO_3, $MgCO_3$, TiO_2, FeS_2, MnS, Mn_nP, CaF_2, P_2O_5, $Ca_5(PO_4)_3(F, Cl, OH)$. In ores phosphorus is mostly present in the form of phosphorus-calcium salt, included into the composition of apatite minerals [6]. In addition, material of the electrodes and lining − carbon (for arc furnaces) and firebrick (for open gas furnaces) − will participate in the interaction reactions.

At consideration of the first stage, analysis of chemical reactions in the solid state − gaseous compounds formation and removal − is traditionally performed. This is exactly the stage at which melting of the flux charge proceeds, i.e. charge transition from the solid into the liquid

state. The charge, which later on forms the slag melt, is first present in the form of separate components, the melting temperature of which is much higher than that of the melting space. The charge melting process proceeds at the expense of contact melting of charge particles with simultaneous thermal dissociation of carbonates and higher oxides.

In the contacting surfaces of flux charge particles interdiffusion takes place, which results in formation of a eutectic layer and contact melting at temperatures below the melting temperature of individual charge materials. This results in formation of partially molten dispersed phase, which promotes further charge melting at melting space temperatures, and flux forming process takes place. The lowest-melting eutectics can form as a result of contact interaction of flux charge particles already at temperatures of 900–1100 °C [7, 8].

Processes of thermal dissociation of charge components are accompanied by intensive gas evolution, thus leading to increase of charge melting rate due to mixing of the forming liquid phase. It should be noted that formation of gaseous compounds should influence the kinetic features of charge material interaction, and can change the concentrational conditions of the reactions between the components in the solid and semi-liquid state.

At the first stage reactions of carbonate decomposition with carbon dioxide gas evolution, as well as reduction of higher manganese oxides (Figure 1, *a*) with formation of gaseous oxygen, take place. Manganese, calcium and magnesium sulphides do not decompose (Figure 1, *b*). Interaction of oxygen with sulphides results in appearance of gaseous sulphur oxide SO_2, which is removed from the melting space (Figure 2, *a*). Therefore, it is believed that for maximum removal of sulphur at the first stage of melting it is necessary to create oxidizing conditions, which can be formed due to dissociation of higher oxides, for instance MnO_2 (see Figure 1, *a*). Besides oxygen, sulphur can be removed from the compounds as a result of interaction of calcium sulphide with higher manganese oxide (Figure 2, *a*).

Manganese phosphides can decompose with formation of solid and gaseous phosphorus (see Figure 1, *b*). The thus formed manganese can here interact with phosphorus oxide also with formation of solid and gaseous phosphorus, which can also be reduced by other metals, for instance, silicon (Figure 2, *b*). However, their presence at the first stage of melting is improbable. Reaction of phosphorus oxidation at interaction with silicon oxide is more probable. Reduction of phos-

Figure 1. Change of Gibbs energy for reactions of dissociation of carbonates, higher oxides of manganese (*a*), phosphides of manganese and sulphides (*b*)

phorus oxide by iron at this melting stage is improbable (see Figure 2, *b*).

Proceeding from the calculation data, it can be anticipated that phosphorus, similar to sulphur, should be removed already at the first stage of melting. This process, however, is prevented by two interrelated factors: under oxidizing conditions sulphur is removed at the first melting stage during a reaction of interaction of solid and gaseous phosphorus with formation of P_2O_5, which, in its turn, comes into a reaction with calcium and magnesium oxides, forming the respective phosphates (Figure 3, *a*). At the same
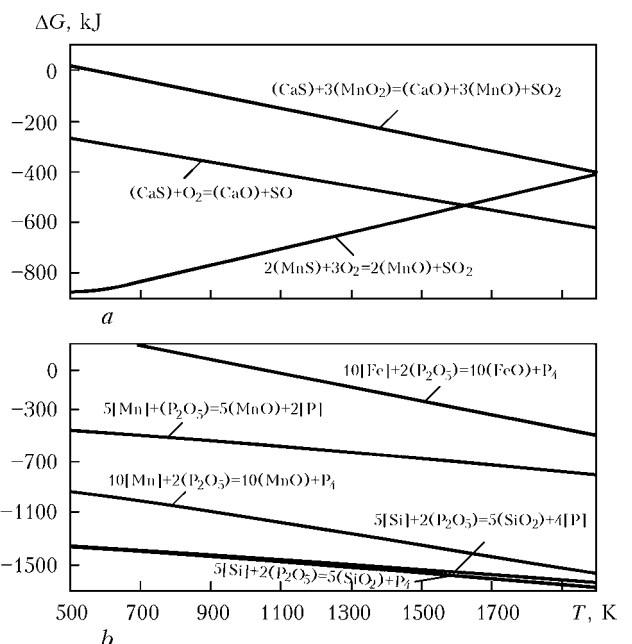
Figure 2. Change of Gibbs energy for reactions of formation of sulphur oxide (*a*) and phosphorus precipitation (*b*)
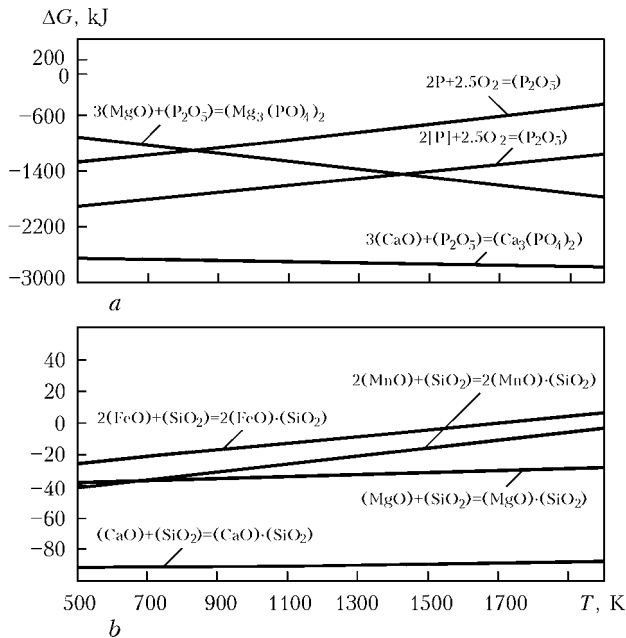
Figure 3. Change of Gibbs energy for reactions of formation of phosphorus oxide and complex compounds with phosphorus oxide (*a*) and silicon oxide (*b*)

time, these oxides can form complex compounds based on silicon oxide. The known property of silicon oxide to form silicon-oxygen chains in the melt leads to phosphorus oxide being bound into extremely strong aggregated complex compounds, which further on at high contents of silicon oxide in the melt are built into the silicon-oxygen lattice of the slag melt and can be removed from the melt only when reducing conditions are created. The probability of these reactions is higher (Figure 3, *b*). Temperature, at which this melting stage is over, can be conditionally taken to be equal to about 1000—1200 °C (±50 °C). The process of charge melting is determined by the kinetics of the processes of gas evolution and contact melting of charge particles. It is exactly the kinetics of these processes at this stage that determines the completeness of removal of gaseous products from the melt, namely phosphorus and sulphur oxides. The main factor, determining the completion of this melting stage, is removal of oxygen and carbon dioxide gas from the melt.

The flux forming (slag forming) stage is characterized by that all the charge mass turns into the melt as a result of interaction of eutectics formed at contact melting with the charge bulk. Charge homogeneity is not achieved [2]. Its mass contains a large number of gas bubbles and has a non-uniform structure. At traditional conducting of the melting process, formation of thermodynamically stable complex compounds — calcium, magnesium, manganese, iron and phosphorus silicates goes on at this stage in the presence of silicon oxide in the charge (see Figure 3, *b*). Calculation results show that due to known property of silicon oxide, mentioned above reactions

proceed in the entire temperature range characteristic for the flux melt, i.e. complex formation accompanies the entire process of flux melting. These are exactly the complex compounds that do not allow phosphorus to be removed from the flux melt in the process of flux melting. Note the fact that the probability of $CaO \cdot P_2O_5$ formation rises with temperature, thus making phosphorus removal from the slag melt difficult.

The objective of phosphorus removal from the melt can be implemented by creation of certain concentrational conditions, in which complex formation will be limited, for instance, by addition of silicon oxide (or part of it) separately from the other charge components.

The main outcome of the second stage, which corresponds to temperature interval of 1200—1270 °C (±50 °C), is charge transformation into the slag melt, in which unmolten charge particles are absent.

At the third stage the processes of slag melt homogenizing and degassing proceed. An important requirement to oxide fluxes for steel welding is lowering of their oxidizing ability relative to metal in the reaction welding zone. Therefore, during their manufacture the slag melt is further oxidized through reactions of carbo-thermal reduction of the melt components with the carbon of the lining (in the case of arc furnaces) or coke breeze additives (in the case of open gas furnaces). As a result, oxidizing conditions in the furnace are replaced by reducing conditions, flux components interact with carbon, forming the metal phase, containing iron, manganese and silicon (Figure 4). Appearing metals interact with phosphorus oxide with formation of gaseous and solid phosphorus (see Figure 2, *b*), taking it out of the slag melt.

Thus, the most important in terms of slag melt dephosphorization is the reaction of phosphorus transfer into the metal phase, which is realized exactly at this stage of the process. Phosphorus reduced by metals goes into the metal phase together with other metals and precipitates on the furnace bottom plate. Temperature and concentrational conditions of this process running have the main role here. On the one hand, reactions of intermediate manganese oxides of Mn_2O_3 type are highly probable, and on the other — probability of the reactions of iron oxide reduction exceeds the possibility of MnO reduction. This enables controlling the processes of manganese loss as a result of its transition into the metal phase. In particular, such a lowering can be achieved due to complete transfer of higher oxides into the lower (MnO) oxide at the first and second melting stages.

In addition, carbon reduces phosphorus from complex compounds based on calcium and man-
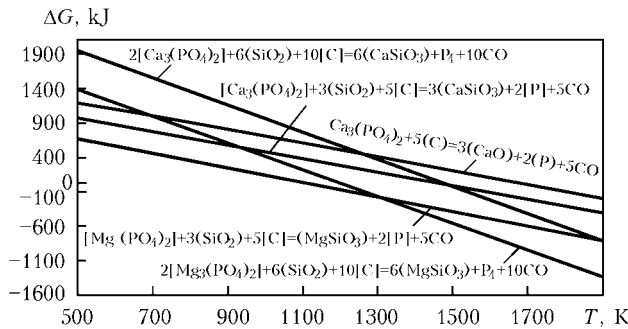
Figure 4. Change of Gibbs energy for reactions of oxide reduction by carbon

Figure 5. Change of Gibbs energy for reduction of phosphates by carbon and silicon oxide

ganese oxides in the presence of silicon oxide (Figure 5). However, some of these reactions start running only after 1200 °C, and their bulk — after 1500 °C, i.e. at the final stage of melting. The thus formed phosphorus precipitates on furnace bottom. In arc furnaces the probability of the reactions is enhanced in near-electrode regions. The simultaneously precipitating carbon oxide promotes homogenizing of the slag melt.

Completeness of phosphorus oxide removal from the slag melt is determined by the presence of the metal phase. Melting conditions can be selected so that it will mainly consist of iron, whereas silicon and manganese transition will be minimum. Temperature range of the last melting stage is determined by technological capabilities of arc furnaces. For open gas furnaces it is over at the temperature of 1470 °C (±10 °C), and for flux melting — at 1800−1900 °C.

CONCLUSIONS

1. Proceeding from analysis of temperature-time conditions of welding flux melting in arc and open gas furnaces, the possibility of application of the laws of equilibrium thermodynamics for analysis of physico-chemical reactions was determined. Here the heat capacity of the elements and their compounds should be taken into account, and the calculation proper should be performed by Uhlich formula.

2. As a result of thermodynamic analysis of the reactions of charge components used in welding flux manufacture it is established that:

• reactions of sulphide decomposition do not proceed, and their removal requires the presence of oxidizing conditions;

• reactions of phosphide decomposition run in the entire temperature range, but under oxidizing conditions phosphorus oxide forms, which goes into difficult to remove complex compounds;

• in the presence of carbon, exchange reactions proceed in the melt, which result in formation of metals reducing phosphorus from the oxide up to the metallic and gaseous state, and oxides of the same metals, i.e. this group of reactions are
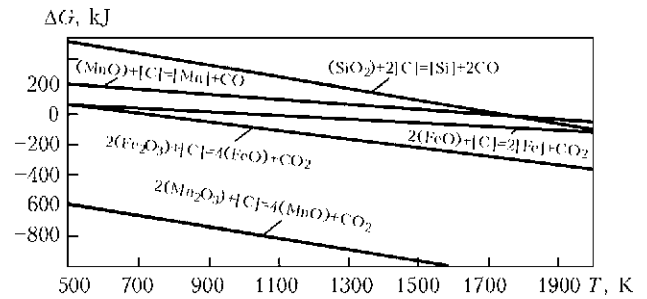
interrelated and should be regarded as one thermodynamic system;

• as a result of exchange reactions with participation of carbon, silicon oxide and phosphates, which are present in complex compounds, reactions of phosphorus reduction with simultaneous formation of carbon oxide run at the third stage of melting. There are ten CO molecules for one P_4 molecule that should promote removal of gaseous phosphorus from the melt. Carbon monoxide further oxidizes in the slag melt, promoting lowering of oxidizing ability of the ready flux.

3. Methods to control the processes of slag melt refining are as follows:

• creating oxidizing conditions at the initial melting stage by adding higher oxides of variable valency for sulphur transfer into gaseous oxides;

• separate addition of charge components, in particular silicon oxide, separately from the rest of the charge bulk to prevent formation of complex compounds in the slag melt, hindering phosphorus removal;

• mandatory simultaneous addition of carbon and silicon oxide at the final stage of melting process for decomposition of phosphates present in the complex compounds;

• mandatory presence of the metal phase, forming through reactions of reduction of iron, manganese and silicon oxides by carbon, to remove solid phosphorus from the slag melt. It is possible to create such concentration and temperature conditions, under which the metal phase will consist mainly of iron and phosphorus, and manganese transition into it will be minimum.

1. Podgaetsky, V.V., Lyuborets, I.I. (1984) *Welding fluxes*. Kiev: Tekhnika.
2. Podgaetsky, V.V. (1947) *Production of AN-3 flux for automatic welding*. Kiev.
3. (1965−1982) *Thermal constants of materials*: Refer. Book. Ed. by V.P. Glushko. Moscow: VINITI.
4. (1978) *Thermodynamic properties of individual materials*. Ed. by V.P. Glushko. Moscow: Nauka.
5. Kazachkov, E.A. (1988) *Calculations on theory of metallurgical processes*. Moscow: Metallurgiya.
6. Leontiev, L.I., Yusfin, Yu.S., Malysheva, T.Ya. et al. (2007) *Raw and fuel materials base of iron industry*. Moscow: Akademkniga.
7. Zalkin, V.M. (1987) *Nature of eutectic alloys and effect of contact melting*. Moscow: Metallurgiya.
8. Savin, V.S., Mikhalyova, O.V., Zubova, Yu.A. (2007) Diffusion of atoms from liquid to solid phase in contact melting. *Zhurnal Tekhn. Fiziki*, 33(**10**), 27−32.

REPAIR WELDING OF INTERMEDIATE CASES OF AIRCRAFT ENGINES FROM HIGH-TEMPERATURE MAGNESIUM ALLOY ML10 WITH APPLICATION OF ELECTRODYNAMIC TREATMENT

L.M. LOBANOV[1], **N.A. PASHCHIN**[1], **A.V. CHERKASHIN**[1], **G.I. TKACHUK**[1], **V.V. SAVITSKY**[1],
O.L. MIKHODUJ[1], **K.V. SHIYAN**[1], **V.K. LEVCHUK**[1], **V.V. ZHYGINAS**[2] and **A.P. LYASHCHENKO**[2]
[1]E.O. Paton Electric Welding Institute, NASU, Kiev, Ukraine
[2]SC «Plant 410 of Civil Aviation», Kiev, Ukraine

Technology was developed for repair welding of damages in aircraft engine intermediate cases from magnesium alloy ML10. The technology comprises electrodynamic treatment of welds aimed at reducing the level of residual welding stresses. It was experimentally proved that treatment practically eliminates residual stresses in the weld. At charging voltage of up to 200 V electrodynamic treatment operator can perform maximum 1100 electrodynamic impact operations per shift, and at 500 V voltage — not more than 100 operations, that fully meets the requirements of production cycle of repair welding of aircraft intermediate case.

Development of modern technologies of repair of aeronautical engineering equipment is related to searching for new ways of extension of service life of metal structures from high-temperature magnesium alloys, reconditioned by repair welding. One of the causes for shortening of the service life of flying vehicles are residual welding stresses in repair welds, which adversely affect the fatigue strength, corrosion resistance and residual distortion of aircraft structural elements. This necessitates investigation of advanced methods to control the stressed state of welded joints, one of which is treatment by electric current pulses [1, 2].

Method of realization of pulsed current impact on metals is electrodynamic treatment (EDT) based on initiation of electrodynamic forces in the material, arising at passage of a current discharge in the treated material [3]. The mechanisms of EDT impact on the treated material are described in detail in [4].

One of the structural components of the aircraft, in which the damage is repaired by welding, is the aircraft engine intermediate case (AEIC). AEIC purpose is aircraft engine fastening on the aircraft wing and thermal insulation of the airframe structural components from thermal impact of an operating engine. Figure 1, *a*, shows AEIC appearance as-assembled with D-36 engine. Conditions of AEIC operation make high requirements to fatigue and static strength characteristics of the structure at high (up to 400 °C) temperatures, as well as to its dimensional stability, determining the aerodynamic and propulsion performance characteristics of D-36 engine. Proceeding from that, static and fatigue strength of AEIC repair welded joints should correspond to mechanical characteristics of base metal, and level of residual welding stresses — to minimum values. Thus, it is believed to be reasonable to assess EDT capabilities to lower the level of residual welding stresses in AEIC repair welds.

The objective of this work is development of the technology of repair welding of AEIC damage with EDT application.

AEIC is a large-sized cast structure from magnesium alloy ML10 (Figure 1, *b*) which consists of outer *1* and inner *2* cylindrical shells, connected by stiffeners — posts *4*. One of the design features of the posts is presence of inner cavities in them, through which the coolant circulates, which is designed for minimizing the thermal impact of operating engine on AEIC. Outer shell is designed for mounting AEIC on aircraft wing, and the inner shell — for fastening the aircraft engine *3*.

The most characteristic damages of AEIC (Figure 2) rectified by repair welding, are fatigue cracks, disturbing the integrity of the post in the

points of their connection to outer and inner shells (Figure 2, weld 1, view *A*). Formation of fatigue cracks on the external surface of outer shell in the zone of reinforcement for cooling pipeline flange (Figure 2, weld 2, sectional view *A–A*) and on reinforcement for the system of AEIC fastening to the wing is less common. In terms of design the assembly of AEIC fastening to the wing is similar to that shown in sectional view *A–A*. The result of mentioned service defects are a partial loss of the load-carrying capacity of the structure and violation of leak-tightness of AEIC cooling cavities.

Repair of AEIC damages was performed using manual single- and multipass nonconsumable electrode arc welding (TIG) in shielding gas atmosphere (argon) in the following modes: $U_a = 20$ V, $v_w = 1.5$ mm/s. Shielding gas was pure argon of grade A, recommended for welding tight joints, to which welds 1 and 2 belong (argon flow rate was 0.25–0.30 l/s). Post repair (see Figure 2, weld 1) was performed at current of 200–350 A in five passes, repair of reinforcement for the cooling main pipeline (Figure 2, weld 2) — at current of 200–250 A in two passes. Joint preparation for welding was performed by mechanical cleaning of the repair joint to the width of 15–30 mm from both sides using a steel brush (stainless steel diameter of 0.2 mm) and scraping. Time interval between mechanical cleaning and welding did not exceed 24 h. Filler rods of ML9 grade of 6 mm diameter were used, the surface of which was treated by chemical etching before welding. Preparation of crack edges was performed with the angle of opening of 50–70°, with more than 3 mm radius of opening in the root up to residual thickness of 0.3–0.5 mm. TIG welding was performed with concurrent local preheating of the welding zone, which was realized by placing specialized heaters based on tubular electric heating elements on the base metal. Heating temperature was equal to 150–200 °C. The first pass was made at minimum current with the initial and final sections of the repair weld reaching the base metal. Here smooth transition of the deposited to base metal was ensured with welding up of the crater in the mode of smooth extinction of the arc. At forced stopping of the welding process, because of filler rod replacement, overlapping of earlier deposited weld by 20–30 mm was performed. The overlapped surface was first cleaned mechanically.

Presence of residual stresses in AEIC repair welds in a number of cases requires performance of postweld heat treatment of the item in large-sized electric furnaces that is a highly energy-consuming operation. Application of heat treatment is required when repair welding of more
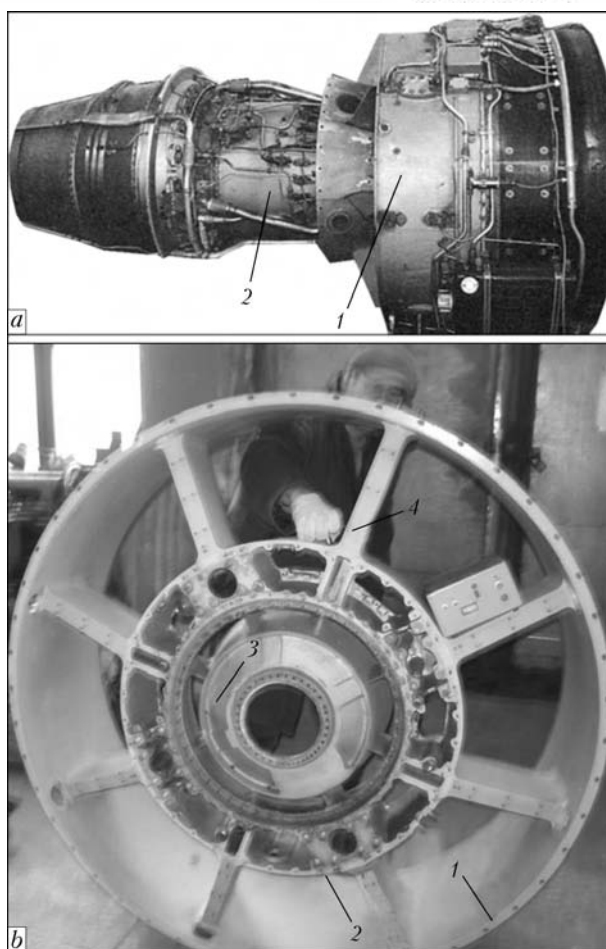
Figure 1. Appearance of AEIC (*1*) as-assembled with D-36 aircraft engine (*2*) (*a*) and AEIC (*b–f* for *1–4* see the text)

than two AEIC damages is performed. At the same time, there are cases, when a unit defect of small depth and length is to be repaired. Then application of total heat treatment is not rational. Practical experience of application of postweld local heating of the repair weld with tubular electric heating elements used for welding, demonstrated its low effectiveness as a result of high heat conductivity of ML10 alloy. Application of
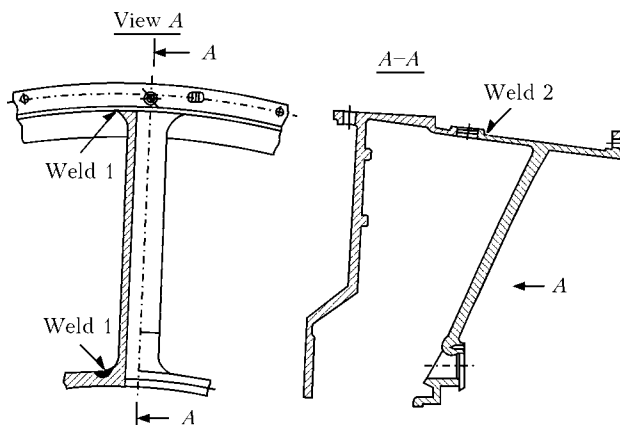
Figure 2. Schematic of location of repair welds at service damage of AEIC in the zone of connection of the post to the outer and inner shells (weld 1) and in the zone of fastening the cooling pipeline (weld 2)

σ_{xx}, MPa
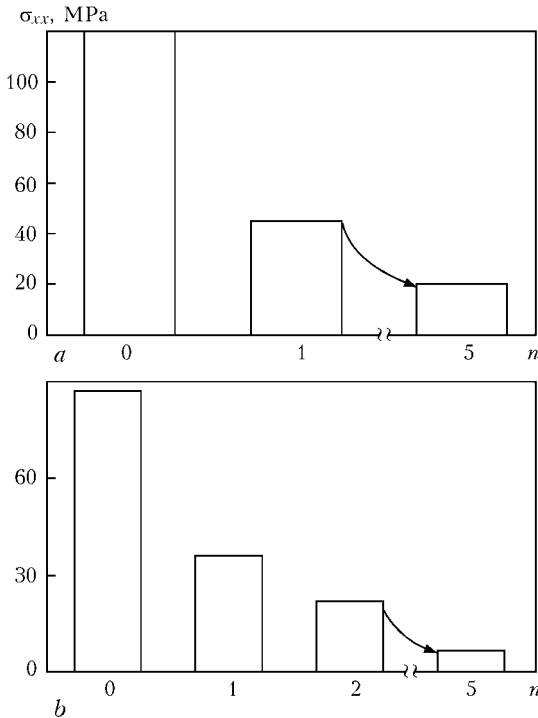
Figure 3. Change of values of stresses σ_{xx} in single-pass 1 (*a*) and two-pass 2 (*b*) welds depending on the number of current discharges *n*

EDT will allow not only lowering the level of residual stresses in short repair welds without heat treatment application, but also replacing it in the future that will lower the cost of AEIC reconditioning. It should be noted that by the results of testing by static tension, EDT does not have any negative influence on mechanical characteristics of AEIC repair welded joints.

EDT influence on distribution of residual stresses arising at two-pass deposition of weld 1 was studied on samples of $350 \times 200 \times 8$ mm size. Before bead deposition a cut of the length, width and depth of 200, 1.6−2.0 and 8−10 mm, respectively, was made with a hand cutter along the weld by a procedure described above. In order to reproduce the operations of AEIC repair, two-pass welding was performed in the cut section in the mode given above. Here, the geometrical characteristics of the deposited weld corresponded to parameters of the repair joint made in AEIC on the shop floor.

Table 1. Modes of EDT of welded joints of magnesium alloy ML10 (capacitor storage $C = 6600$ µF, discharge ratio $t_r = 60$ s)

EDT mode number	Charging voltage U, V	Charging current[*] I, A	Electrode pressure[*] P, N	Discharge time[*] t_d, ms
1	200	1195	2792	1.2
2	500	3080	20461	1.6
[*]Procedure of determination of EDT parameters is described in [4].				

EDT influence on the magnitude and distribution of residual stresses when making weld 2 was studied on samples of $300 \times 200 \times 8$ mm size, containing elements of reinforcement for the flange of the cooling pipeline, shown in Figure 3 (sectional view *A−A*). Before deposition a cut of the length, width and depth of 50, 1.6−2.0 and 8−10 mm, respectively, simulating the fracture, was made between the bosses, and its edge preparation was made similar to weld 1. In order to simulate repair welding performed at damage reconditioning, single-pass deposit 50 mm long was made between the bosses, in the mode mentioned above. After bead deposition and complete cooling of the samples, EDT of welded joints of the samples was performed in the modes given in Table 1.

Welded joints were treated along the weld axis in the direction from the middle towards the edges.

Before performance of TIG welding, evaluation of the initial level of stresses in ML10 alloy was performed by the method of electron speckle-interferometry on sample surface. After welding, values of longitudinal component σ_{xx} of residual stresses were determined in repair weld zone before and after EDT performance. Treatment effectiveness was assessed by the results of comparison of stressed state parameters before and after EDT.

Evaluation of initial stressed state on the surface of ML10 alloy samples before welding showed that stress distribution on their outer surface was uniform, while σ_{xx} values were in the range of 4−6 MPa.

EDT of samples with deposited welds 1 and 2 was performed by series of five current discharges in modes corresponding to charging voltage $U = 200$ and 500 V. Sections on the surface of deposited beads were treated by application of current pulses with monitoring σ_{xx} variation in EDT zone. Initial and final weld sections of 10 mm length, in which values of initial stresses are minimal, were treated in mode 1, and the other bead surfaces — in mode 2 from Table 1.

Initial σ_{xx} values in the metal of single-pass weld 2 before and after treatment were equal to 120 and 20 MPa, respectively. Initial σ_{xx} level in two-pass weld 1 before treatment was lower and was equal to 87 MPa. This is due to local tempering of weld metal deposited in the first pass after making the second pass. After EDT σ_{xx} values did not exceed 6.5 MPa in the measured zone that is comparable with the stress level in the base metal before deposition. Changes of σ_{xx} values in welds 1 and 2, depending on the

number of current pulses *n* are shown in Figure 3, from which it is seen that the maximum effectiveness of electrodynamic impact is achieved after the first current discharge ($n = 1$) that allows lowering initial σ_{xx} values by more than 50 %.

Results of experiments conducted on AEIC fragments lead to the conclusion that EDT of repair deposits in the zone of characteristic damage of the structure allows lowering the level of initial welding stresses practically to base metal level.

EDT of full-scale AEIC was conducted in the locations of repair cladding in the areas of post damage (see Figure 1, *b*) and reinforcement for the flange of cooling pipeline fastening (Figure 4). EDT was performed in modes shown in Table 1 in the sequence corresponding to treatment of full-scale samples. During EDT cycle initial stress level was recorded before and after cladding, as well as after EDT. Analysis of current measurements of parameters of repair deposit stressed state leads to the conclusion that after EDT the level of stressed state in repair deposits is close to that of AEIC base metal.

It should be noted that manual tool for EDT (see Figure 4) enables access to AEIC repair welds in all the positions. Power source for EDT, the weight of which does not exceed 3 kg, is quite compact, that allows placing it on the surface of the treated structure in the working zone of EDT operator. EDT operators are exposed to the impact of pulsed electromagnetic fields. This is related to the fact that the tool, which is the source of magnetic radiation, is in direct contact with the operator's hand during EDT. Values of intensity *H* of the magnetic field (MF) should not exceed limit permissible levels (LPL) specified by «State Sanitary Norms and Rules of Operation with Electromagnetic Field Sources» (DSN 3.3.6.096–2002). Determination of MF parameters, corresponding to AEIC treatment modes, is an urgent task, related to taking measures for industrial safety of EDT operators.

The main MF source is a flat inductor, which is part of the working tool [4]. Amplitude value of MF intensity at EDT operator workplace depends on pulse current, dimensions and shape of discharge circuit, as well as the distance between the performer and field source. Such MF sources as discharge circuit and capacitor storage module were not considered, in view of small values of magnetic radiation.

Proceeding from analysis of amplitude-frequency characteristics of current pulses, applied at EDT [4], conditions of MF radiation at EDT are at the lower limit of radio frequency range. This allowed isolating a frequency range from 1 up to 10 kHz, in which it is necessary to determine MF level, corresponding to electrodynamic impacts with charging voltage of 200–500 V.

Figure 4. AEIC EDT in the zone of repair cladding of reinforcement for the flange of fastening the post cooling pipeline: *1* — reinforcement for flange; *2* — manual tool for EDT; *3* — power source for EDT

A flat inductor was a source of MF radiation, and the operator's wrist located at the distance of 70 mm from the inductor, was selected as the zone closest to MF source.

Plate with deposited bead from ML10 alloy was used for evaluation of MP parameters.

Intensity *H* of pulsed MF was determined using instrumentation system GFI-1 (Hall sensor), the analog signal from which was recorded by TDS-1002 oscillograph with Fourier transformation function. Certified sensor and oscillograph ensured measurement of the spectrum of MF in-

Figure 5. GFI-1 system for measurement of pulsed MF intensity at EDT: *1* — power source for EDT; *2* — Hall sensor; *3* — flat inductor; *4* — welded joint sample; *5* — MF intensity recorder
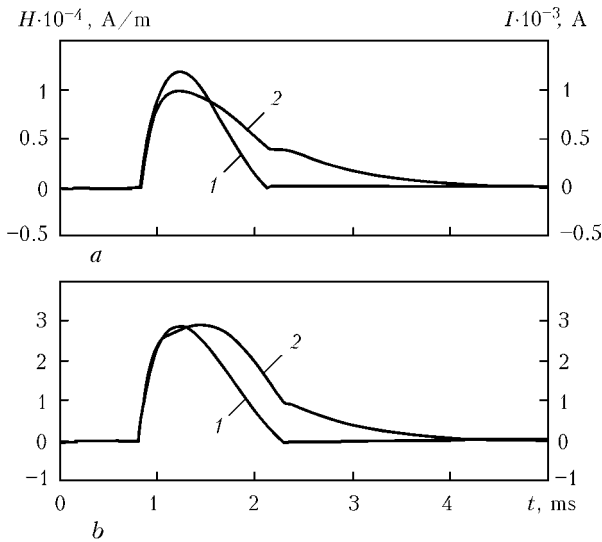
Figure 6. Amplitude values of pulsed current I (*1*) and magnetic field intensity H (*2*) at charging voltage of 200 (*a*) and 500 (*b*) V

tensity H from 8 up to 16,000 A/m. Amplitude values of pulsed current were recorded using Rogowski's belt by a procedure described in [4]. Three ranges of MF frequency were studied at capacitor storage discharge, namely: 0–5, 50–1000 and 1000–10,000 Hz. Values of charging voltage of capacitor energy storage, at which MF intensity H was measured, were taken to be equal to 200 and 500 V, that ensures the charge energy of 300 and 800 J, respectively, and is close to EDT parameters, used at treatment of AEIC repair welds. Hall sensor was fastened on inductor outer surface in the zone of operator hand location that allowed studying the parameters of horizontal and vertical components H of magnetic flux at EDT. Recording H values was conducted during an isolated discharge of capacitor storage through an inductor mounted on a welded joint sample (Figure 5).

Values of pulsed current I and vertical component of intensity H of pulsed MF at EDT with charging voltage of 200 and 500 V are shown in Figure 6. It should be noted that the ratio of intensity H values in the vertical and horizontal planes is equal to 10/1 that allows ignoring the latter at calculation of MF characteristics.

It is found that amplitude values I at $U = 200$ and 500 V are equal to 1200 and 3000 A, respec-

tively, and the time of current running does not exceed 1.4 ms (see Figure 6, curves *1*). Amplitude H values at similar U values are equal to 10,000 and 30,000 A/m, respectively, and time of MF impact is equal to 2.2 ms (Figure 6, curves *2*). It should be noted that comparison of curves *1* and *2*, reflecting the ratio of values of pulsed current and MF intensity during the current discharge shows that at I attenuation to zero values residual magnetic flux was recorded in the measured zone, the period of action of which is equal to 0.75–0.90 ms. At the moment of I achieving zero values, intensity H of residual MF at $U = 200$ and 500 V was equal to 4000 and 10,000 A/m, respectively. Presence of MF after current action in the discharge circuit is over, is attributable to residual magnetization of flat inductor, as well as running of attenuating current in a disc from non-ferromagnetic material, incorporated into the working tool.

Proceeding from the obtained data, calculation-based estimate of relative energy load (REL) in the studied spectrum of MF frequencies was performed by the following procedure [5]:

$$REL = \frac{H_m}{LPL}, \qquad (1)$$

where H_m is the MF intensity, A/m (Hall sensor readings); LPL are the data from standard DSN 3.3.6.096–2002.

Time of operator working t_{op} was assigned as an 8-hour shift, which is equal to 28,800 s. Full period of action t_d of pulsed MF, as shown in Figure 6, *a*, was equal to 2.2 ms for all the studied values of charging voltage.

Admissible values of operator exposure t_{adm} and number of tool switching on operations n_{adm} in the studied MF were calculated by the following procedure [5]:

$$t_{adm} = \frac{t_{op}}{2\sum REL}, \qquad (2)$$

$$n_{adm} = \frac{t_{adm}}{t_d}. \qquad (3)$$

Data of calculation of MF parameters, given in Table 2, lead to the conclusion that at charging voltage of up to 200 V, EDT operator can perform not more than 1100 actions of thermodynamic impact per a work shift, and at 500 V voltage — not more than 100.

The number of electrodynamic impacts per one item does not exceed 20–30 discharges. Thus, production cycle of AEIC reconditioning, including EDT, provides safe working conditions for EDT operators under the condition of charging the capacitor storage up to maximum voltage value of 500 V.

Table 2. Spectral composition and relative energy load of MF at AEIC EDT (discharge time $t_d = 0.0022$ s)

Charging voltage U, V	MF REL			Admissible discharge time t_{adm}, s	Admissible discharge number n_{adm}
	Frequency range, Hz				
	0–5	50–1000	1000–10000		
200	0.64	4197	1705	2.45	1100
500	8.35	51968	13426	0.22	100

CONCLUSIONS

1. Technology of repair welding of damage in AEIC from magnesium alloy ML10 was developed, including EDT of welds to lower the level of residual welding stresses.

2. By the results of EDT of full-scale AEIC fragments with characteristic damage of the item reconditioned by repair welding, it is established that EDT allows eliminating residual stresses in the weld.

3. Experimental procedure was developed, on the basis of which the influence of charging voltage on magnetic field intensity at EDT of welded joints of magnesium alloy ML10 was studied.

4. It is established that at up to 200 V charging voltage EDT operator can perform not more than 1100 actions of electrodynamic impact per a working shift, and at the voltage of 500 V — not more than 100, that supports the production cycle of repair welding of AEIC from magnesium alloy ML10.

1. Stepanov, G.V., Babutsky, A.I. (2007) Modeling of stress relaxation under action of pulsed electric current of high density. *Problemy Prochnosti*, **2**, 113–120.
2. Antonov, Yu.A., Ragozin, Yu.I. (2001) Pulse method of residual stress relieving. *Fizika i Khimiya Obrab. Materialov*, **3**, 91–95.
3. Lobanov, L.M., Pashchin, N.A., Loginov, V.P. et al. (2007) Change of the stress-strain state of welded joints of aluminium alloy AMg6 after electrodynamic treatment. *The Paton Welding J.*, **6**, 7–14.
4. Lobanov, L.M., Pashchin, N.A., Cherkashin, A.V. et al. (2012) Efficiency of electrodynamic treatment of aluminium alloy AMg6 and its welded joints. *Ibid.*, **1**, 2–6.
5. Levchenko, O.G. (2010) *Occupational safety and health in welding engineering*. Kiev: Osnova.

PROCEDURE FOR CALCULATION OF DIMENSIONS OF NOZZLES IN WELDING USING TWO SEPARATE GAS JETS

V.M. BELOKON and **A.O. KOROTEEV**

State Institution of Higher Professional Education «Belarusian-Russian University», Mogilyov, Republic of Belarus

Advantages of the process of welding without short-circuiting with double gas shielding of the arcing zone are shown. The arc is shielded by argon, and the weld pool — by carbon dioxide gas, fed through two concentrically located nozzles. Calculation of arc radius in its largest cross-section was performed. Calculation of weld pool length allows determination of the diameter of nozzle for carbon dioxide feed. Application of higher welding parameters requires increasing the diameter of nozzles, which can be calculated by similar procedures.

Keywords: *arc welding, consumable electrode, shielding gases, separate jets, dimensions of nozzles, calculation procedure*

Gas shielded welding finds wide application in production of various structures. At that CO_2 welding or welding in its mixtures with oxygen, argon etc. are often preferred. Welding without short-circuiting with double gas shielding, i.e. welding arc is shielded by Ar and weld metal by CO_2 is presented to be promising method. This method allows significantly reducing losses for electrode metal spattering, expenses for cleaning of near-weld zone from spatters and shielding gas costs [1–4].

Main parameters of each jet of shielding gas were experimentally determined by a number of domestic and foreign researchers and recommendations were provided for selection of dimensions of welding torch nozzles [5 et al.].

The aim of the present work is a development of procedure for calculation and determination of dimensions of nozzles (for Ar and CO_2) in reversed polarity current welding with two radial jets of shielding gases.

An electric arc consisting of three areas (anode, cathode and column) is used as a power source in consumable electrode welding. The anode and cathode areas have small dimensions. Anode spot in Ar welding can cover the whole end surface of the electrode and transfer to its side surface. At that transfer of electrode metal takes place in a form of small drops or jet that has positive effect on process of the electrode metal transfer, reducing spattering and splashing.

Argon shield of the cathode and anode areas, as well as arc column, can provide welding process, connected with positive effect of arcing in argon in welding with two concentric gas flows.

Putting of arc column to homogeneous channel with uniformly distributed within it tempera-
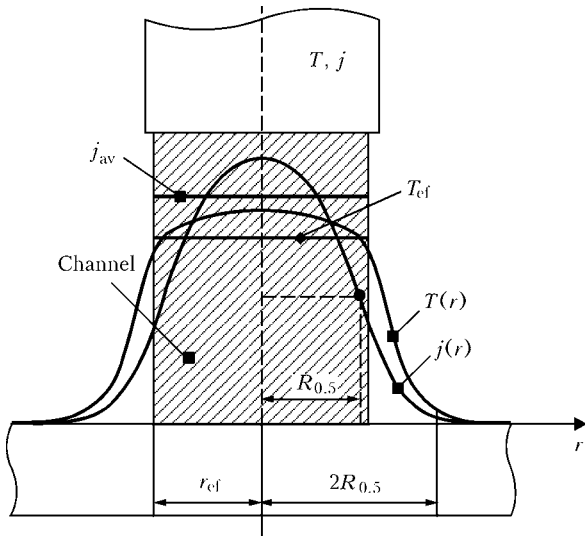
Figure 1. Scheme of «channel» model of arc column: r_{ef} — arc effective radius; j_{av} — average density of arc current; T — average effective temperature of arc; $R_{0.5}$ — conventional radius of arc column

ture and current is a reasonable idealization being sufficiently close to practice and does not violating the main physical representations in series of assumptions, considering that welding arc burns in iron vapors (in steel welding). Figure 1 shows the accepted scheme known as «channel» model of arc column [6, 7]. According to this model an average current density in the arc is distributed along the section with effective radius r_{ef}.

The average current density based on «channel» model is determined on formula

$$j_{av} = 5.5 \cdot 10^{-8} \frac{U_i^{38/12} a^{2/3}}{g_e^{2/3} I_a^{1/3}}, \qquad (1)$$

where $U_i = 7.87$ V is the ionization potential of metal vapors; a is the ratio of static weights of ions and atoms of iron vapors ($a^2 = 12/5$); $g_e = 35 \cdot 10^{-20}$ m^2 is the section of collision of atoms with electrons in Ar welding; I_a is the welding arc current, A.

Effective radius of arc column

r_{ef}; R, mm
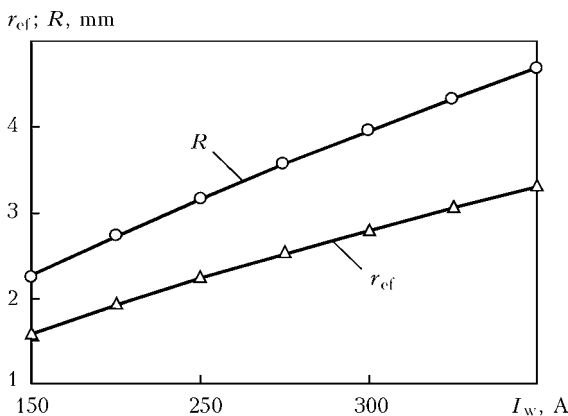
Figure 2. Dependence of effective r_{ef} and actual R radiuses of arc column on welding current

Table 1. Width of weld and active zone in welding using 1.2 mm diameter wire

Welding current, A	Arc voltage, V	Weld width, mm	Active zone width, mm	Dimension of active zone 2R acc. formula (5), mm
250	27	7.33	5.62	6.30
300	30	8.47	6.49	7.12
350	35	9.88	7.57	7.89
400	38	11.01	8.43	8.63

$$r_{ef} = \frac{\sqrt{I_a}}{\pi j_{av}} = \frac{2.4 \cdot 10^3 I_a^{2/3} g_e^{1/3}}{U^{19/12} a^{1/3}}. \qquad (2)$$

The whole arc current according to «channel» model passes through section with radius R determined on formula

$$R = 2R_{0.5}, \qquad (3)$$

where $R_{0.5}$ is the conventional arc radius related with effective radius by relationship

$$r_{ef} = 1.4 R_{0.5}. \qquad (4)$$

The next will be obtained solving simultaneously expressions (2)–(4):

$$R = \frac{3.4 \cdot 10^3 \, I_a^{2/3} \, g_e^{1/3}}{U^{19/12} a^{1/3}}. \qquad (5)$$

The results of calculation of effective and actual radius of the arc column depending on welding current intensity, represented in Figure 2, show that an internal nozzle feeding argon jet of around 9 mm diameter ($R = 4.5$ mm) is sufficient for complete shielding of welding arc from ambient environment by argon using normal welding modes (up to 450 A). The diameter of nozzle should be increased for welding modes of ≥450 A.

Shielding of welding arc only is obviously not enough for obtaining of quality weld. Shield of a surface of weld pool molten metal from interaction with atmosphere is necessary to be provided.

Table 2. Width of weld and active zone in welding using 1.6 mm diameter wire

Welding current, A	Arc voltage, V	Weld width, mm	Active zone width, mm	Dimension of active zone 2R acc. formula (5), mm
250	28	7.46	5.72	6.30
300	31	8.60	6.59	7.12
350	33	9.60	7.35	7.89
400	35	10.55	8.10	8.63
450	37	11.51	8.83	9.33
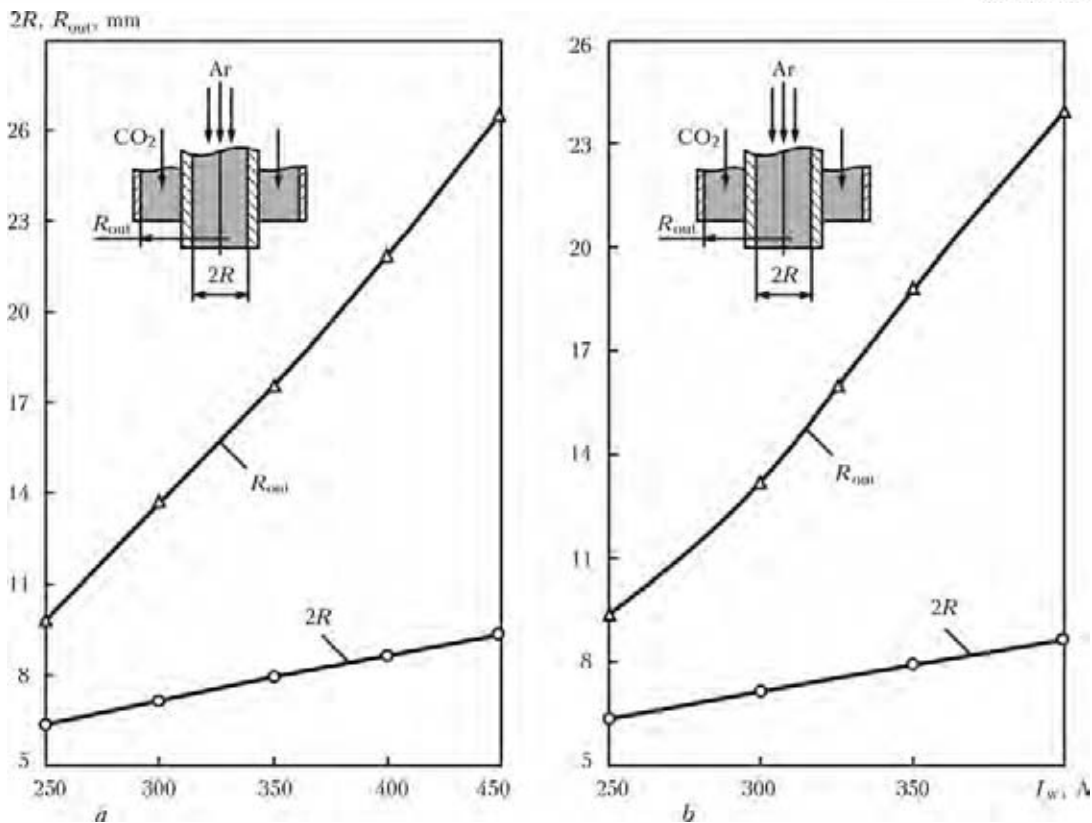
Figure 3. Dependence of dimensions of torch nozzles on welding current in welding using 1.2 (*a*) and 1.6 (*b*) mm diameter wire

The weld pool consists of specific zones. A central zone includes a head part of the weld pool and part of a tail. Cross-section of the central active zone, based on some sources, coincides with weld width [8]. In fact it is somewhat smaller.

Weld width can be determined on the following formula [9, 10]:

$$b = 2\sqrt{\frac{2q}{\pi e c \gamma v_\mathrm{w} T}},\qquad(6)$$

where $q = \eta I_\mathrm{a} U_\mathrm{a}$ is the effective heat power of arc; U_a is the arc voltage, V; $\eta = 0.8$ is the efficiency; $c\gamma = 4.8\ \mathrm{J/(cm^3 \cdot K)}$ is the volumetric heat capacity; v_w is the welding speed, m/h; T is the steel melting temperature, K.

Formula (6) can also be used for calculation of cross dimension of the weld pool active zone. For this temperature equal to metal evaporation

temperature should be assumed in this formula. Calculation results show that the dimension of active zone virtually coincides with the actual dimension of arc column section, calculated on formula (5), through which all the arc current passes. Deviation makes not more than 5–10 %. Tables 1 and 2 show the results of calculation of the weld width and cross dimension of the weld pool active zone.

Weld pool length is determined on formula [10]

$$L = \frac{q}{2\pi\lambda T},\qquad(7)$$

where $\lambda = 47\ \mathrm{W/(m \cdot K)}$ is the coefficient of heat conductivity of steel.

Radius of outer nozzle for CO_2 feed, considering shield of surface of the weld pool from

Table 3. Results of calculation of weld pool length and radius of outer nozzle in welding using 1.2 mm diameter wire

Welding current, A	Arc voltage, V	Length of weld pool, mm	Radius of outer nozzle acc. formula (8), mm
250	27	13.07	9.40
300	30	17.43	13.20
350	35	23.73	18.79
400	38	29.44	23.94

Table 4. Results of calculation of weld pool length and radius of outer nozzle in welding using 1.6 mm diameter wire

Welding current, A	Arc voltage, V	Length of weld pool, mm	Radius of outer nozzle acc. formula (8), mm
250	28	13.56	9.82
300	31	18.01	13.71
350	33	22.37	17.58
400	35	27.12	21.84
450	37	32.25	26.50

interaction with atmosphere, can be calculated using formula

$$R_{out} = L - b/2. \qquad (8)$$

Results of calculations are summarized in Tables 3 and 4.

Formula calculations show that application of 20 mm radius nozzles is enough for arcs with up to 350 A welding current and 1.2 and 1.6 mm diameter wires. Radius of the nozzle for outer gas jet should be larger in the case of welding with higher currents. The outer nozzle for the purpose of economy of shielding gas can be made in ellipse form, the cross dimension of which equals the weld pool and the longitudinal dimention equals its length.

The next sequence of calculation is proposed for welding torch nozzles: calculation of average current density in the arc column; determination of effective and actual radiuses of the welding arc; after that using values of these parameters determination of diameter of nozzle for argon feed (see Figure 2) and dimensions of the weld pool; determination of diameter of outer nozzle for CO_2 feed (Figure 3) considering the dimensions of active zone. Diameter of the outer nozzle can be reduced considering spreading of shielding gas flow in welding of flat joints [11].

Diagrams, shown in Figure 3, simplify the processes of practical fulfillment of the proposed procedure.

Analysis and calculations performed allowed determining the optimum relationship of shielding gases which should make 1:4, i.e. 20 % Ar and 80 % CO_2, from the general necessary consumption.

Primitive technical and economic calculations show that welding with two separate gas jets can be applied not only to special materials, but to low-alloyed as well as low-carbon steels. Economy only of electrode metal at that makes 20−95 kg per 1 t of wire that is character for pure argon welding without short-circuiting and it covers an insignificant increase of shielding gas

consumption in comparison with CO_2 welding, welding with double and triple mixtures. Five time reduction of argon consumption is observed in comparison with pure argon welding.

CONCLUSIONS

1. Sequence and procedure for calculation of diameter of welding torch nozzle in welding with two separate jets of shielding gas is proposed. The optimum ratio of Ar and CO_2 in general consumption of shielding gas makes 1:4, i.e. Ar + + 80 % CO_2.

2. Calculation of diameter of nozzles for argon feed based on «channel» arc model was carried out, and calculation of dimensions of nozzles for CO_2 feed was performed considering the weld pool dimensions. It was determined that internal nozzle feeding argon jet of around 9 mm diameter is enough for welding in normal modes (up to 450 A).

1. Laevsky, V.S., Dyurgerov, N.G., Lenivkin, V.A. et al. (1969) Consumable electrode welding of low-carbon steels in combined shielding. *Svarochn. Proizvodstvo*, **10**, 21−22.
2. Potapievsky, A.G. (1973) *Consumable-electrode gas-shielded welding*. Moscow: Mashinostroenie.
3. Paton, B.E. (1974) *Technology of fusion arc welding of metals and alloys*. Moscow: Mashinostroenie.
4. Malyshev, B.D., Akulov, A.I., Alekseev, E.K. et al. (1989) *Welding and cutting in industrial engineering*. Ed. by B.D. Malyshev. Vol. 1. Moscow: Strojizdat.
5. Fedko, V.T., Kiyanov, S.S., Shmatchenko, V.S. et al. (2003) Application of double-jet nozzles for gas-shielded welding. *Avtomatizatsiya i Sovr. Tekhnologii*, **3**, 12−18.
6. Leskov, G.I. (1971) *Welding electric arc*. Moscow: Mashinostroenie.
7. Pavlyuk, S.K., Belokon, V.M. (1974) About stability of arc ignition process in consumable electrode welding. *Svarochn. Proizvodstvo*, **4**, 51−53.
8. Erokhin, A.A. (1973) *Principles of fusion welding*. Moscow: Mashinostroenie.
9. Akulov, A.I., Belchuk, G.A., Demyantsevich, V.P. (1977) *Technology and equipment for fusion welding*. Moscow: Mashinostroenie.
10. Petrov, G.A., Tumarev, A.S. (1967) *Theory of welding processes*. Moscow: Vysshaya Shkola.
11. Popravka, D.L., Khvorostov, N.E., Proskurin, V.N. (1973) Some principles of flow of shielded gas jet. *Svarochn. Proizvodstvo*, **6**, 33−36.

BRAZE-WELDING WITH WELD METAL PEENING DURING ITS SOLIDIFICATION

A.S. PISMENNY, I.V. PENTEGOV, V.M. KISLITSYN, E.P. STEMKOVSKY and **D.A. SHEJKOVSKY**

E.O. Paton Electric Welding Institute, NASU, Kiev, Ukraine

Advantages of the process of braze-welding of zinc-plated steel, including impact peening of metal in the joint zone at metal cooling stage, are considered in comparison with the widely accepted process of brazing by copper-based filler metals with arc heating.

Keywords: *resistance spot welding, braze-welding, peening, explosion compression mechanism, joint strength*

At present the process of brazing by Cu-based filler metals with arc heating became widely accepted for joining sheet Zn-plated steel. Selection of this variant of the joint is due, unfortunately, not to the desire to achieve a high quality of the joint, but to a possibility of improvement of process efficiency using currently available equipment for automatic or semi-automatic arc welding in the atmosphere of active shielding gases [1].

Main difficulties in welding Zn-plated steel are caused by that zinc starts evaporating much earlier than base metal melting temperature. Because of appearance of zinc vapours over the weld pool, electric arc loses its stability that promotes appearance of weld porosity, undercuts and other defects.

In this connection, in arc welding of Zn-plated steel the mode of heating with lower heat input is used, and Cu-based alloys, for instance of CuSn6P, CuSi3, CuSi2Mn, CuSi3 composition, are applied as filler wire [1, 2].

As in case of application of the above filler materials it is possible to avoid base metal melting, joints of this kind can be included into the category of brazed joints, even though in this process the fluxes, which are compulsory for conducting the process of brazing in an uncontrolled atmosphere, are not used. Here, the arc is a heat source, comparable in its intensity with the heat evolved, for instance, at flame heating.

Unfortunately shielding gasses (argon, helium) used in arc welding do not provide the necessary degree of wetting and spreading of Cu-based filler metal over Zn-plated steel surface. This circumstance leads to appearance of undercuts in the joint zone, and promotes initiation of microcracks lowering the joint strength at its operation under the conditions of cyclic load application.

In view of such shortcomings of the process of brazing Zn-plated steel with arc heating, the question of selection of an optimum variant comes up, which would provide not only high efficiency of the technological process, but also high quality of the joint.

One of the promising variants of producing joints of coated metals is braze-welding, which is a unique method to produce joints of similar- and dissimilar metallic and nonmetallic materials. A significant difference of braze-welding from other joining methods is preliminary addition of low-melting (compared to materials being joined) interlayer between the materials being joined or its formation during heating. In the case of joining Zn-plated steel, such an interlayer is the zinc coating which melts at the temperature much lower than that of steel melting.

In addition, braze-welding process is characterized by application of single or multiple compression force (peening), required for removal of the greater part of low-melting interlayer from the joint zone, that greatly increases joint strength.

Attempts to apply metal peening at the final stage of the welding process to improve welded joint strength were realized, for instance, in the units for resistance spot welding of metal [3, 4].

This variant became applied in welding of metals prone to formation of cracks, looseness and pores, in order to improve the fatigue strength of welded joints. However, in practice this kind of «peening» did not lead to any noticeable increase of joint strength, because of the low speed of compression force application, caused by the use of a pneumatic drive of displacement of mobile welding electrode and inertia of its suspension assembly. As a result, instead of high-speed peening the weld spot metal was exposed to static compression force.

Delaying of the moment of peening force impact on the weld spot metal at temperature below

the points of structural transformations of treated metal crystalline lattice, for instance, point A_{c1}, did not lead to any significant deformation of weld spot metal or development of mechanical compressive stresses in the near-weld zone. In addition, application of peening force to solidified metal did not promote removal of the greater part of low-melting interlayer from the joint zone, particularly, in braze-welding processes that might have essentially improved the joint strength.

Improvement of the effectiveness of peening of welded or brazed joint metal turned out to be possible due to an abrupt increase of the speed of compressive force application. Results of the conducted comparative studies of the produced joint strength show the obvious advantages of impact application of the compressive force, compared to the strength of joints, produced at application of static compressive force [5].

Impact peening of metal in the joint zone, conducted at its solidification stage, leads to development of several technologically important phenomena, promoting an improvement of welded joint strength.

The features of this variant of thermomechanical treatment of metal in braze-welding or welding processes include development of mechanical compressive stresses, both in the connecting weld metal, and in the HAZ, which are preserved in the process of further cooling of the metals being joined. In addition to that, improvement of welded joint strength is further promoted by the processes of refinement of metal crystalline structure in the joint zone caused by high-speed deformation at higher temperature.

Results of technological studies described in [5] were obtained at application of an electromagnetic drive of the system of compressive force impact. However, inertia of the mobile part (suspension) of welding electrode limited the speed of compressive force application on the level of 300 m/s [6].

The assumption of a good potential for increasing the upsetting speed in the processes of resistance spot welding or braze-welding is based mainly on the experience of forge welding with indirect heating of the metals being joined. Moreover, an abrupt increase of the compressive force speed, in all probability, should inevitably be accompanied by appearance of new technological effects.

Speed of compressive force application can be increased by using an explosion of hydrogen-oxygen mixtures, in which the velocity of propagation of the shock wave front reaches 3000 m/s [7]. Even higher speeds (up to 6000 m/s) can be achieved at application of the electrohydraulic effect [8].

This work presents a variant of the process of resistance spot braze-welding with application of a compressive force on weld metal, which is created as a result of an explosion of hydrogen-oxygen mixtures of a stoichiometric composition, produced by electrolysis of water in portable gas generators. For instance, a generator of P-105 type which was developed by PWI for flame brazing and welding of small-sized products provides the efficiency of hydrogen-oxygen mixture of up to 350 l/h at up to 0.07 MPa excess pressure.

Schematic of explosive drive of displacement of electrode assembly of the unit for spot braze-welding, which does not differ so much from the known schematics of the units using peening, is given in Figure 1. As shown in the Figure, the hydrogen-oxygen mixture is generated in electrolyzer *1* and comes to the electrode assembly through electropneumatic valve *2*, which is switched on by controller *3*. The latter ensures switching on the heating current, regulation of the number of alternating current pulses, time of delay of electropneumatic valve switching on after completion of a series of current pulses for heating the samples being joined, switching on generator *4* of high-voltage pulses applied to the device for firing the combustible mixture *5*. Electrode component is made in the form of cylinder *6*, the lower part of which accommodates bellows *7* with the assembly for fastening replaceable welding electrode *8* and drainage hole for discharging the combustion products *9*.
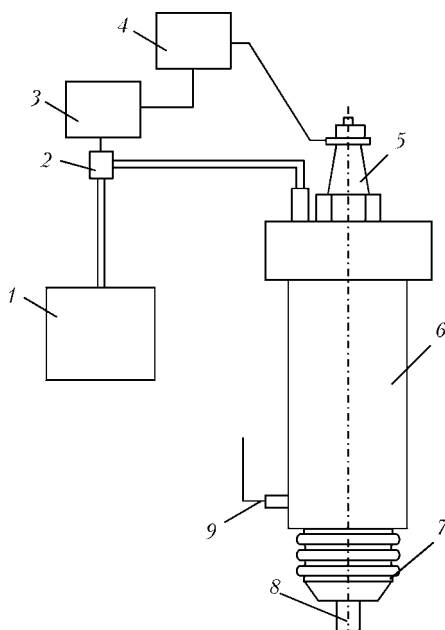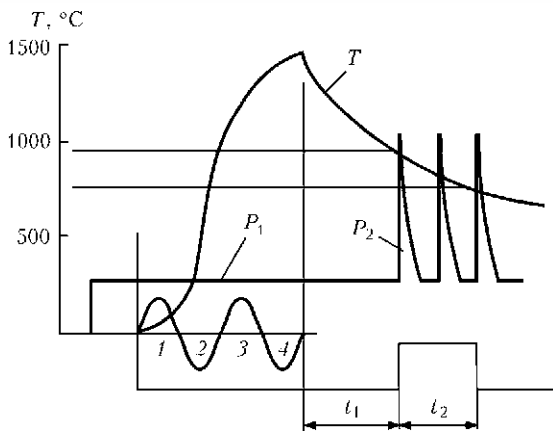

Figure 1. Schematic of the drive of electrode assembly for spot braze-welding (for *1–9* see the text)

Figure 2. Cyclogram of the process of braze-welding with impact application of the peening force

Figure 3. Welding head with explosion type mechanism of impact treatment of the weld

The assembly of fastening the welding electrode is made on the basis of bellows, the corrugations of which close completely at the initial moment to ensure the preliminary compressive force, but allow additional displacement of welding electrode in the vertical direction under the impact of pressure pulse formed in the explosion chamber at firing of the combustible mixture.

Process cyclogram (Figure 2) shows the sequence of impact of the following technological parameters: application of compressive force (preliminary P_1 and impact action P_2); curve of temperature rise in the joint zone when going through four half-cycles (1–4) of heating current; time interval of delay of the impact of compressive force t_1 and moment of application of high voltage to the firing device of the system of electrode suspension with an explosion drive of electrode assembly of the unit for spot braze-welding (in this case a unit pulse of peening force application is implemented) or with an electromagnetic drive, providing the impact of several pulses of the peening force.

As is seen from the cyclogram, after creating a preliminary compressive force in the joint zone, the electropneumatic valve connecting the gas volume of electrolyzer with the explosion chamber operates at switching on the heating current. Blowing of explosion chamber volume through the drainage hole is performed, with its subsequent filling with the combustible mixture. After disconnection of explosion chamber volume from the electrolyzer volume the controller ensures connection of electric circuit of power source of combustible mixture firing system. Drainage hole remains open after blowing of explosion chamber volume, as it was experimentally established that the small diameter of this hole (about 1 mm), high velocity of explosion wave propagation and short time interval between the moment of completion of explosion chamber filling and moment of application of the high-voltage pulse of mixture firing almost do not lower the effectiveness of the explosion wave.

Welding head with the mechanism of impact treatment of the weld of explosion type is shown in Figure 3.

Figure 4 gives a typical oscillogram of arrangement of welding current pulses (four half-cycles in this case) and pulses of current, ensuring firing of the combustible mixture.

Signal for firing the combustible mixture comes from the controller of welding circuit power unit after counting the time of delaying the time interval from the moment of completion of welding current pulse, set by the operator. This completes the cycle of welding an individual spot and it is repeated many times in this sequence at process realization, similar to the process of resistance seam brazing.

Technological studies of the process of braze-welding with explosive application of unsetting force were performed using samples of Zn-coated St3 steel 0.3 mm thick. Process of braze-welding was conducted in a laboratory unit for resistance
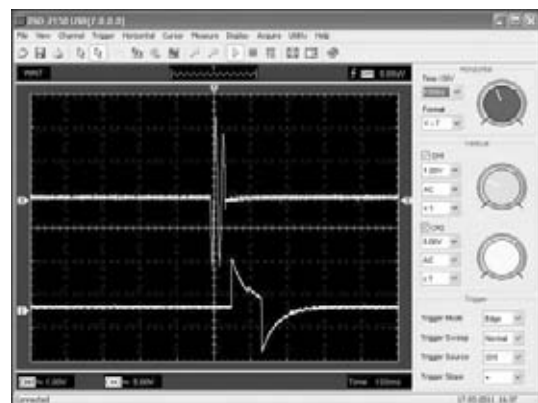
Figure 4. Oscillogram of welding current pulses and current pulses in the circuit of explosive application of the compressive force
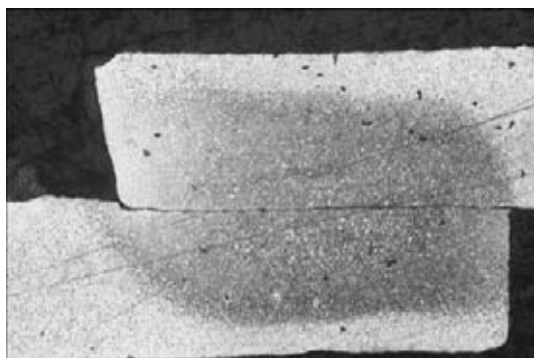
Figure 5. Typical macrosection (×50) of brazed joint with impact peening of the joint zone

Figure 6. Macrosection (×50) of braze-welded joint across the section near the joint center

spot welding, in which the upper electrode holder supported the electrode assembly with an explosion upset drive.

Results of technological experiments show the ability to preserve the continuity of zinc coating in the zone of contact of the sheets being joined with welding electrodes due to lowering of the level of heat evolution on transient resistances and intensive heat removal from this zone into forcibly cooled electrodes, ensuring the compressive force in braze-welding zone.

Impact action of pressure at the stage of metal solidification in the joint zone promotes an abrupt increase of heat removal from the surface layers of the metals being joined, which were subjected to peening, thus leading to narrowing of the HAZ.

As is seen from the photograph of macrosection of brazed joint with zinc coating (Figure 5), dimensions of HAZ can be essentially reduced even at joining sheets of greater thickness (0.4 mm).

One of the features of braze-welding process with impact upsetting in some cases is an almost complete ousting of the low-temperature interlayer at minimum thinning of the joined sheets in the zone of Zn-plated sheet joint (Figures 5 and 6).

As shown by experimental results, the effectiveness of impact application of upsetting force can be realized not only at heating by electric current, but also for other variants of joint zone heating, for instance, flame, microplasma and arc. Advantages of flame heating (hydrogen-oxygen mixtures) include high accuracy of the parameters, purity of gas mixture, and possibility of fine adjustment of the required thermal energy, applied to the joint zone (in the pulsed heating mode).

Possibility of application of indirect heating is the only technological variant allowing welding of nonmetallic materials to be performed.

In order to realize the variant of indirect heating of the parts being welded it is sufficient to fit the welding head with a plasmatron or flame torch. In this case the controller should ensure

a continuous sequence of commands for feeding a thermal energy pulse of specified value to the heating zone and impact treatment of the joint zone. In the future transition from pulsed heating to continuous heating is possible, which can be controlled by selection of heating source power, speed of welding head displacement, and distance between indirect heating source and joint zone.

CONCLUSIONS

1. Impact peening of metal during spot braze-welding of Zn-coated sheet steel is not only the most acceptable, but also the only, in our opinion, variant of producing the joints, the good prospects of which are proved by the possibility of preservation of the initial coating layer after heating of the sheets being joined above zinc melting point and improvement of corrosion resistance of the joints in service due to elimination of copper and its alloys from the joint zone.

2. Impact application of the compressive force during welding at the stage of metal cooling in the joint zone promotes an increase of braze-welded joint strength due to refinement of metal structure, and lowering of the probability of defect development in the joint zone, particularly, pores, cracks, and gas inclusions.

1. (2010) Arc brazing of galvanized sheets. *Welding and Cutting*, 9(1), 20.
2. (2010) Investigations into the material failure of resistance weld spots on ultrahigh-strength steels. *Ibid.*, 9(3), 167–173.
3. (2000) *Equipment for resistance welding*: Refer. Book. Ed. by V.V. Smirnov. St.-Petersburg: Energoatomizdat.
4. Moravsky, V.E., Vorona, D.S. (1985) *Technology and equipment for spot and projection capacitor-discharge welding*. Kiev: Naukova Dumka.
5. Pismenny, A.S., Kislitsyn, V.M. (2010) Influence of weld metal impact treatment on welded joint strength. *The Paton Welding J.*, **1**, 38–40.
6. Pismenny, A.S., Pentegov, I.V., Kislitsyn, V.M. et al. (2011) Devices for impact treatment of the weld in the process of resistance spot welding. *Ibid.*, **1**, 45–47.
7. (1973) *New technological processes in precise instrument engineering*. Ed. by R. Zeviga. Moscow: Energiya.
8. Yutkin, L.A. (1955) *Electrohydraulic effect*. Leningrad: Mashgiz.

COMPARATIVE ANALYSIS OF ISO 18841:2005 STANDARD AND RF 26389−84 STANDARD ON EVALUATION TO HOT CRACK RESISTANCE IN WELDING

B.F. YAKUSHIN

N.E. Bauman Moscow State Technical University, Moscow, Russian Federation

Differences between the EU standard on tests to hot crack resistance in welding and standard 26389−84 in force in the Russian Federation are considered, and specific variants for their harmonization to quantitative evaluation of the sensitivity of steels and welding consumables to hot cracking are suggested.

Keywords: *arc welding, hot cracks, brittleness temperature range, ductility margin, crack physical simulation, critical rate of deformation, technological and machine methods of testing, EU and RF standards*

The first standard of such designation GOST 26389−84 was developed at Welding Faculty of the N.E. Bauman Moscow State Technical University with the assistance of author. Monograph of Prof. N.N. Prokhorov and works of other researchers studying the problems of hot crack (HC) resistance, the results of which were widely discussed during two meetings on problem of HC formation in the welds, castings and ingots in 1958 and 1962 [1], became a theoretical basis of this standard.

As a result, a theory of production strength of metals during solidification in welding was stated. Based on this theory, the HC appear in the alloys under effect of welding stresses in a brittleness temperature range (BTR) as a result of exhausting of ductility margin δ_{BTR} in a period of solid-liquid state t_{BTR}. Possibility of HC formation is determined by ratio of three main factors: BTR, minimum ductility δ_{min} of metal in the BTR, and intensity of deformation rise in the BTR, depending on rigidity of welded structure. If accumulated deformation ε_i exceeds current value $\delta_i(T)_{min}$ (Figure 1) in the BTR limits the HC will appear.

Critical tension speed V_{cr}, equal δ / t_{BTR} ratio, was taken as an index of weld metal HC resistance for specific welding mode, and at comparison of modes [2] critical tension rate B_{cr}, equal δ_{min} / BTR, at which HC formation is possible, was considered. These indices are to be determined by means of increase of deformation rate of welded samples from studied alloys up to HC appearance.

There are two variants of determination of V_{cr} and B_{cr} in GOST 26388−84:

• technological methods, i.e. by means of welding of the samples under conditions of increase of rigidity (thickness, level of fastening, mode of welding up to HC formation);

• machine methods, i.e. by means of increase of deformation intensity of weld being solidified using testing machine.

Testing machines of three types, i.e. LTP1-4, LTP1-6 and MIS, allowing tension or bending of small-dimension samples in welding with adjusted speed up to HC appearance [1], were developed at the Bauman MSTU for practical application. This provided a wide implementation of a testing technique at the E.O. Paton Electric Welding Institute, main research institutes, at plants, as well as abroad [3−5]. Effect of standard 26389−84 on the territory of the Russian Federation was reinstated since 2000.

ISO 17641 standard, developed by European Committee for Standardization (CEN) in collaboration with Technical Committee ISO/TC44 «Welding and related processes» in 2005, consists of preface and two independent parts. The preface of ISO 17641-1:2004 describes the methods of testing to HC resistance and areas of their application.

The first part of standard ISO 17641-2:2005 describes in details a test procedure applying welding of butt and tee samples of natural rigidity, and methods for testing of the welded samples with forced loading are characterized in the third part of ISO 17641-3:2005.

Its configuration corresponds with that of the RF standard. General favorable reception of standard ISO 17641 is given in work [5].

However, insignificant selectivity in comparative testing as well as inapplicability for testing of sheet samples of not less than 10 mm thickness should be noted proceeding from proposed production tests and types of welded joints of «natural» rigidity. Therefore, formation of HC is un-

likely in testing of modern quality electrodes of many grades and modes of testing do not reproduce welding conditions of more rigid structures to significant extent. Besides, limitation of dimensions on length of the tee joint with double-sided weld and gussets prevent performance of automatic welding and weld failure after welding for detection of cracks on fracture type. The process of result evaluation is extremely complicated and long due to manufacture and testing of special rod and plate samples from the welded joints. No data on thickness of metal to be welded and method of fastening, which eliminats deformation in welding, are provided by procedure of application of the sample with butt weld.

In contrast, the RF standard provides for possibility of wide variation of thickness of samples being welded, modes and methods of welding which make more effect on crack formation process in comparison with chemical composition change. The universal samples with butt and circumferential welds in sheet plane are as well represented for this in the RF standard together with rigid single-sided tee weld [6]. They allow changing a metal thickness (1–12 mm), diameter of circumferential weld, modes and methods of welding in a wide range and, thus, obtaining critical values at which formation of HC in sample welding is possible.

Change of width of plates to be welded in the sample with butt joint allows increasing high-temperature welding deformations up to the level
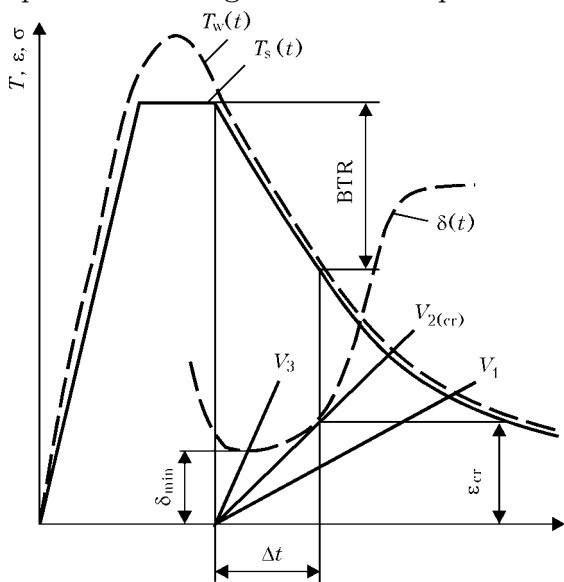
Figure 1. Scheme of weld and near-weld metal tests to HC resistance in welding by means of deformation growing developed using test machine: $T_w(t)$ — welding thermal cycle; $T_s(t)$ — simulation of thermal cycle; V_1–V_3 — growing of deformation in the BTR; V_{cr} — deformation resulting in crack formation; $\delta(t)$ — predicted character of ductility change in the BTR; $V_{cr} = \varepsilon_{cr}/\Delta t$ — critical rate of deformation

sufficient for obtaining of quantitative result of testing from weld metal of any composition (GOST 26389−84) that is very important for consumable selection.

The second part of standard ISO/TR 17641-3 is represented in a form of engineering report on tests with forced «loading» in welding and can be considered as its first project. It contains description of American procedures Varestraint, TransVarestraint, Gleeble, as well as PVR procedure developed in Austria [7].

A series of notes should be made on this document.

1. High-speed deformation by bending of solidifying weld metal on Varestraint and Trans-Varestraint procedures violates the principles of physical simulation in sample testing and conditions promoting failure in real welded structures. This note also refers to Gleeble procedure, in accordance to which speed of high-temperature tension of investigated samples in the BTR makes 0.15−0.25 m/s (6−10 inch/s) [7].

2. Evaluation of degree of deformation in mandrel bending on formula $\varepsilon = h/2R$ is suitable for homogeneous, i.e. isotropic material. However, solidifying metal in welding has double-phase structure and defomations are accumulated along the grain boundaries which is a reason for HC formation.

3. Evaluation to HC resistance in bending testing of the welded joint from thin-sheet metal, including pass, is impossible since the critical values are not achieved in mandrel bending.

4. Proposed criterion of total length of cracks L_{tot} does not consider ductility margin of metal in it being the main factor of crack formation.

5. Diffusion processes and high-temperature creep preparing conditions for HC nucleation are limited by a dynamic deformation of weld being solidified. Elimination of these processes in the dynamic deformation develops seeming increased HC resistance that can result in unpredicted failure of the welded structures.

It should be noted that as a rough approximation HC length can only characterize the BTR value in the dynamic deformation. Another factor, i.e. ductility margin δ_{BTR}, can not be evaluated by number of cracks and their length, therefore, L_{tot} does not considered to be a qualitative criterion of tendency to HC (see Figure 1).

Inter-grain ductility of metal in the BTR according to Gleeble procedure is proposed to be evaluated on degree of its change outside the BTR, i.e. in area of high-ductility weld metal condition that violate validity of tests [8].

Tests to HC, types of cracking and designation according to ISO 17641:2005 standard

Test type	Type of cracking	Results	Designation
Method of deformation along the weld axis	Solidification	L_{tot}	Base metal (selection and confirmation)
	Liquation	L_{tot}	Consumable (selection and confirmation) Welding procedure
	Ductility reduction	L_{tot}	
Method of deformation across the weld axis	Solidification	L_{tot}	Selection of consumable. Welding procedure
Tensile test of flat sample along the weld (PRV test)	Solidification	V_{cr}	Metal selection. Multipass welded joints. Welding procedure. Metal combination
	Liquation	V_{cr}	
	Ductility reduction	V_{cr}	Selection and confirmation of material
Tensile test in hot state (Gleeble™)	Solidification	BTR	
	Liquation	BTR	

The advantage of the RF standard is that $V_{cr} = \delta / t_{BTR}$ index can be evaluated using a method requiring no direct measurement of ductility of the weld metal and the BTR limits. At that, the sample is subjected to continuous, i.e. static, deformation in the temperature range from upper to lower limits of the BTR up to $0.5 T_{melt}$ temperature in the investigated section with weld being solidified.

At that, intergranular shifts are not accumulated in deformation out of the BTR. They appear only in the BTR that is the main advantage of static tension or bending in HC resistance tests.

Inclusion of procedure of static deformation (programmable deformation cracking PVR) procedure in project of ISO/TR 17641-3 standard is its positive moment. However, testing of PVR sample having deposited bead of large length results in heating and increase of length of the sample between the machine grips that distort predicted linear distribution of deformations along the sample.

Besides, a local concentration of deformations under the arc, to large extent machine v_m, is inevitable as a result local arc heating of the sample and reduction of metal resistance to deformation. Its level depends on thermophysical properties of steels and alloys being compared and duration of deformation can be smaller than the BTR time.

In the RF standard the similar tests to HC resistance, oriented along the weld axis («paling»), are carried out with growing tension speed within one series of the samples. This allows determining V_{cr} index and using it in selection of alloys and consumables.

Large number of mutually exclusive indices (Table) and absence of correlation coefficients between them should be noted at general evaluation of ISO 17641 standard. This provides a

necessity of purchase and operation of large number of testing machines.

One conditional index of HC resistance V_{cr} (mm/s) is regulated in RF standard. Comparison of its values is possible at equal speed w_{BTR} of metal cooling in the BTR. In other cases physical index B_{cr} (mm/°C) equal V_{cr} / w_{BTR} is determined. This index allows evaluating resistance of weld metal and near-weld zone to formation of longitudinal and transverse cracks in different welding methods [8].

New model of testing machine MIS (Figure 2) equipped with a fixture for static tension and bending of samples (Figure 3) in process of welding, welding head with possibility of movement along x, y and xy axes (circumferential weld) and fixture for electric contact heating and tension of the samples for evaluation of metal tendency to formation of HC in the near-weld zone

Figure 2. General view of machine MIS for HC testing on the RF standard: *1* — box for control of test parameters, their imaging and registration; *2* — manipulator of welding head for its movement along x, y and xy axes; *3* — force measure device; *4* — machine for welding of samples and their bending or tensile tests; *5* — machine for simulation of welding cycle in the samples and HC tests at cooling stage
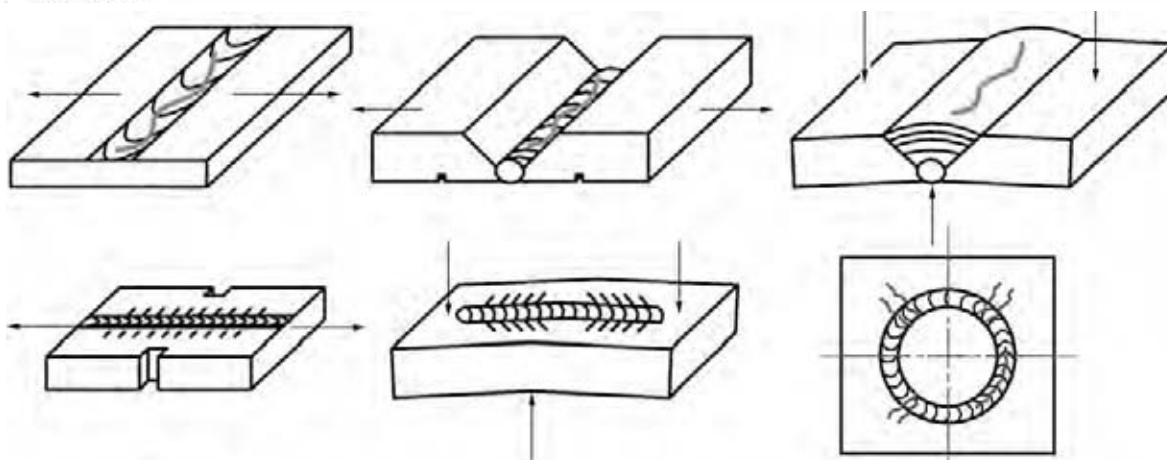
Figure 3. Types of samples applied for MIS machine testing

was designed for performance of metal tests to HC resistance. Presence of dynamometer in power mains and dilatometer allows applying MIS machines for testing of joints to cold crack resistance etc.

CONCLUSION

1. Theory of production strength is the basis of standard for quantitative evaluation of metal to HC resistance. In accordance to it the HCs are the result of exhaust of ductility margin in the BTR under effect of welding stresses and deformations.

2. Critical rate of deformation, determined based on a fact of exhaust of ductility of the samples with weld in the BTR at static machine deformation, is quantitative index of metal HC resistance.

3. Machine methods of evaluation of metal to HC resistance in testing of small dimension samples should provide the possibility of physical modelling of conditions resulting in HC formation at manufacture of real welded structures.

4. Machine tests on ISO/TR 17641-3 standard project using impact bending of the samples with weld (Varestraint and TransVarestraint) or impact rupture of the samples (Gleeble) do not have sufficient ground, since convective and diffusion processes, determining metal ductility in

the BTR, are not considered in determination of L_{tot} and high-temperature ductility dip (BTR) and not suitable for qualitative evaluation.

5. Technological tests of metal to HC resistance on GOST 26389−84 provide for application of samples with butt and tee welds as well as widely used [8] samples with circumferential weld of various thickness (1−20 mm) that guarantee their suitability for comparison of consumables and technological variants of welding and, thus, widening their versatility in comparison with samples of ISO 17641−2 standard.

1. (1991) *Welding and welded materials*: Refer. Book. Vol. 1: Weldability of materials. Ed. by E.L. Makarov. Moscow: Metallurgiya.
2. Yakushin, B.F. (1969) Assessment of technological strength depending on welding conditions. *Svarochn. Proizvodstvo*, **1**, 19−21.
3. Bernasovsky, P. (2005) *Contribution to HAZ liquation cracking of austenitic stainless steels. Phenomena in welds*. Berlin: Springer.
4. Zhelev, A. (1988) *Complex thermokinetic approach in assessment of hot cracks during welding*: Syn. of Thesis for Dr. of Techn. Sci. Degree. Sofia.
5. Wilken, K. (1999) Investigation to compare hot cracking tests. *IIW Doc. IX-1945−99*.
6. Tsarkov, V.A., Chuprak, A.I. (2010) Ways of harmonisation of national and European standards for assessment of metal resistance to hot cracking. *Svarka i Diagnostika*, **6**, 58−62.
7. Yakushin, B.F. (2003) Harmonisation of RF and EU standards on weldability tests. *Svarochn. Proizvodstvo*, **1**, 39−43.
8. Steklov, O.I. (1976) *Strength of welded structures in aggressive media*. Moscow: Mashinostroenie.

MULTICHANNEL MICROPROCESSOR CONTROLLER FOR DATA COLLECTION FROM THERMOCOUPLES

V.V. DOLINENKO, T.G. SKUBA, O.Yu. VASHCHENKO and **N.F. LUTSENKO**

E.O. Paton Electric Welding Institute, NASU, Kiev, Ukraine

Development of 9-channel microprocessor controller of the system of welding thermal cycle recording with digital interface for communication with PC of Ethernet-100Base-TX is presented. CAT and WRT type thermocouples are used as temperature sensors. Application of Internet-protocol of data exchange with PC of TELNET type allows designing automated system for research performance in the field of multipass welding at minimum cost.

Performance of experimental studies of mechanical properties of welds in critical structures involves application of expensive welding equipment and consumption of considerable material resources, such as welded samples metal, electrode wire, shielding gas, as well as power. Therefore, one of the main objectives at experiment performance is ensuring reliable recording of maximum possible scope of information to obtain the most complete idea of the nature of structural changes in the HAZ metal of the item being welded. Of considerable interest is the information on dynamics of variation of spatial temperature field in the welded item during performance of mutlipass arc welding. The most widely accepted in welding are contact methods of temperature measurement using chromel-alumel (CAT) and tungsten-rhenium (WRT) (VR5/VR20) thermocouples which allow measuring temperature in the item up to 1300 (CAT) and 2500 °C (WRT), respectively, with ±1 °C error.

At present use of corporate Internet network is an effective method of creating computerized systems for research performance. During applied research in the field of arc welding using Internet
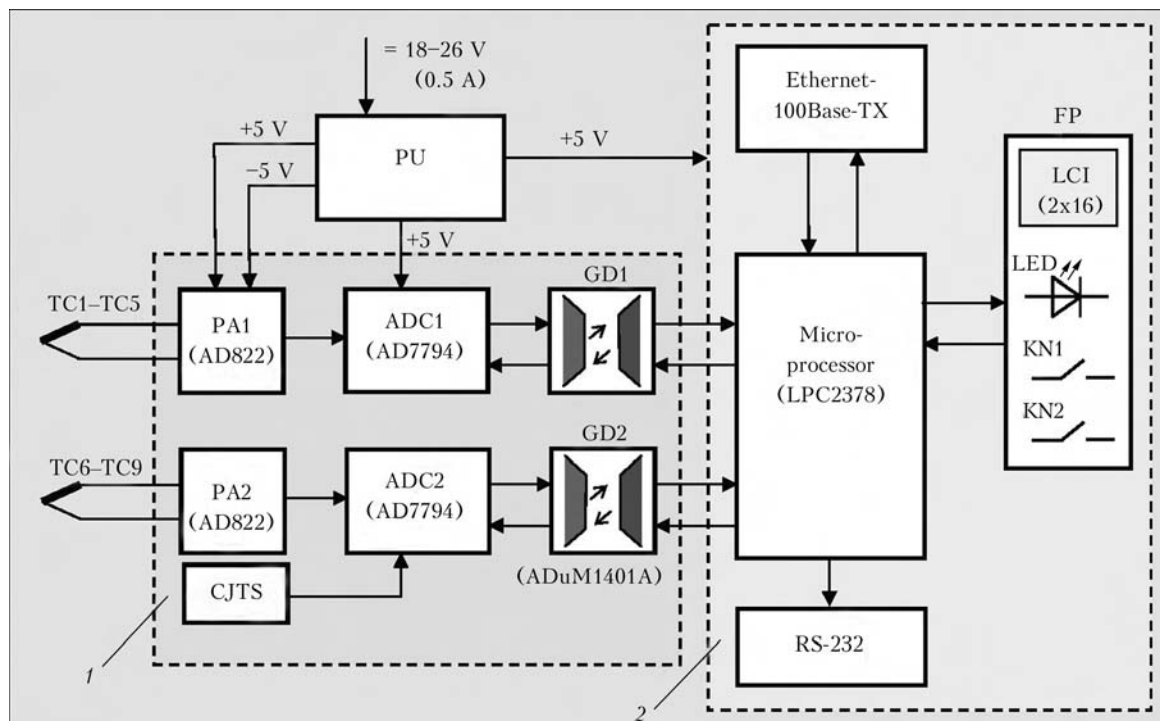
Figure 1. Block-diagram of MCRTC: *1* — analog module; *2* — digital module; PU — power unit; GD — galvanic decoupling; LCI — liquid-crystal indicator; KN1, KN2 — control buttons; FP — front control panel; PA — preamplifier; LED — light-emitting diode; TC — thermocouples; CJTS — sensor of «cold junction» temperature

T, °C
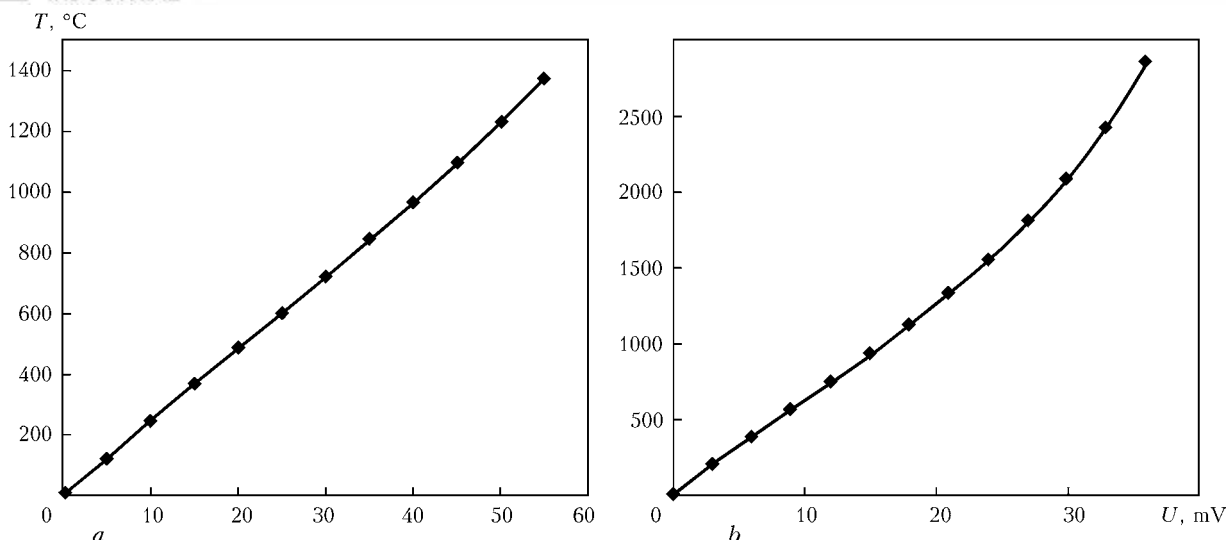
Figure 2. MCRTC metrological characteristics: a — mode of thermocouple of CAT type; b — mode of thermocouple of WRT type (A1)

technologies it is possible to solve the problems of both galvanic decoupling and reliable data exchange between the controllers and PC. Ethernet-100Base-TX bus is usually used as physical interface, and Internet-protocols of TCP/IP and TELNET type ensure reliable connection and error-free data transmission. In connection with the fact that batch-produced thermocouple controllers with Internet connection are not available now, PWI developed a microprocessor controller, designed for recording thermal cycles of multipass welding [1] (further on referred to as MCRTC) which ensures digitizing signals from 9 thermocouples and issuing the results to PC by TELNET protocol with real-time labels (Figure 1).

MCRTC is designed as an analog and digital modules, connected to each other through galvanically decoupled interface of SPI type. Digital module uses 32-bit microprocessor LPC2378 (NXP Company). Analog module is realized on the basis of OA microcircuits of AD822 type and

Figure 3. Recorded thermal cycle of multipass welding (fragment): $\Delta t_{Ac3} = 15$ s; $t_{8/5} = 37$ s

24-bit sigma-delta ADC of AD7794 type (Analog Devices Company). «Cold junction» temperature is measured by thermistor B57861S with 10 kOhm resistance (EPCOS Company). Range of measured temperatures for thermocouples of CAT type is equal to 0–1300 °C, and for thermocouples of VR5/VR20 type it is 0–2500 °C. Sampling rate is 3 Hz for all the channels.

Application of galvanically decoupled interface of Ethernet-100Base-TX type allows placing MCRTC in the immediate vicinity of the object of studies, and removing the PC to up to 100 m distance, that will shorten the length of thermocouple wires to 1 m, and minimize the level of electromagnetic noise and interference.

Information exchange with the computer is performed through network protocol of TELNET type, which ensures storing the data received from the controller into the file specified by the user. MCRTC operation is controlled using three special commands: TIME — current time setting; TP — thermocouple type selection, and MEAS — sending thermocouple readings to the computer.

Calculation of thermocouple readings (in Celsius degrees) is performed by the known method based on the read value of thermocouple emf using calibration charts [2] and allowing for cold junction temperature. To assess the controller metrological characteristics, constant voltage was applied to its inputs through a resistance divider from a galvanic power source. Voltage at controller input was monitored by digital voltmeter MASTECH MS8218 (measurement pitch of 0.001 mV). After program displacement compensation at shorted inputs, metrological characteristics of all the measurement channels practically coincided. Differences of obtained «volt-

age-temperature» characteristics (Figure 2) from graduation charts [2] did not go beyond the limits of error ±0.2 °C.
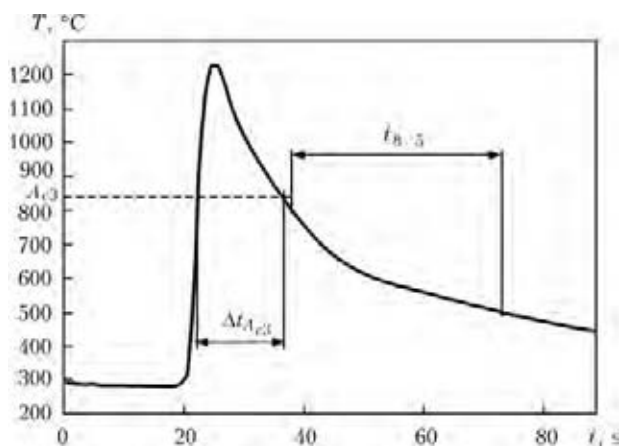
Figure 3 shows a fragment of thermal cycle obtained in an experiment with multipass welding of V-shaped groove by short sections, using the developed controller and subsequent data processing by MS Excel program. A thermocouple of CAT type with 0.6 mm wire diameter was used in the experiment, which was caulked in on the surface on an item from low-carbon steel at 5 mm distance from the groove edge. From Figure 3 it is not difficult to assess the time of metal staying above point A_{c3} (15 s), and time $t_{8/5}$ of cooling from the temperature of 800 to 500 °C (37 s). Maximum temperature in the controlled zone was 1240 °C.

Developed microprocessor controller used for identification of mathematical model of the heat source in MIG/MAG welding, as well as during investigations of structural transformations in steel in multipass welding, demonstrated a high stability to welding interference and reliability of data transmission in PC.

1. Dolinenko, V.V., Skuba, T.G., Vashchenko, O.Yu. (2012) Microprocessor controller for registration of thermal cycles of multipass arc welding. In: *Abstr. of 11th Int. Conf. on Instrument Engineering: State-of-the-Art and Prospects* (24–25 April 2012, Kiev). Kiev: NTUU KPI, 223.
2. *GOST R 8.585–2001*: Nominal static characteristics. Instead of GOST R 50431–92, MI 2559–99. Introd. 21.11.2001.

NEWS

DEPOSITION OF NICKEL COATINGS ON COPPER PLATES OF MOLDS OF MCCB USING FRICTION STIR SURFACING METHOD

Intensive wear-out of the internal surfaces of the molds takes place in a process of continuous casting of steel that makes extremely high demands to quality of surfaces of the copper plates. Copper plates with the nickel coating have the highest working capacity. This results in increased wear resistance of the copper plates in 3–4 times.

Fragment of 10 mm copper plate deposited by 3.5 mm thick nickel

Process of coating using FSS method

Technology for deposition of nickel on the copper plates of machines for continuous casting of billets using friction stir surfacing (FSS) based on friction stir welding method was developed at the E.O. Paton Electric Welding Institute of the NAS of Ukraine.

Welding is performed by a face of rotating tool having an extended pin which moves in a weld metal in welding direction. Plastification of the metal takes place in the metal-to-tool friction along the butt of surfaces being welded that results in its stir and formation of weld.

Material of the surfacing tool should be high-temperature and heat-resistant that allows working at 1000–1200 °C temperatures. Shape of the tool has an important role at that. Thus, the best results were obtained in application of a tool with conical pin.

Working tools were manufactured from ultra-hard materials, i.e. tungsten-cobalt hard alloys with microadditions of refractory compounds and cubic boron nitride, and they had complex configuration.

Lap slot weld is formed in a tool movement. Successive overwelding of such welds with overlaying allows nickel surfacing on the copper plate.

TECHNOLOGICAL INNOVATIONS — BASIS FOR INCREASE OF COMPETITIVENESS OF THE U.S. WELDING PRODUCTION

O.K. MAKOVETSKAYA

E.O. Paton Electric Welding Institute, NASU, Kiev, Ukraine

The tasks and problems of materials joining in industrial production are given. The model of development and implementation into production of technological innovations, offered by the Edison Welding Institute (USA), was considered.

The risk of loosing the leadership in the world economy causes ever more anxiety among the state and business spheres of the USA. In the recent years the country has lost its position in the world rating of competitiveness having moved from the first place in 2009 to the fifth one in 2011, and in 2010 the USA let China have the first place as to the volume of industrial production [1].

The sector of industrial production is the corner-stone for the US economy. Its volume amounts 11 % in the GDP of the country, and in the total volume of export the volume of goods of industrial production exceeds 60 %. About 13.4 Million people are engaged in industry which amounts about 9 % of all employees. The labor payment in the sector of industrial production is 20 % higher than that in the other non-industrial sectors of economy.

Since 2008 the crisis remains the main problem for the US economy. However negative tendencies in the economy of the country were revealed as long ago as 2001. By that time in the period of one year more than 2.5 Million working places were reduced in the sector of industrial production. Among the most anxious tendencies in the US sector of industrial production, experts outline the following:

• reduction of output of industrial products. The volume of industrial sector in GDP of the country for the period of 2000—2010 was reduced from 17 to 11 %;

• reduction of number of working places. In the period of 2000—2010, 37 % (6.5 mln) of working places were reduced in industry;

• reduction of volume of foreign trade (the volume of USA at the world market decreased from 19 to 11 % (2000—2010) that resulted in growing of the trade deficit;

• increase in prices on goods of industrial production (increase of costs connected with safety and protection of environment, taxation, labor payment, reclamation, etc. was reflected on the price of ready products which became one of the factors deteriorating its competitiveness at the world market);

• lack of qualified personnel. Only in the field of welding production the lack of qualified welders amounts 500 persons per year [2].

The technologies for materials joining are the indispensable part of industrial sector of economy. Welding and related technologies of joining are closely integrated into the production process of fundamental branches of industry and considered as the key non-alternative technologies for them. Taking into account such a decisive role of joining technologies for the economy, the Edison Welding Institute (EWI) together with the American Welding Society in 2010 initiated the wide-scale study of state-of-the-art and possible ways for growing competitiveness of industrial production where the materials joining is widely applied. In the frames of the project «The future of materials joining in the North America» the survey of goods manufacturers of six leading branches of industry was conducted to determine the basic problems of those branches and their needs in technologies for joining materials. The results of research were studied in 2011 at the final conference «The growth of competitiveness of industry: the future of materials joining in the North America» in the work of which the scientific, governmental and social organizations, leading manufacturers of welding technologies «Lincoln Electric», «Trumpf», «Miller Electric», etc. took part. In the final document the basic problems of materials joining in industrial

Table 1. Problems and priority tasks in the field of materials joining in the USA for the nearest five years (four first ranks on branches of industry are mentioned)

Problems and tasks	Rank on branches of industry					
	Automobile industry	Oil-and-gas industry	Military industry	Aerospace industry	Heavy-machine building	Power engineering
Deficit of qualified engineers and specialists in the field of quality control of joints		1	4			
Deficit of qualified workers-welders and workers of other professions		3			1	
Growth of competitiveness in countries with low payment of labor	3					
Increase of expenses for development and implementation of new processes, products, methods				2		2
Increase of time for evaluation of joints quality					3	
Broadening of application of new materials and their combinations	1	4	3	4	4	1
Implementation of new technological processes			2	1		
Decrease of time from designing to putting technologies into production			1	3		4
Creation of on-line system for informing about innovative technologies and methods, providing access to them	2					3
Increase of requirements to the quality of joints performance	4	2			2	

production and tasks of its development in the nearest five years were defined.

Under the modern conditions of globalization of world economy the only possible way for the growth of competitiveness in industry is innovative development, i.e. improvement of level of developments, reduction of time for implementation of technical innovations into production, improvement of level of education and qualification of personnel. The innovative development of economy implies also a high level of correlation between science, production and personnel training. According to the survey of enterprises of six leading branches of US industry carried out by the EWI, the problems available in the branch of materials joining are closely connected with the solution of namely these tasks. The results of survey are given in Tables 1 and 2 [3].

According to the results of research given above over the recent years the volumes of application of new progressive structural materials and their combinations will grow in all branches of industry (see Table 1). This is the basic task of the branch of automobile industry and power engineering, it is also included into the specified four tasks of other branches of industry. The designers and manufacturers are ever more interested in the application of new materials which improve technical characteristics of products and reduce their cost. For example, the need in re-

duction of mass of automobile resulted in increase of application of high-strength steels, aluminium, magnesium alloys and composites. The growth of application of new structural materials requires development of the new technologies for joining (see Table 2). It was mentioned by representatives of all the surveyed branches of industry, and for space-aircraft and military industry this problem is the most challenged. According to estimates of correspondents it is also necessary to reduce the cycle period «R&D — implementation of new developments into industrial production», to find the ways of reduction of costs on development and implementation of innovations, creation of on-line system for informing about innovative developments in the field of materials joining. In total, these tasks reflect the need in development of strategy for development of joining technologies (Table 2).

The next important task is involvement of qualified personnel into the field of joining technologies. According to the data of the US Statistics Bureau the number of employees and specialists of all welding professions in the period of 2002−2009 decreased from 1,076,498 to 968,037 people, or by 10.08 %. Nowadays the deficit of welders on long-term contracts amounts approximately 500 people per year. However this number can be higher as far as mastering the professional skills of welder is required else in

Table 2. Necessary industrial technologies of materials joining and other types of works (four first ranks on branches of industry are mentioned)

Required technologies/types of works	Rank on branches of industry					
	Automobile industry	Oil-and-gas industry	Military industry	Aerospace industry	Heavy-machine building	Power engineering
Development of technology for joining the new progressive materials	1	3	1	1	3	3
Increase in number and improvement of level of education of engineers and designers in the field of joining technologies		2	2			1
Development of arc welding process (efficiency, quality, etc.)		1	3		1	
Development of new methods for joining dissimilar materials	2			2		2
Providing the on-line access to the databases on technologies for materials joining		4				
Development of more sensitive, accurate, reliable methods of non-destructive testing	3		4	4		
Development of high-efficient technologies for welding thick-sheet materials					2	
Improvement of methods for education of welders (making them more perfect, purposeful, less expensive)					4	
Development of strategy of development of new joining processes						4
Improvement of resistance welding technology (quality, reliability, etc.)	4					
Development of additive industrial technologies				3		

more than 25 professions. According to the data of survey confirmed by the statistic data, the branches of US industry lack in qualified workers-welders, engineers and also other specialists in the field of welding and quality control. Thus, the main problem in oil industry is the lack of qualified engineers and specialists in the field of quality control of joints, and in heavy-machine building the main problem is the deficit of workers-welders (see Table 1). The lack of qualified personnel is closely connected with modernization of system of personnel training, development and implementation of system of constant improvement of qualification for the specialists of all professions [4].

The main source of innovations is R&D. According to the estimates of American experts the total costs on financing of research and developments in the world will grow by 5.2 % in 2012 and reach 1.4 Trillion USD, among which the volume of USA will amount 36 % or 436 Billion USD. The industry finances 64 %, the federal government 29 %, meantime 71 % of all R&D, carried out in the country, are performed in the industry. Table 3 gives data on structure of distribution of financing of R&D in USA on basic sources of financing and performers.

The field of R&D becomes ever more opened for cooperation in USA as well as in the whole world. The data of Table 3 show considerable growth of finances by the industry of both its own R&D as well as fundamental ones carried out by academic organizations in the interests of the industry. The federal government attracts also considerable investments into the industrial R&D and other organizations. According to the data of survey of «R&D Magazine» 80 % of industrial companies finance joint research with academic organizations and other companies. Not only industry but also federal government shows ever growing interest in obtaining income from the investments into the R&D. If several years ago only 10 % of companies planned and obtained income from investments into R&D, nowadays already more than 50 % of companies consider this value as a key indicator of their activity.

The Act of Bayh-Dole accepted in 1980 laid grounds for the new state scientific and technical policy of USA directed to the growth of competitiveness of the national economy. The Act allowed transferring intellectual property, created at the federal costs, to such non-federal performers of R&D as universities, private companies and other subjects, and also allowed exclu-

Table 3. Structure of distribution of financing of R&D in the USA on the basic sources of financing in 2012, Million USD (percent of changes by 2011)

Financing source	Performer of R&D					
	Federal government	Governmental funds, centers, national laboratories	Industry	National fund and other academic organizations	Non-profitable organizations	In total
Federal government	29,152 (−2.5)	14,666 (−3.69)	37,577 (−2.42)	37,440 (093)	6817 (−2.29)	125,652 (−1.61)
Industry	–	202 (2.20)	237,487 (3.37)	3868 (26.49)	2129 (8.89)	279,685 (3.75)
National scientific fund and other academic organizations	–	–	–	12,318 (2.85)	–	12,318 (2.85)
Other governmental organizations	–	–	–	3817 (2.72)	–	3817 (2.72)
Non-profitable organizations	–	–	–	3491 (2.70)	11,055 (2.70)	14,546 (2.70)
In total	29,152 (−2.51)	14,868 (−2.36)	311,063 (2.63)	60,934 (2.85)	20,001 (1.55)	436,018 (2.07)

sive licensing of inventions which is the key condition for their commercialization. This and another accepted acts and decrees of the government, state programs of USA and stimulated integration of fundamental and applied science, strengthened interest of industry in performance of fundamental research, activated the inter-discipline research, changed the policy as applied to research infrastructure [5, 6].

To stimulate the carrying out of technological R&D in the field of joining technologies, to strengthen correlation among scientific and industrial sector, to reduce significantly the time and broaden the branches of implementation of innovation products, the EWI together with the Institute of Industry (USA) created a model of development and implementation of technological innovations into industry in the field of joining technologies and successfully approbated it in practice. The proposed model is based on the idea of creation of new organizational structures which could promote the closer integration of all participants of innovation process: from the idea to development commercialization and wide implementation of innovations into production, namely:

• focused industry consortia, and

• manufacturing technology application centers.

Consortium is the temporary union of industrial enterprises interested in development of new progressive technology. The members of consortium define the basic technological problems which require attention, form project program and team of performer. As the performers for solution of different specific tasks the consortium can attract centers of development and imple-

mentation of industrial technologies, research laboratories, commercial structures and other organizations. The support of innovations development to the stage of commercialization is performed by the state through the state programs. The implementation of innovations into industry implies wide attraction of funds of industrial foundations and other sources. Table 4 shows scheme of interaction of consortium and development centers and implementation of industrial technologies. This scheme demonstrates one of the possible ideas of functioning of consortium, i.e. the possibility of attraction in the course of development of innovation for the solution of definite tasks of specialized centers of development and implementation of industrial technologies and material resources which have available highly qualified personnel and necessary material resources.

The aim of the model of consortium developed by the EWI is to reveal the needs in new technologies of materials joining arising in the branches of industry, to realize the development of these technologies and develop programs of partner cooperation for the creation and wide implementation of new technologies into production. The example of realization of this model in practice is the Consortium of Additive Technologies and the Consortium of Technologies of Nuclear Power Engineering created by the EWI in 2010.

For example, the Consortium of additive technologies combined the efforts of large corporations of US space-aircraft industry, the clients of the EWI and other private, social and state organizations interested in the development and wide implementation into production of ad-

Table 4. Scheme of interaction of the purposeful industrial consortia and centers of development and implementation of industrial technologies

Purposeful industrial consortia	Centers of development and implementation of industrial technologies							
	Automation	Casting	Assembly of electronics	Stamping	Control	Joining	Additive technologies	Treatment
Production of metal for aircraft industry using additive technologies	×				×	×	×	×
Decrease in automobile mass		×		×	×	×	×	
High-speed assembly of batteries	×		×		×	×		
Ecologically clean production of electronics	×		×			×		
Manufacturing of equipment for nuclear power plants		×			×	×	×	×
Automation of process of production of equipment for heavy-machine building	×				×	×	×	×

vanced additive technologies. In total the Consortium united 24 industrial members and partners for performance of research. The industrial members of Consortium are the companies-producers and consumers and investigation partners: five universities and such organizations as Army, Air Force, Navy, NIST, NASA. The development and implementation of this model was supported by the state. The state Ohio allotted the many-million grant for realization of this project.

If the aim of consortia is to solve the strategic and organizational tasks on development of the new technology, the centers of development and implementation of industrial technologies are the basic performers of this project. These organizations should be recognized as the world class leaders in their field, equipped with the innovative equipment and having the highly qualified personnel. The example of such center in the field of materials joining is the EWI. It closely cooperates in the work with research universities and industrial sector which allows realizing of innovation developments and their successful implementation into production. Since 1984 the Institute has a constant state support according to the Ohio Edison Program. The constant development, efficiency of work and high level of return of investments attract private investors. In 2010 the volume of private investments into the developments of the EWI 20 times exceeded the volume of state financing [7].

The innovation model of development and implementation of technologies proposed by the EWI was approved by the government of the USA. The National Institute of Standards and Technologies at the Trade Ministry accepted the new state program on its basis to support the development of technological innovations in the USA «Advanced Manufacturing Technology Consortia» in 2011. The budget of the program for 2012 amounted to 12 Million USD. It envisages the support of development of such innovation directions as robotic technologies, nanomaterials, new progressive materials, new progressive production technologies. In total, the state allotted 75 Million USD to support the innovation programs in 2012 [8].

1. Bucher, K. US competitiveness ranking continues to fall: Emerging markets are closing the gap. *www*.weforum.org
2. (2011) Strengthening manufacturing competitiveness: Report from Conference 2010 on the Future of Materials Joining in North America. EWI, Febr. 2. *www*.ewi.org
3. Conrardy, C. Materials joining and technology. *www*.weldingandgasestoday.org
4. State of the welding industry report: executive summary. In: Weld-Ed. *www*.weld-ed.org
5. 2012 Global R&D Funding Forecast. In: Battelle. The Business of Innovation. *www*.battelle.org
6. Dezhina, I. (2011) Support of fundamental science in USA: Lessons for Russia. *Bytie Nauki*, **94**, 6–7.
7. Revitalizing American's manufacturing innovation infrastructure. Response to the NIST AMTech Request for Information. EWI. *www*.ewi.org
8. President Obama Launches Advanced Manufacturing Partnership. *www*.nist.go

EXPERIENCE OF APPLICATION OF HF ELECTRIC WELDING APPARATUS EK-300M1 IN SURGERY

O.N. IVANOVA[1], **A.T. ZELNICHENKO**[2], **D.D. KUNKIN**[1], **V.V. PEREKREST**[3] and **V.A. TODORENKO**[3]
[1]International Association «Welding», Kiev, Ukraine
[2]E.O. Paton Electric Welding Institute, NASU, Kiev, Ukraine
[3]NTUU «Kiev Polytechnic Institute», Kiev, Ukraine

Presented are the data illustrating advantages and areas of application of HF electric welding apparatus EK-300M1 in surgery.

Keywords: *electric welding, soft live tissues, high-frequency apparatus EK-300M1, area of application, advantages*

Development of equipment and technology for high-frequency electric welding (HFEW) of soft live tissues became a priority for Ukrainian scientists, engineers and doctors.

In 1991 Prof. B.E. Paton and Prof. V.K. Lebedev put forward a hypothesis and proposed mathematical model which were proved by series of experiments on animals. This allowed stating a possibility of electric welding of soft live tissues with preservation of their viability. It is time to develop the laboratory samples of techniques and experimental substantiation of the technology [1].

For this purpose an international project was developed in 1996 under the leadership of Prof. B.E. Paton with assistance of the E.O. Paton Electric Welding Institute (PWI), A.A. Shalimov National Institute of Surgery and Transplantology, International Association «Welding» and commercial credit company «Consortium Service Management Group Technologies Inc.», as well as series of medical institutions of Ukraine. Common work was successful. The first variants of system with dosed power supply, prototypes of samples of power sources and surgical instruments were proposed at the beginning.

Development of the power sources was stepwise. The first experimental variant was developed in 1992, the second in a period from 1995 to 1996, and the third one in 2003. EK-300M1 power source was developed in 2004 and its updated variant in 2007–2008 together with RI of Applied Electronics of NTUU «Kiev Polytechnic Institute» [2] and plant «Schyotmash» (Lubny, Poltava region). Experimental work was kept on during indicated periods in the PWI laboratories as well as in the clinics with assistance of the specialists of engineer and medical orientation.

The first State Certificate about registration of HFEW apparatus EK-300M1 in Ukraine was issued in January, 2001. This is a date of beginning of practical application for new method of tissue saving HFEW technology in surgery. The further State Registration Certificates were issued in 2004 and 2010. The State Certificates about registration in the Russian Federation (2006) and in Belarus (2009) were also obtained. Technology, method of HFEW and welding instruments were patented in Ukraine, Russia, USA, European Union, Canada, China, Japan and Australia [3–15]. All these allowed proceeding to the application of method of soft live tissue welding in different spheres at the clinics of 16 regions of Ukraine as well as in Russia, namely, three Moscow and Saint-Petersburg clinics.

Medical instruments being a constituent of the HFEW complex is developed simultaneously with work over the power source. Such main parameters as dimensions, form, weight of electrodes as well as requirement to design, i.e. comfortable operation, access to place of HFEW, workability of instrument in manufacture and repair are determined. All the types of electric welding medical instruments (forceps, clamps and laparoscopes) are the instruments of bipolar type. Instruments used for endoscopic and thoracoscopic surgical procedures are of a great interest. Experience of manufacture and practical application of such type of the instruments is accumulating. At that the experimental work is proceeded with and positive results are immediately transferred in the clinical conditions.

Large scope of experimental and research work promoted accumulation of experience of clinical application of HFEW and corresponding equipment.

The new electric welding technology is confidentially introduced in practice of surgery treatment of the patients with different pathologies. Continuous accumulation of experience in this direction allowed creating atlas «Tissue saving HFEW technology in surgery» in 2009. All the participants of development of this technology, i.e. specialists of engineer and medical orientation, became the authors of this book.

The atlas reflects the whole way from the first steps of researches up to the practical progress of clinicians who mastered around 130 types of surgical techniques as for 2009.

Development of given technology, improvement of HFEW equipment and new surgical techniques, increase of number of users of this equipment is observed today. Data on clinical application given by users of EK-300M1 equipment to new (after 2009) surgical techniques can be an example of this technology development. These are Odessa Regional Oncology Dispensary, Kiev Center of Endocrine Surgery, Institute of Pediatrics, Obstetrics and Gynecology of the NAMS of Ukraine, Donetsk Regional Anti-Cancer Center, V.P. Filatov Institute of Eye Diseases and Tissue Therapy, Zhitomir Regional Children's Hospital. These organizations successfully apply new techniques of surgery treatment using EK-300M1 for:

• septoplasty in children, in particular, in nooks;
• laryngeal cancer;
• treatment of pathologies of thyroid gland;
• organ saving operations on removal of tumor on ovaris in woman;
• bladder cancer;
• stomach cancer and breast cancer;
• metastatic lesions of liver (hepatic resection, marginal biopsy of liver, left and right hemihepatectomia, trisegmentectomia and bisegmentectomia);
• regmatogenous retinal detachment for blocking of retina rupture;
• endoresection of intraocular neoplasms;
• microsurgery of trabecular apparatus of eye and iris.

Original instruments for work in cavity of vitreous body of eye and technique for obtaining adequate devitalization of tumorous focuses that reduces a risk of uncontrolled bleeding in endoresection of uveal melanoma are developed up to present time. HFEW technology is used at endoscopic, mainly laparoscopic operations in pediatric surgery for treatment of different pathologies.

Application of EK-300M1 apparatus in opinion of medical staff allows achieving:

• significant reduction of blood loss at operative surgical intervention;
• minimization of thermal and mechanical injury of tissue that result in preservation of living cells and faster regeneration of tissues in place of coagulation at retention of functional activity of organ, including the possibility of preservation of reproductive function;
• change of scheme of performance of operative intervention with achieving of more simplified access to injured organ (experience of neurosurgical and urological operations);
• possibilities of performance of tissue saving operative interventions;
• reduction of time of operative interventions, i.e. time of patient being under effect of narcotic drugs;
• reduction of period of postoperative rehabilitation;
• decrease of time of patient hospital stay;
• elimination of application of foreign suture material;
• reduction of number of necessary medical instruments;
• improvement of work conditions for surgery team, lighten the work of surgeon, in particular, at nooks;
• elimination of infiltration formation;
• reduction of postoperative pain.

Thus, we already have excellent instrument for fight against illnesses and method of alleviating human's physical suffering.

The present technology develops as a living organism. Control of power complex is improved and new design solutions for apparatus and instruments are developed. These efforts are directed at quality improvement and increase of scope of surgical operations performed. The new electric welding complex has been already tested under clinical conditions. It will be added to surgeons' arsenal in the nearest time, i.e. the possibilities of fight against the illnesses and render the qualified help to the patients are expanded. It should be noted that principle of operation of EK-300M1 power sources in improvement remain the same in accordance with acquired patents.

1. Paton, B.E. (2004) Electric welding of soft tissues in surgery. *The Paton Welding J.*, **9**, 6–10.

2. Zelnichenko, A.T., Mironichev, A.V., Perekrest, V.V. et al. (2008) Hardware-software complex for investigation of electric welding process of live soft tissues. In: *Welding and Related Technologies into the Third Millennium*: Abstr. Kiev: PWI.

3. Paton, B.E., Lebedev, V.K., Vorona, D.S. et al. *Method of bonding of vessels and other animal and human hollow organs and device for its realisation*. Pat. 39907 Ukraine. Prior. 25.03.98. Publ. 16.07.2001.

4. Paton, B.E., Lebedev, V.K., Vorona, D.S. et al. *Method of bonding of soft biological tissues and fixture for its realisation*. Pat. 44805 Ukraine. Prior. 25.03.98. Publ. 15.03.2002.

5. Paton, B.E., Lebedev, V.K., Vorona, D.S. et al. *Bonding of soft biological tissues by passing high frequency electric current therethrough*. Pat. 2002/0091385 A1 US. Publ. 11.06.2002.

6. Paton, B.E., Lebedev, V.K., Lebedev, A.V. et al. *System and method for control of tissue welding*. Pat. WO 03/070284 A2. Prior. 13.02.2003.

7. Paton, B.E., Lebedev, V.K., Vorona, D.S. et al. *Bonding of soft biological tissues by passing high frequency electric current therethrough*. Pat. 6,562,037 B2 US. Publ. 13.05.2003.

8. Paton, B.E., Lebedev, V.K., Lebedev, A.V. et al. *System and method for control of tissue welding*. Pat. 2003/0158551 A1 US. Publ. 21.08.2003.

9. Paton, B.E., Lebedev, V.K., Lebedev, A.V. et al. *System and method for control of tissue welding*. Pat. 6733498 US. Prior. 19.02.2002. Publ. 21.08.2003.

10. Paton, B.E., Lebedev, V.K., Masalov, Yu.A. et al. *System and method for control of tissue welding*. Pat. 6,733,498 B2 US. Publ. 21.08.2003.

11. Paton, B.E., Lebedev, V.K., Lebedev, O.V. et al. *Instrument for bonding of soft biological tissues of animals and human*. Pat. 72901 Ukraine. Prior. 09.01.2004. Publ. 15.02.2006.

12. Paton, B.E., Lebedev, V.K., Vorona, D.S. et al. *Bonding of soft biological tissues by passing high frequency electric current therethrough*. Pat. 2005/0234447 A1 US. Publ. 20.10.2005.

13. Paton, B.E., Lebedev, V.K., Lebedev, O.V. et al. *Method of welding of animal and human soft tissues*. Pat. 75342 Ukraine. Prior. 19.06.2002. Publ. 17.04.2006.

14. Paton, B.E., Lebedev, V.K., Lebedev, A.V. et al. *Method of welding of biological tissue and device for welding of biological tissue (variants)*. Pat. 77064 Ukraine. Prior. 13.02.2003. Publ. 15.10.2006.

15. Paton, B.E., Lebedev, V.K., Lebedev, A.V. et al. *Method of welding of animal and human soft tissues*. Pat. 2294171 RF. Prior. 19.06.02. Publ. 27.02.07.

NEWS

REGULATOR FOR RESISTANCE WELDING

Regulator for resistance welding RKSM designed for control of welding cycle in multispot AC resistance welding machines was developed by «Obert» Ltd (Kiev) being specialized on development and manufacture of electric automated mechanisms for welding machines.

Capability of setting of up to 99 welding modes with their cyclic change in a process of operation of welding machine is the peculiarity of the regulator.

Immediately 8 valves and up to 32 valves using external expander of the outlets can be controlled by the welding cycle regulator.

Main technical parameters of regulator

Power consumed, V·A .... not more than 30
Dimensions, m .... 0.16 × 0.16 × 0.29
Weight, kg .... not more than 4
Number of welding current pulses 1–99
Regulation of welding cycle time periods
(compression–welding–pause between the pulses of
welding–cooling–forging), s 0–399
Regulation of real values of welding current, % 0–99
Duration of welding current rise (modulation)
is programmed in the ranges, % 0–99
Regulation of load power factor 0.2–0.8
Parameters of hyristor activation pulses:
    voltage, V 24
    duration of pulse, μs .... 200 ± 150
Parameters of signal for power supply of output
DC devices:
    voltage, V .... 24 ± 2
    current, A .... not more than 0.4
Number of actuating devices, pcs .... up to 8
Number of outputs (including pedal) 4

SCIENTIFIC-TECHNICAL CONFERENCE «MODERN PROBLEMS OF METALLURGY, TECHNOLOGY OF WELDING AND SURFACING OF STEELS AND NON-FERROUS METALS»

On October 25–26, 2012, the Scientific-Technical Conference «Modern Problems of Metallurgy, Technology of Welding and Surfacing of Steels and Non-ferrous-Metals», devoted to the 100th anniversary of Prof. I.I. Frumin and Prof. D.M. Rabkin, two famous scientists in the field of metallurgy and technology of welding and surfacing of steels and non-ferrous metals, was held at the E.O. Paton Electric Welding Institute of the NAS of Ukraine (PWI) in Kiev. The Conference was organized by PWI, Society of Welders of Ukraine and International Association «Welding».

More than 100 scientists and specialists in the field of welding and allied processes from research institutes, higher educational institutions and enterprises of Ukraine, Russia and Poland participated in the work of the Conference.

The plenary session of the Conference was opened by Prof. L.M. Lobanov, academician of the NAS of Ukraine. He described the course of life of Prof. Frumin and Prof. Rabkin.

Isidor I. Frumin was given an employment at the PWI by Evgeny O. Paton in 1937. Since 1941 to 1945 he took part in the Great Patriotic War. He finished the war in Berlin having a military rank of major and being the officer of chemical service of anti-aircraft division.

After demobilization, I.I. Frumin returned to the PWI, where he headed the chemical and flux laboratories, and then he was a chief for almost 30 years of the Department of physical-metallurgical problems of surfacing the wear-resistant and heat-resistant steels. Together with his team he accomplished a complex of fundamental works in the field of metallurgy of welding, theory of formation of pores and cracks in welding, developed and implemented the first fused fluxes in the industrial production.

A great contribution was made by I.I. Frumin to the creation of scientific and practical bases of the mechanized surfacing. Under his supervision the first flux-cored wires for surfacing, new methods and technologies of surfacing were developed which found the wide application in different branches of industry. I.I. Frumin became the first laureate of Evgeny Paton Prize of NASU for research, development and implementation of the mechanized surfacing of hot milling rolls. The State Prize of the USSR was awarded to him in the team of scientists for the development of flux-cored wires for welding and surfacing.

Daniil M. Rabkin began to work at the PWI in 1939 after graduation from the Kiev Industrial Institute (now NTUU «Kiev Polytechnic Institute»). In 1941–1943 he joined the ranks of Red Army. In 1943 he was recalled from the front to the PWI for urgent solution of problems connected with the development and implementation of technologies of welding of armor structures and shells at the plants of Ural and Siberia. All his further activity is connected with the PWI where he was dealing with the problems of metallurgy of welding of light alloys.

D.M. Rabkin showed himself as a talented researcher of processes of melting of aluminium alloys in arc welding and physical-chemical reactions in arc and weld pool. He fulfilled the fundamental studies both in the field of metallurgy and materials science of aluminium alloys and also in the development of new technologies of their welding, such as mechanized semi-open arc using halogenide fluxes, electroslag, electron beam, etc. He was awarded the Evgeny Paton Prize of NASU for the monograph «Metallurgy of fusion welding of aluminium and its alloys».

Then, Prof. I.A. Ryabtsev, the Chief of PWI Department of physical-metallurgical problems of surfacing the wear- and heat-resistant steels, made a speech. He said, in particular, that those investigations and traditions are continued and further developed in the Department which were established by I.I. Frumin. Over the recent years the Department is dealing with research and development of the new methods of optimization of structure and properties of the deposited metal. For this, the effect of structural heredity is used. To realize this effect, the nano-sized carbide compositions, which have an influence on structure and properties of the deposited metal without change of its chemical composition, are added into composition of surfacing flux-cored wires.

In collaboration with the S.P. Timoshenko Institute of Mechanics of NASU the Department is dealing with the development of mathematical models and methods of calculation of structural and stress-strain states of plane and cylindrical parts in surfacing and service under the conditions of simultaneous action of cyclic thermal and mechanical loads. Mathematical models make it possible to evaluate the service life of deposited mill rolls, dies and other similar parts using the method of calculation. In collaboration with the PWI Department of mathematical investigations an expert system «Naplavka» (Surfacing) was developed. The development of this system allowed systematizing the comprehensive knowledge on surfacing materials, technologies and technique of surfacing of almost all the parts which are subjected to surfacing in CIS countries. Taking into account the present feasibilities in obtaining the practical knowledge and experience on surfacing, the expert system can be used successfully in the process of education at the higher educational institutions.

Prof. A.Ya. Ishchenko (PWI), Corr.-Member of NASU, delivered a paper «Challenging technologies of welding the high-strength aluminium alloys». Aluminium alloys of different systems of alloying are widely used in aircraft, aerospace and defense engineering. In the paper the physical-metallurgical processes, proceeding in their welding, such as formation and measures of prevention of inclusions of oxide film in weld metal, causes and measures of prevention of porosity in weld metal in fusion welding, peculiarities of crystallization of multi-component alloys, formation and measures of prevention of hot cracks, chemical and structural heterogeneities, were analyzed. Characteristic of new and updated methods and technologies of welding using an electric arc, electron beam and laser source of heating was given. Over the recent years, the complexly-alloyed aluminium alloys with microadditions of scandium and zirconium have been developed, which are characterized by the high manufacturability and strength. Their weldability by fusion using updated technologies of welding is characterized as good or satisfactory, and the tensile strength of heat-hardened deformed semi-products reaches 750 MPa. The improvement of characteristics of weldability of these materials will provide the progressive design of many new products of transport purpose, such as airbuses, cars of high-speed trains, products of defense purpose, that will increase the technical and economic characteristics of their production and service.

Paper of Dr. E.F. Pereplyotchikov (PWI) was devoted to the achievements of the Institute in the field of plasma-powder surfacing (PPS), the progress of which is indispensably connected with the name of Frumin I.I. Under his supervision, the integrated and purposeful investigations of technological features of plasma surfacing, development of surfacing powders and equipment, as well as implementation of the process in the different branches of industry were carried out. PPS is especially effective under the conditions of manufacture of different-purpose reinforcement with sealing surfaces, deposited by alloys on cobalt, nickel, iron, copper base. A large experience is gained in surfacing of parts as small gates, stop valves (DN50), and also large ones (DN1000 and larger) for stationary and transport power plants, chemical enterprises, oil-and-gas pipeline, Technology and surfacing powder PR-X18FNM for PPS of worms of extruders of polymeric machines, operating under the conditions of abrasive wear and corrosion effect of environment, developed at the PWI, represent a great interest. The plasma surfacing in repair of worms is especially effective, as it allows at small expenses not only restoration of expensive part, but also increase its serviceability, and, moreover, restoration of worn-out worms several times. PPS is used in industry for surfacing of exhaust valve of internal combustion engines of different types and sizes, staring from valves of motor cars of 20–35 mm diameter and finishing by valves of ship diesels of 300–450 mm diameter. In surfacing of valves the most important advantage of PPS is greatly manifested, i.e. possibility of deposition of thin layers at low thermal effect on the parent metal.

The paper of Dr. O.G. Kuzmenko (PWI) described the developments of the Institute in the field of electroslag surfacing (ESS). A unique design of a non-consumable electrode, i.e. current-carrying mould (CCM), was made at the Institute. With use of the CCM the filler materials can be fed to a slag pool in the form of a tubes, bars, wires, shot, liquid filler material, etc. The grainy material is most promising for surfacing in CCM. With its use it is possible to produce the deposited layers of preset sizes and chemical composition, as well as to influence actively on the processes of deposited metal crystallization and its properties. The largest experience was gained in manufacturing and restoration surfacing of mill cast iron rolls using a shot. At PWI a method of producing the multi-layer metal by ESS with liquid metal was developed and implemented in industry. The process is

started with pre-fusion of a hard billet, then the metal, melted in a separately-standing furnace, is poured on the pre-fusion surface and the electroslag process is maintained by non-consumable graphitized electrodes. The deposited metal is solidified gradually by decreasing the electroslag process power. Owing to this, the metal is well refined and solidified in upward direction without defects of a shrinkage nature. At the present time, the developed technology passed successful test in industry for producing billets of bimetal dies, restoration of dies of hot deforming, etc.

Engineer A.Yu. Pasechnik (Donetsk National Technical University) described the works carried out at the laboratory of welding and surfacing in DNTU. The laboratory is dealing with the development and implementation of technologies of repair, strengthening and manufacturing of parts and components of mining and metallurgical equipment using the electroslag process. Indispensable specifics of the developed technologies is the possibility of their industrial realization directly in the sites of the equipment service, and also the use as initial materials of metal wastes.

Prof. V.Yu. Konkevich (All-Russian Institute of Light Alloys, Moscow) presented the paper about technologies of production and application of granulated aluminium alloys. The main advantages of a granular production of aluminium alloys consists in a feasibility of using the simpler technological scheme of producing the thin-walled semi-products; providing the economical production of products due to reduced cycle in combination with a high yield of an efficient metal; producing of semi-products of complexly-alloyed alloys, containing components in their composition in the amounts exceeding their limiting solubility in an equilibrium state.

Prof. E. Turyk (Institute of Welding, Gliwice, Poland) presented the paper «Experimental investigations of thermal resistance and resistance at cyclic temperature and constant mechanical loads of metal used for surfacing of rollers of machines for the continuous casting of billets». These experimental investigations were carried out using the metal deposited by wires which are used at Polish metallurgical plants for restoration and strengthening of rollers of MCCB. For comparison, the base metal of rollers (steel 34KhM) was tested using the same procedures. As a result of investigation, it was found using both procedures that during these tests specimens of steel 34KhM had the best properties. Among the deposited specimens the austenitic deposited metal Kh18N10 had the best prop-

erties. Properties of metal of martensitic 10Kh13 and martensitic-austenitic Kh13N4 classes had the lower properties. The lower resistance of specimens of deposited metal of steel types Kh18N10, 10Kh13 and Kh13N4 is, probably, connected with precipitations of chromium carbides at the boundaries of grains.

The paper of Dr. V.N. Matvienko (Priazovsky State Technical University, Mariupol, Ukraine) described the problems of increasing the life of mill rolls using surfacing and arc metallization. The work was fulfilled in collaboration with the Illjich Metallurgical Works. Because of increasing the cost of mill rolls, as well as due to growth in prices for surfacing materials, not only restoration of rolls, but also the development and mastering the production of surfacing materials directly at the Works become of current importance. At present, the production of alloyed surfacing strip 20Kh4MFB has been mastered at the Works for surfacing of mill rolls. The application of this strip (alongside with steel strips 08 (rimmed), 20 (semi-killed)) in combination with fused or agglomerated fluxes make it possible to surface the layers, the mechanical and service properties of which correspond to the service conditions of rolls. The surfacing of mill rolls using the surfacing materials manufactured at the Illjich Metallurgical Works provides a lower fraction of expenses (33–45 %) for restoration of worn-out rolls as compared with the cost of the new ones.

The paper of Dr. K. Madej (Institute of Welding, Gliwice, Poland) included the problems of welding of as-heat-treated structural steels of high strength with 690–1100 MPa yield strength. The brief characteristic of these steels, purpose, chemical composition, mechanical properties were given. Peculiarities of technology of welding of high-strength steels, in particular, the effect of heat input of arc welding on structure and mechanical properties of welded joints were considered. One of the main defects in welding of steels of similar type is the cracks, and the paper presented data on causes of their initiation and possible measures of their prevention.

Dr. A.G. Poklyatsky (PWI) presented paper at the Conference about the efficiency of application of friction stir welding for producing the permanent joints of aluminium alloys. The formation of welds in solid phase prevents the formation of pores, macroinclusions of oxide film, hot cracks and other defects. The absence of arc discharge and molten metal allows producing the permanent joints without application of shielding gas, as also avoiding the ultra-violet radiation

of arc, fumes, burn-out of alloying elements. The reduction of heat effect on metal promotes the decrease in residual stresses and deformations, thus leading to the lower distortion of welded structures and increasing their resistance to fracture. FS-welded joints of aluminium alloys have a large resistance to initiation and propagation of service cracks and a high fatigue strength.

In total, 27 papers and presentations were made at the Conference plenary session. In addition, more than 10 poster papers were presented in the reading-hall of the PWI library, representing a great interest to the Conference participants.

Prof. Ryabtsev I.A., PWI

NEWS

SPHERICAL TUNGSTEN CARBIDE

Technology for manufacture of powder refractory materials, in particular cast tungsten carbides WC + W_2C with spherical-shaped granules, using thermal centrifugal spraying was developed at the E.O. Paton Electric Welding Institute. Special unit SFERA-2500 was developed for centrifugal thermal spraying allowing obtaining of the granules from 50 up to 850 μm size at 15–20 kg material per hour efficiency.

Drill pipe lock cladded by spherical tungsten carbide

Unit for thermal centrifugal spraying SFERA-2500

Granulated tungsten carbides with $HV0.1 \geq$ ≥ 3000 MPa hardness exceeded the similar materials on its physical-mechanical and technological properties, and are successfully used for increase of wear resistance of the parts of drilling equipment and tool.

Developed material is widely used for plasma-powder, laser and oxy-acetylene cladding as well as strengthening of parts by impregnation method.

Strip cladding material of 8.0×3.0 mm section was developed on the basis of fused tungsten carbide

powders. It is delivered in the bundles for automatic plasma cladding or rods for oxy-acetylene and atomic-hydrogen cladding of parts of drilling equipment.
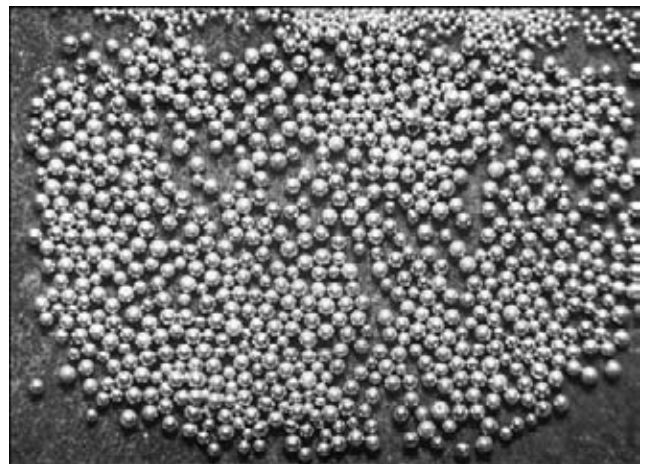
General view of spherical granules of fused tungsten carbides

SUBSCRIPTION
FOR «THE PATON WELDING JOURNAL»

If You are interested in making subscription directly via Editorial Board, fill, please, the coupon and send application by fax or e-mail.

The cost of annual subscription via Editorial Board is $324.

Telephones and faxes of Editorial Board of «The Paton Welding Journal»:

Tel.: (38044) 200 82 77, 200 81 45

Fax: (38044) 200 82 77, 200 81 45.

«The Paton Welding Journal» can be also subscribed worldwide from catalogues of subscription agency EBSO.

SUBSCRIPTION COUPON
Address for journal delivery

Term of subscription since   20   till   20
Name, initials
Affiliation
Position
Tel., Fax, E-mail

Subscription to the electronic version of «The Paton Welding Journal» can be done at site: *www: rucont.ru*

РУКОНТ
национальный цифровой ресурс

We offer for the subscription all issues of the Journal in pdf format, starting from 2009. You can subscribe to individual issues or to the entire archive including all issues over a period of 2009–2011. The subscription is available for natural persons and legal entities.

ADVERTISEMENT
IN «THE PATON WELDING JOURNAL»

External cover, fully-colored:
First page of cover
(190×190 mm) – $700
Second page of cover
(200×290 mm) – $550
Third page of cover
(200×290 mm) – $500
Fourth page of cover
(200×290 mm) – $600

Internal cover, fully-colored:
First page of cover
(200×290 mm) – $350
Second page of cover
(200×290 mm) – $350
Third page of cover
(200×290 mm) – $350
Fourth page of cover
(200×290 mm) – $350

Internal insert:
Fully-colored (200×290 mm) – $300
Fully-colored (double page A3)
(400×290 mm) – $500
Fully-colored (200×145 mm) – $150
Black-and-white (170×250 mm) – $80
Black-and-white (170×125 mm) – $50
Black-and-white (80×80 mm) – $15

• Article in the form of advertising is 50 % of the cost of advertising area
• When the sum of advertising contracts exceeds $1000, a flexible system of discounts is envisaged

Technical requirement for the advertising materials:
• Size of journal after cutting is 200×290 mm
• In advertising layouts, the texts, logotypes and other elements should be located 5 mm from the module edge to prevent the loss of a part of information

All files in format IBM PC:
• Corell Draw, version up to 10.0
• Adobe Photoshop, version up to 7.0
• Quark, version up to 5.0
• Representations in format TIFF, color model CMYK, resolution 300 dpi
• Files should be added with a printed copy (makeups in WORD for are not accepted)